

# DIAGNOSTIC IMAGING OF THE PITUITARY GLAND IN DOGS

**Roselinda van der Vlugt - Meijer**

*Voor mijn allerliefste vader  
die mijn grote voorbeeld was en altijd zal blijven*

*Voor Lex, Vera en Alex*

# **DIAGNOSTIC IMAGING OF THE PITUITARY GLAND IN DOGS**

## **Diagnostische beeldvorming van de hypofyse bij de hond**

(met een samenvatting in het Nederlands)

### **Proefschrift**

ter verkrijging van de graad van doctor aan de Universiteit Utrecht  
op gezag van de rector magnificus Prof. Dr. W.H. Gispen,  
ingevolge het besluit van het college voor promoties in het openbaar  
te verdedigen op donderdag 9 november 2006 des middags te 2.30 uur

door

**Roselinda Henrica van der Vlugt – Meijer**

geboren op 2 mei 1967 te Hellevoetsluis

Promotor: Prof. dr. P.Y. Barthez

Co-promotoren: Dr. G. Voorhout  
Dr. B.P. Meij

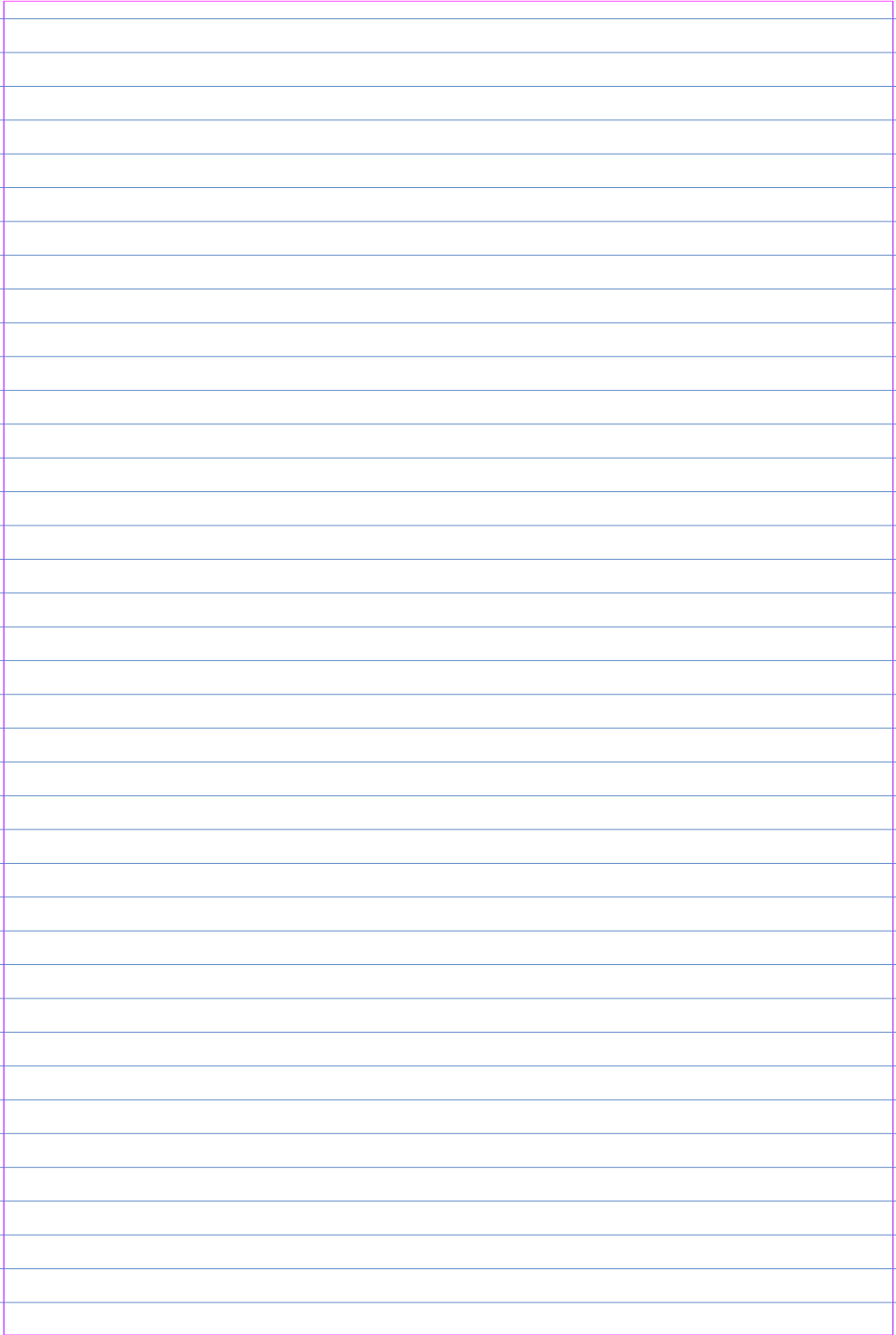
The studies described in this thesis were conducted at and financially supported by the Division of Diagnostic Imaging, the Department of Clinical Sciences of Companion Animals, Faculty of Veterinary Medicine, Utrecht University, Utrecht, The Netherlands.

Publication of this thesis was financially supported by

**ACE Pharmaceuticals BV and**

**ACE Veterinary Products BV**

## DIAGNOSTIC IMAGING OF THE PITUITARY GLAND IN DOGS



A large, empty rectangular box with a purple border, occupying the majority of the page below the title. This box is likely intended for a student to draw a diagram or insert an image related to the diagnostic imaging of the pituitary gland in dogs.

Cover Karin Bosch  
Figures Aart van der Woude, Joop Fama and Yvonne Pollak  
Lay-out Studio.karin@casema.nl  
Print Drukkerij De Jong Driebergen BV  
ISBN-10: 90-393-4379-9  
ISBN-13: 978-90-393-4379-1:

## Contents

List of Abbreviations	8
Chapter 1: General introduction and aims of the thesis	9
Chapter 2: Intraobserver and interobserver agreement, reproducibility, and accuracy of computed tomographic measurements of pituitary gland dimensions in healthy dogs	29
Chapter 3: Dynamic computed tomographic evaluation of the pituitary gland in healthy dogs	45
Chapter 4: Dynamic computed tomography of the pituitary gland in dogs with pituitary-dependent hyperadrenocorticism	65
Chapter 5: Dynamic helical computed tomography of the pituitary gland in healthy dogs	87
Chapter 6: Thin-slice 3-dimensional gradient-echo magnetic resonance imaging of the pituitary gland in healthy dogs	103
Chapter 7: Summarizing discussion and conclusions	121
Chapter 8: Samenvatting en conclusies in het Nederlands	135
Dankwoord	147
Curriculum vitae	151

## Abbreviations

CT	Computed Tomography
PDH	Pituitary-Dependent Hyperadrenocorticism
BW	Body Weight
P:B ratio	Pituitary gland Height to Brain area ratio
HU	Hounsfield Units
WW	Window Width
WL	Window Level
AI	Agreement Index
MRI	Magnetic Resonance Imaging
MPR	MultiPlanar Reconstruction
SE	Spin Echo
GE	Gradient Echo
SNR	Signal to Noise Ratio
CNR	Contrast to Noise Ratio
ROI	Region of Interest
SI	Signal Intensity
T	Tesla
HAH	Hypofyse afhankelijk hyperadrenocorticisme

# CHAPTER I

## General introduction and aims of the thesis

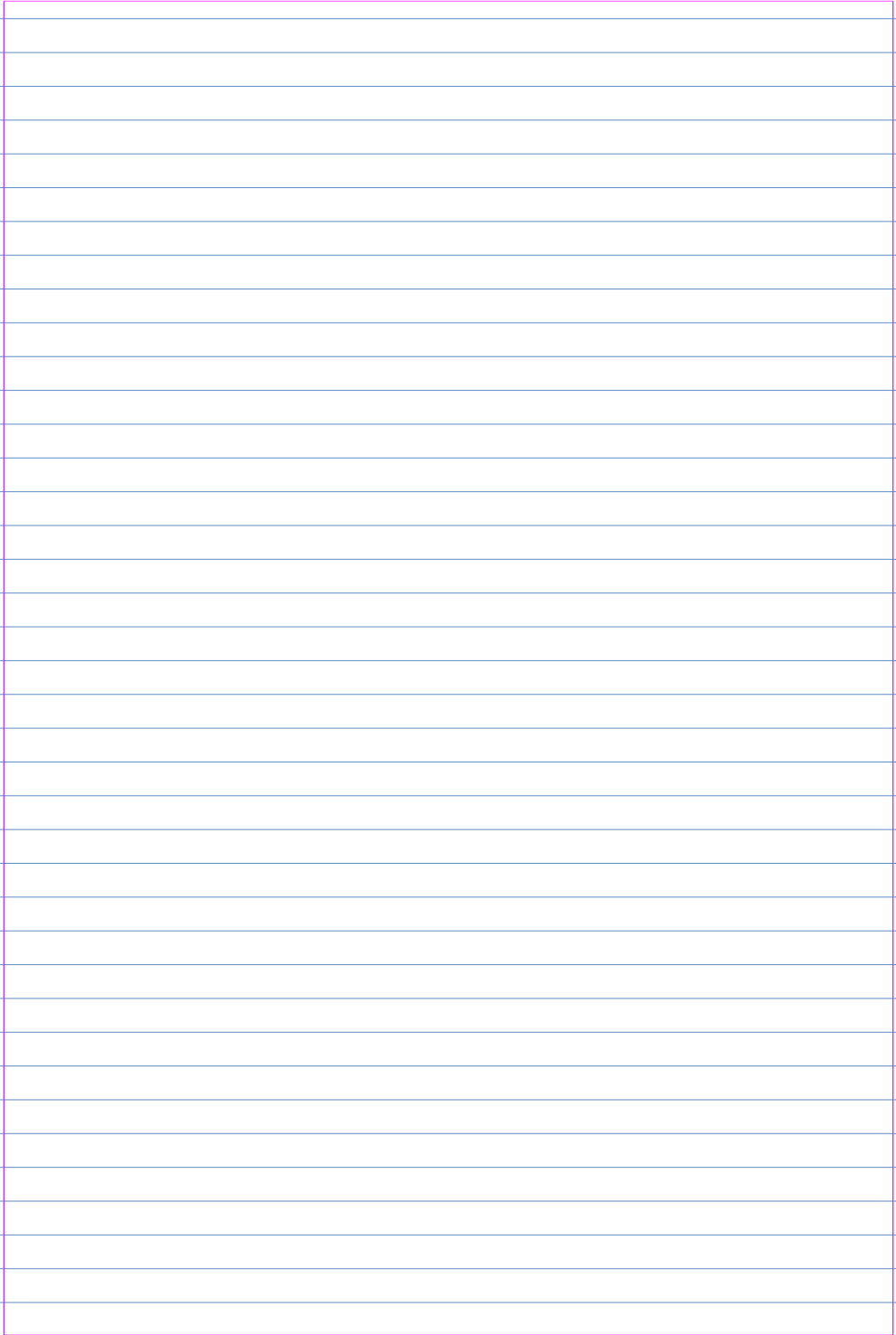
Based (in part) on:

Van der Vlugt-Meijer RH, Voorhout G, Meij BP.

Imaging of the pituitary gland in dogs with pituitary-dependent hyperadrenocorticism

**Molecular and Cellular Endocrinology 2002;197:81-87**

## DIAGNOSTIC IMAGING OF THE PITUITARY GLAND IN DOGS



A large, empty rectangular box with a purple border, occupying the majority of the page below the title. This box is likely intended for a student to draw a diagram or insert an image related to the diagnostic imaging of the pituitary gland in dogs.

# I. Nomenclature and Anatomy

## I.1. Nomenclature

In this thesis the nomenclature according to the *Nomina Anatomica Veterinaria* and the *Nomina Anatomica* is used for the pituitary gland.<sup>1</sup> According to this terminology the canine pituitary gland is composed of two main parts, the neurohypophysis and the adenohypophysis (Table 1).

Nomina Anatomica Veterinaria	Nomina Anatomica
Adenohypophysis (Lobus anterior)	
Pars infundibularis adenohypophysis	Pars tuberalis
Pars intermedia adenohypophysis	Pars intermedia
Pars distalis adenohypophysis	Pars distalis
Neurohypophysis (Lobus posterior)	
Pars proximalis neurohypophysis	Infundibulum
Pars distalis neurohypophysis	Lobus nervosus

**Table 1.** Terminology for the parts of the pituitary gland (*Glandula Pituitaria*) according to the *Nomina Anatomica Veterinaria* (NAV) and the *Nomina Anatomica* (NA, for man).

## I.2. Pituitary Gland

The canine pituitary gland lies in a shallow depression in the basisphenoid bone, the fossa hypophysialis, and is directed rostrocaudally with its long axis almost parallel to the ventral surface of the brain (Figure 1).<sup>1,2</sup> There is no real sella turcica, such as is found in man. Although the caudal clinoid processes may be well developed and arise from a prominent elevation, there is only a slight rostral elevation, the tuberculum sellae, corresponding to the anterior clinoid processes in man.

The pituitary gland is suspended from the midline of the hypothalamus by a cylindrical stalk (Figures 1 and 2). This stalk is an extension of the median eminence from the tuber cinereum of the hypothalamus and is the proximal part of the neurohypophysis, the pars proximalis neurohypophysis or infundibulum. The third ventricle continues as an invagination, the recessus neurohypophysis or infundibular recess, into the infundibulum. The pars proximalis neurohypophysis is continuous with the distal enlargement, the pars distalis neurohypophysis which is the major portion of the neurohypophysis. The major

part of the pars distalis adenohypophysis, lies rostroventral to the pars distalis neurohypophysis, and, unlike in man, it almost entirely surrounds the pars distalis neurohypophysis. The pars proximalis adenohypophysis also extends as a cuff or collar around the pars proximalis neurohypophysis. The inner portion of the pituitary gland, which is in direct contact with the neurohypophysis, is termed the pars intermedia adenohypophysis. The pars intermedia remains separated from the pars distalis adenohypophysis by a remnant of Rathke's pouch, the hypophyseal cleft.

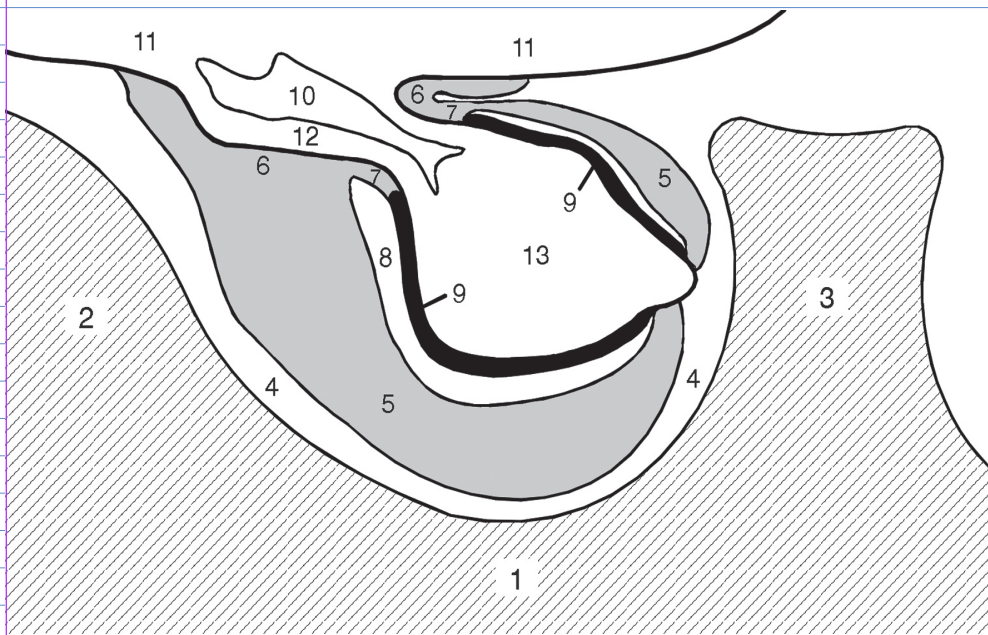


**Figure 1.** Schematic representation of the pituitary gland in relation to the pituitary fossa. The diagram was reconstructed from a sagittal median microscopic section of the canine pituitary gland. Left is rostral, right is caudal.<sup>42</sup>

- |   |  |
|---|--|
| 1 = Sphenoid bone                       | 8 = Hypophyseal cleft or cavity            |
| 2 = Tuberculum sellae                   | 9 = Pars intermedia adenohypophysis        |
| 3 = Dorsum sellae                       | 10 = Third ventricle (infundibular recess) |
| 4 = Pituitary fossa                     | 11 = Hypothalamus (median eminence)        |
| 5 = Pars distalis adenohypophysis       | 12 = Pars proximalis neurohypophysis       |
| 6 = Pars infundibularis adenohypophysis | 13 = Pars distalis neurohypophysis         |
| 7 = Transitional zone                   |  |

The pituitary gland is enveloped by two layers of dura mater: an outer layer that follows the pituitary fossa and blends with the endosteum and the capsule of the pituitary gland, and an inner layer that passes over the dorsal aspect of the pituitary gland, as diaphragma sellae, and also blends with the capsule of the pituitary gland.<sup>1,3,4</sup> The two layers of dura mater also envelop the paired cavernous sinuses at the ventrolateral aspect of the pituitary gland (Figure 2).<sup>1,3-5</sup> The arachnoid membrane follows the inner layer of dura mater and thus the subarachnoid space covers the dorsal aspect of the pituitary gland and, coursing around the pituitary stalk, connects the chiasmatic and intercruclal cisternae.<sup>1,4,6</sup>

### **1.3. Vascularization of the Pituitary Gland**

The internal carotid arteries run a short distance in the cavernous sinuses to a point just cranial to the pituitary gland, where they perforate the inner layer of dura mater and the arachnoid membrane, and come to lie in the subarachnoid space. The internal carotid arteries then run dorsally along the pituitary gland and optic chiasm, to trifurcate as rostral cerebral, caudal communicating, and middle cerebral arteries. A small rostral intercarotid artery arises from the trifurcation. The rostral cerebral and caudal communicating arteries form the cranial and lateral parts of the cerebral arterial circle. Caudally, the basilar artery, which lies in the subarachnoid space at the ventral aspect of the medulla oblongata and the pons, anastomizes with the cerebral arterial circle just cranial to the pons.<sup>5,7,8,9</sup>

A small caudal intercarotid artery leaves the first part of the internal carotid artery as it enters the cavernous sinus. The caudal intercarotid artery gives off branches, the caudal hypophyseal arteries, which supply the neurohypophysis (Figure 3).<sup>1,5,7</sup> Several arteries leave the cerebral arterial circle and the rostral intercarotid artery and run to the stalk of the pituitary gland where they form the mantle plexus. From this mantle plexus many arterioles enter the median eminence and provide capillaries to the primary blood capillary network. The capillaries of this network receive the releasing hormones from the hypothalamus which are subsequently carried to the capillaries of the adenohypophysis, the secondary blood capillary network, via a portal vascular system, the long hypophyseal portal vessels. So, the neurohypophysis has a direct arterial blood supply, while the adenohypophysis receives blood via portal vessels originating from the mantle plexus. There is some degree of circulatory blood flow within the pituitary gland present.<sup>10,11</sup>

## 2. Pituitary-Dependent Hyperadrenocorticism

Hyperadrenocorticism is one of the most frequently occurring endocrinopathies in dogs and it shares many of the important characteristics with Cushing's syndrome in humans.<sup>12-14</sup> In dogs, the diagnosis hyperadrenocorticism is based on the history, clinical signs, and elevated urinary corticoid / creatinine ratios.<sup>14</sup> Spontaneous hyperadrenocorticism can be caused by autonomous

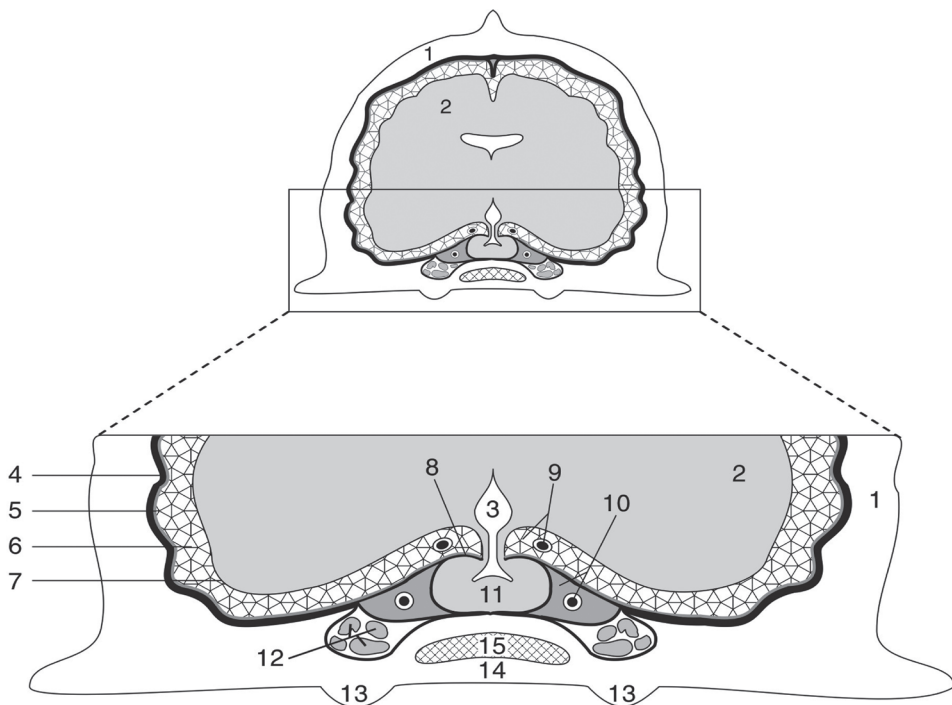


**Figure 2.** Schematic transverse view of canine skull through the centre of the pituitary fossa and a close-up view of the pituitary gland in relation to the meninges.<sup>42</sup>

- |                                       |  |
|---------------------------------------|--|
| 1 = Cranium                           | 9 = Basal cisterna with caudal communicating a.                              |
| 2 = Cerebrum                          | 10 = Cavernous sinus with internal carotid a.                                |
| 3 = Third ventricle                   | 11 = Pituitary gland   |
| 4 = Dura mater                        | 12 = Nerve groove for ophthalmic, abducent, trochlear, and oculomotor nerves |
| 5 = Arachnoid membrane                | 13 = Pterygoid bone  |
| 6 = Subarachnoid space and trabeculae | 14 = Sphenoid bone   |
| 7 = Pia mater                         | 15 = Sphenoid sinus  |
| 8 = Diaphragma sellae                 |  |

secretion of glucocorticoids by an adrenocortical tumor (ACTH-independent) or by excessive adrenocorticotrophic hormone (ACTH) secretion (ACTH-dependent) by a corticotroph pituitary adenoma or an ectopic ACTH-producing tumor. To distinguish between ACTH-dependent and ACTH-independent hyperadrenocorticism, a high dose dexamethasone suppression test is performed.<sup>14</sup> If a high dose of dexamethasone decreases cortisol secretion with at least 50% (dexamethasone-sensitive), hyperadrenocorticism is caused by excessive ACTH secretion. If suppression of cortisol secretion is less than 50 % (dexamethasone-resistant), hyperadrenocorticism may be due to an adrenocortical tumor or due to dexamethasone-resistant ACTH excess secretion. For differentiation of the latter two, measurement of endogenous ACTH is necessary.<sup>14</sup> In dogs with adrenocortical tumors basal ACTH values are suppressed and much lower values are found than in cases of excessive ACTH secretion. ACTH-dependent hyperadrenocorticism, which accounts for about 85% of the dogs with hyperadrenocorticism, originates mainly from adenomas in the pituitary gland and is therefore called pituitary-dependent hyperadrenocorticism (PDH).<sup>14</sup> An ectopic or paraneoplastic ACTH syndrome has recently been described in a dog, characterized by high plasma ACTH levels and dexamethasone-resistant hyperadrenocorticism. The syndrome is very rare in dogs, but should be considered when no pituitary neoplasia can be demonstrated.<sup>15</sup>

### 3. Treatment of PDH

Various therapies have been described for the treatment of PDH, including medical treatment with o,p'-DDD (mitotane), trilostane, and ketoconazole, and surgical therapy by performing a bilateral adrenalectomy.<sup>14,16</sup> These therapies are efficient in decreasing cortisol production by the adrenal glands and reducing the clinical signs.<sup>14,16</sup> However, these therapies are not effective against the ACTH-producing pituitary tumor itself and, in time, neurological signs may develop due to expansion of the tumor mass.<sup>17-20</sup> Furthermore, several other problems remain in the use of these therapies, including the occurrence of severe adverse effects, the need for repeated or continued treatment, and the development of Addison's disease.<sup>16,17,20</sup> Radiotherapy has been described in dogs with macrotumors and neurological signs, but was only moderately successful.<sup>21</sup>

Transsphenoidal hypophysectomy has been demonstrated to be an effective method of treatment in dogs with PDH.<sup>22,23</sup> However, a prerequisite

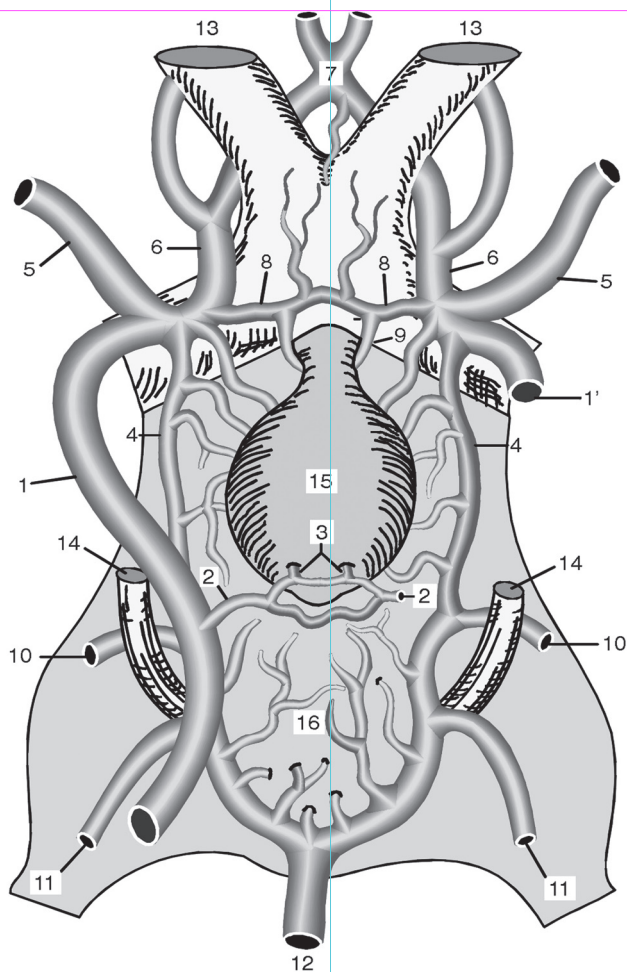


**Figure 3.** Ventral view of the arterial vascularisation of the pituitary gland after complete removal of the dura mater.<sup>42</sup>

1 = Left internal carotid a. in cavernous sinus (not shown)

1' = Left internal carotid a.

2 = Caudal intercarotid a.

3 = Caudal hypophyseal a.

4 = Caudal communicating a.

5 = Middle cerebral a.

6 = Rostral cerebral a.

7 = Rostral communicating a.

8 = Rostral intercarotid a.

9 = Rostral hypophyseal a.

10 = Caudal cerebral a.

11 = Rostral cerebellar a.

12 = Basilar a.

13 = Optic nerve

14 = Oculomotor nerve

15 = Pituitary gland

16 = Position of dorsum sellae (not shown)

for pituitary surgery is some sort of preoperative pituitary imaging assessing the size of the pituitary gland and its exact location in relation to the surgical landmarks.<sup>22,23</sup>

## 4. Diagnostic Imaging

### 4.1. Imaging Planes

Because of the quadruped position of the dog, some of the anatomical planes and directions for the skull, which are used in humans, cannot be used in veterinary diagnostic imaging. Adjectives that have common usage in human anatomy, such as “anterior”, “posterior”, “superior” and “inferior” are not appropriate in veterinary anatomy. This is especially true for the head of the dog, with the nose positioned as an extension of the spine, instead of perpendicular to the spine like in man (Figure 4). The single plane that is identical between humans and animals is the sagittal plane, which divides the body and head in the median plane in two symmetrical halves, i.e., a left and a right part (Table 2). The structures that lie closer to the median plane are classified as medial while structures lying towards the flank of the body are classified as lateral. Sections of the head and trunk that are parallel to the back are classified as the coronal plane in humans, and as the dorsal plane in dogs (Figure 4). The coronal plane in humans usually divides the body in anterior and posterior parts, while in dogs the dorsal plane divides the body in dorsal and ventral parts (Table 2). Sections of the head and back which are at right angles to the axis are referred to as axial in humans and transverse in animals (Figure 4). The axial plane divides the human body in superior and inferior parts, and the human head in cranial and caudal parts. The transverse plane divides the canine body in cranial and caudal parts, and the head in rostral and caudal parts (Table 2).

Human		Dog	
Anatomical plane	Anatomical direction	Anatomical plane	Anatomical direction
Sagittal	Left and right or medial and lateral	Sagittal	Left and right or medial and lateral
Coronal	Anterior and posterior	Transverse	Rostral and caudal
Axial	Cranial and caudal	Dorsal	Dorsal and ventral

**Table 2.** Anatomical planes of the skull in humans and dogs.

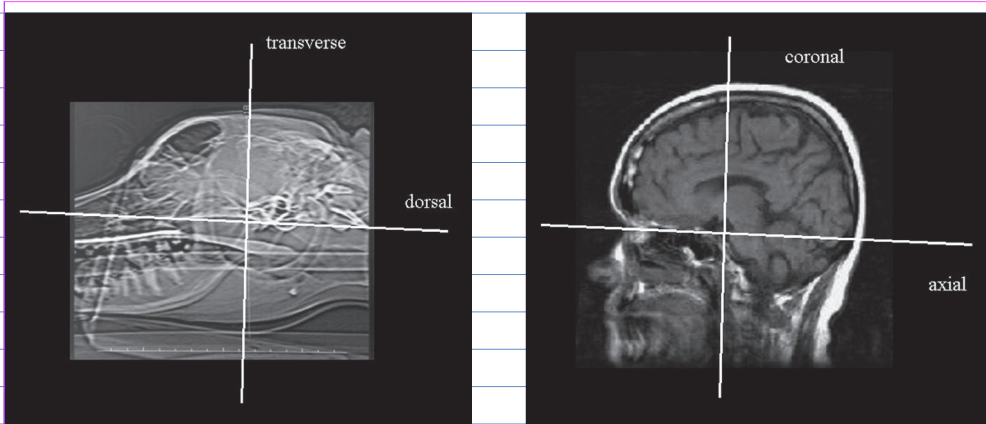


*Figure 4. Anatomical planes of the skull in the dog (A) and in man (B).*

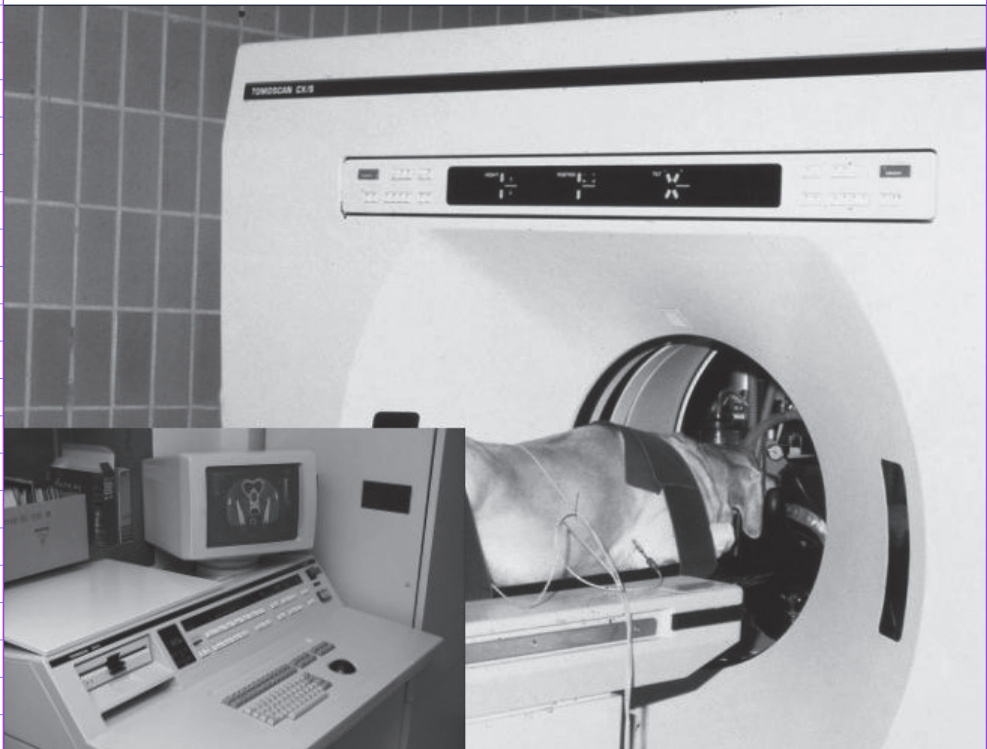


*Figure 5. Third generation CT scanner (Philips Tomoscan CX/S) and working station with console (insert) at the Division of Diagnostic Imaging of the Utrecht University, The Netherlands from 1990 until 2004.*

## 4.2. CT and MRI in Veterinary Medicine

Developments of diagnostic imaging techniques in veterinary medicine, like computed tomography (CT) and magnetic resonance imaging (MRI), have followed the developments in human medicine. The introduction of these techniques in the veterinary field largely depends on costs of purchase and maintenance of the equipment. The owners of companion animals and horses are increasingly willing to pay for advanced diagnostic imaging techniques that may lead to (new) therapies that prolong the life of their animals. CT and MRI usually require a long duration of immobilization which necessitates sedation or anaesthesia of the animals. Anaesthesia is difficult to monitor in a closed MRI scanner and expensive, MRI-compatible, equipment is needed.

Until the 1990's, advanced imaging equipment of human hospitals were occasionally used for animals. Imaging was performed with protocols that were developed for humans. Because of medical hospital regulations which prohibit animals from entering the hospitals, it is nowadays in the Netherlands nearly impossible to make use of equipment intended for human use. At the Division of Diagnostic Imaging, a third generation CT scanner (Tomoscan CX/S, Philips, Eindhoven, The Netherlands) was installed in 1990 (Figure 5). This CT scanner became a very useful and relatively inexpensive diagnostic imaging tool. However, since continuous rotation of the tube was not possible, the imaging protocols were of rather long duration. This machine was replaced by a single-slice helical CT scanner (Philips CT Secura, Philips Medical Systems, Eindhoven, The Netherlands) in 2004, enabling scanning of volumes at shorter duration (Figure 6). In 2000, a 0.2 Tesla open MRI scanner (Magnetom Open Viva, Siemens AG, Germany) was installed (Figure 7). With this machine it was possible to make images of both small and large animals under anaesthesia. Open MRI machines have, however, relatively low field strengths.

## 4.3. Imaging of the Pituitary Gland

Before computer-based imaging modalities, such as CT and MRI, were routinely available in veterinary medicine, several techniques have been described for visualizing the pituitary gland in dogs.<sup>24-27</sup>

### 4.3.1. Cisternography

Cisternography, which involves the injection of radiographic contrast medium into the subarachnoid space, allows imaging of the pituitary gland because of the close anatomical relationship between the dorsal aspect of the



*Figure 6. Helical CT scanner (Philips CT Secura) and working station with console (insert) at the Division of Diagnostic Imaging of the Utrecht University, The Netherlands from 2004 until present.*



*Figure 7. 0.2 Tesla open MRI scanner (Siemens Magnetom Open) at the Division of Diagnostic Imaging of the Utrecht University, The Netherlands from 2000 until present.*

pituitary gland and the subarachnoid space.<sup>28,29</sup> The length and width of the pituitary gland can be measured on a dorsoventral radiograph (Figure 8A), while the height can be measured on a sagittal linear tomogram through the midline of the skull (Figure 8B). Suprasellar expansion of a pituitary tumor can be identified by absence of contrast medium along the dorsal aspect of the gland on a sagittal linear tomogram (Figure 9). The dorsal extension into the suprasellar region is the first sign of pituitary gland enlargement in case of a corticotroph tumor<sup>30</sup> and the slightest increase in height can be assessed using cisternography and linear tomography. However, the magnitude of suprasellar expansion cannot be assessed with this technique.<sup>31</sup>

### 4.3.2 Computed Tomography

Computed tomography (CT) enables imaging of the pituitary gland. The pituitary gland lies outside the blood-brain barrier, and, following the IV administration of radiographic contrast medium, pituitary glands and pituitary adenomas will enhance on CT images. There is some insight in the size of the pituitary gland in healthy dogs and it varies among breeds and among individual dogs of the same breed.<sup>1</sup> However, the reference values do not necessarily cover the wide range of variations that may be found in very small and very large dogs. An accurate distinction between enlarged and non-enlarged pituitary glands in dogs with PDH was made by calculating the ratio between the height of the pituitary gland from a transverse contrast-enhanced CT-image through the center of the pituitary and the area of the brain from the same image (pituitary height/brain area (P/B) ratio).<sup>30</sup> No information is available on observer-dependent variability and the accuracy of the measured values.

Large pituitary tumours with suprasellar extension are readily diagnosed on CT-images (Figure 10). However, in almost 40% of dogs with pituitary-dependent hyperadrenocorticism, the disease is caused by a microadenoma that does not change the size and shape of the pituitary gland.<sup>30</sup> Microadenomas and small macroadenomas often can not be localized on routine contrast-enhanced CT-images, due to isoattenuation.<sup>32,33</sup>

In humans, microadenomas have been identified by use of dynamic CT.<sup>34-36</sup> Dynamic contrast-enhanced CT includes a series of scans of identical slice thickness, at the same slice position through the center of the pituitary gland, during and after IV injection of a bolus of contrast medium.<sup>34,35,37</sup> During dynamic CT in humans, enhancement of the internal carotid artery is observed followed by enhancement of the central part of the anterior lobe

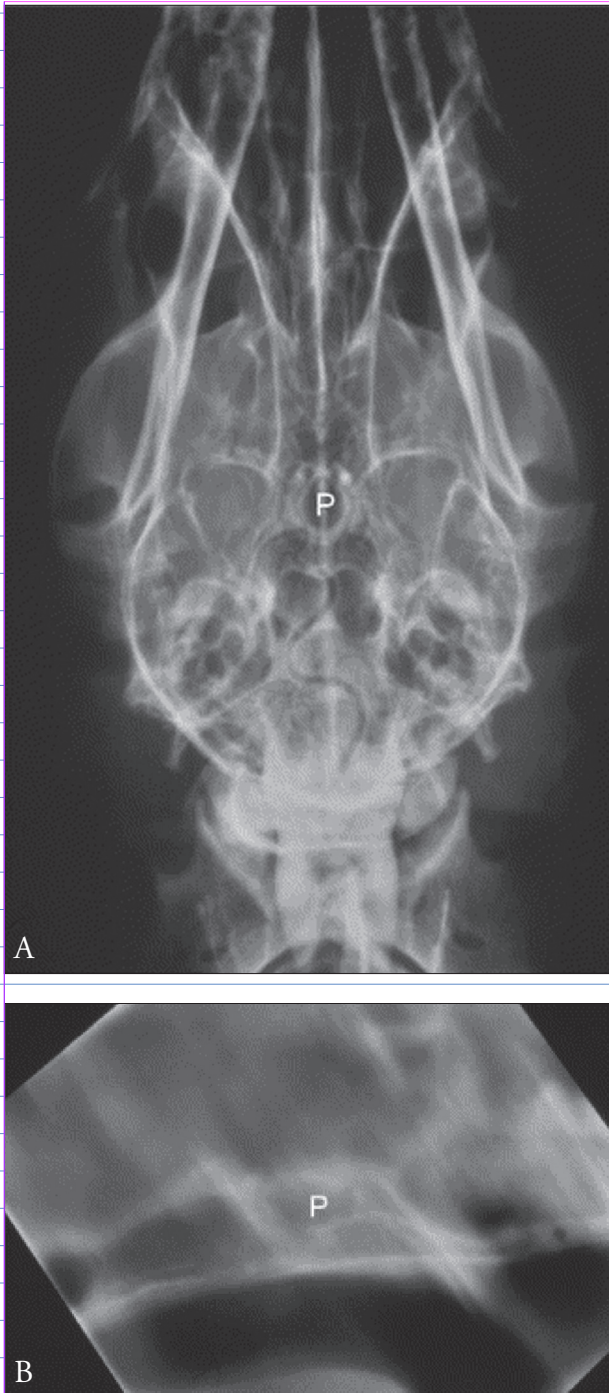


**Figure 8.** Dorsoventral cisternogram (A) and sagittal linear tomogram (B) following cisternography in an adult Greyhound. A: The pituitary gland (P), optic chiasm, basilar artery, cerebral arterial circle, and parts of the internal carotid arteries are visualized in the contrast-filled basal cisterns. B: The pituitary gland (P) is outlined by the pituitary fossa, dorsum sellae and contrast medium over its dorsal aspect. Cross sections of the basilar artery and parts of the rostral cerebral arteries are visualized as filling defects in the contrast-filled subarachnoid space.

(i.e., the secondary capillary bed of the adenohypophysis), which has been called the pituitary tuft.<sup>34,37</sup> Following this, there is a centrifugal enhancement of the peripheral parts of the anterior lobe. Microadenomas may cause a deviation or distortion of the secondary capillary bed (the so-called tuft sign).<sup>34</sup>

Dynamic CT using a conventional single detector array CT unit only provides information about one thin slice of the pituitary gland, because of a long interscan time. Microadenomas may be present outside the scan plane and, when present in the scan plane, no information is obtained about the rostrocaudal dimension of the adenoma. These limitations may be overcome with helical dynamic CT. With a helical CT scanner a relatively large area can be examined with very short scanning times,<sup>38</sup> allowing the dynamic examination of the whole pituitary gland instead of only a thin slice of the pituitary gland.

Apart from information about the size of the pituitary gland, CT also provides information about the exact location of the pituitary gland relative to some important surgical landmarks: the caudal extension of the hamular processes and the level where the ridge of the outer cortical lamina of the presphenoid bone disappears and becomes flat towards the basisphenoid bone. In addition, information is obtained about the thickness of the sphenoid bone.<sup>22,39</sup>

### 4.3.3. Magnetic Resonance Imaging

Magnetic resonance imaging is the imaging modality of choice for the detection of pituitary adenomas in humans.<sup>35</sup> Pituitary adenomatous tissue in patients with pituitary-dependent hyperadrenocorticism is usually hypointense and can be distinguished from normal hyperintense pituitary tissue.<sup>35</sup> Experiences with this diagnostic imaging modality in veterinary medicine is rapidly increasing.<sup>40,41</sup> Preliminary results of low-field MRI examination of the canine pituitary gland revealed the superior differentiation between the pituitary gland and the surrounding structures such as brain tissue and blood vessels. However, the value of MRI for the diagnosis and pre-surgical evaluation of pituitary tumors in dogs remains to be investigated.<sup>39</sup>

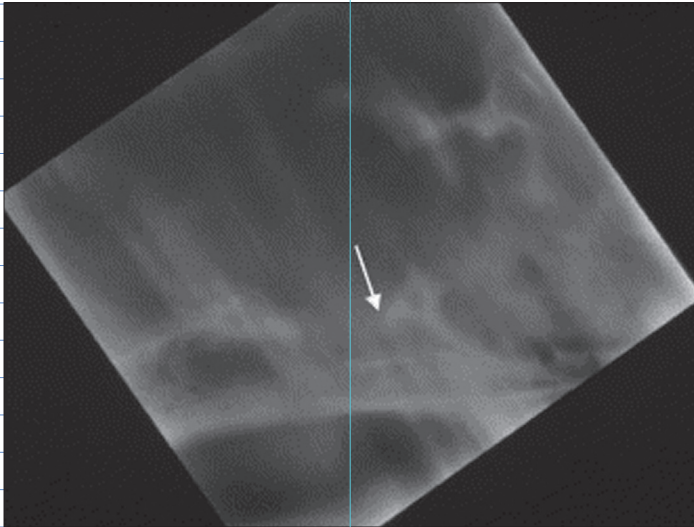


**Figure 9.** Sagittal linear tomogram following cisternography of an 9-year-old Kerry-Blue terrier. Contrast medium is blocked at the edge of the dorsum sellae (arrow) and does not outline the dorsal aspect of the pituitary gland, indicating suprasellar expansion of the pituitary tumor.

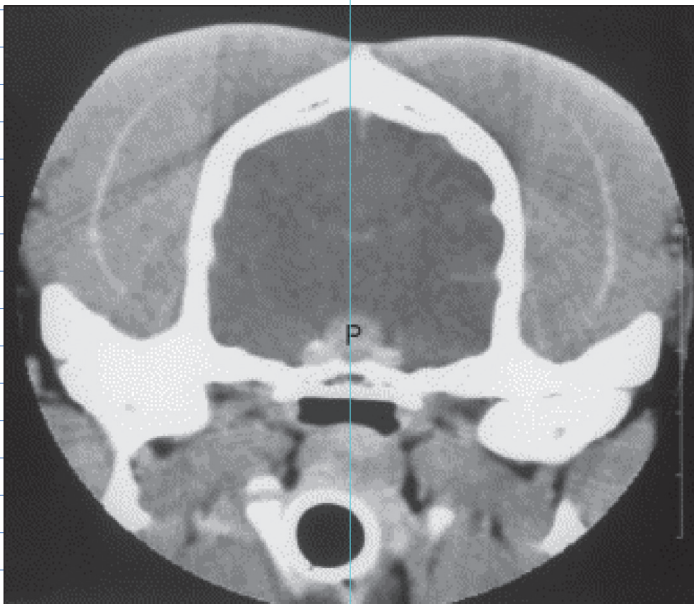


**Figure 10.** Transverse computed tomography image of an enlarged pituitary gland (P) in a 7-year-old mixed breed dog with pituitary-dependent hyperadrenocorticism.

## 5. Aims of the thesis

### **The aims of the present study were:**

- To determine the intra- and interobserver variability of CT measurements of pituitary glands in healthy dogs.
- To determine the accuracy of these measurements using a pituitary phantom.
- To determine the enhancement pattern of the pituitary gland during single slice dynamic CT in healthy dogs.
- To assess the changes in the contrast enhancement pattern of the pituitary gland during single slice dynamic CT in dogs with PDH and to correlate the imaging findings with findings of transsphenoidal hypophysectomy and histopathological findings of the surgical specimens.
- To investigate the dynamic enhancement pattern of the entire pituitary gland in healthy dogs with dynamic helical CT.
- To determine a protocol for MRI of the pituitary gland in healthy dogs using a 0.2 Tesla open MRI scanner.

## References

1. Hullinger RL. The endocrine system. In: Evans, HE (ed.), Miller's anatomy of the dog, 3rd ed. Philadelphia: WB Saunders Co 1996: pp 559-585.
2. Daniel PM, Pritchard MML. Studies of the hypothalamus and the pituitary gland. *Acta Endocrinol* 1975;80:S27-S63.
3. Fletcher TF. Spinal cord and meninges. In: Evans, HE (ed.), Miller's anatomy of the dog, 3rd ed. Philadelphia: WB Saunders Co 1993: pp 800-893.
4. Schwartz HG. The meningeal relations of the hypophysis cerebri. *Anat Rec* 1936;67:35-51.
5. Evans HE. The heart and arteries. In: Evans, HE (ed.), Miller's anatomy of the dog., 3rd ed. Philadelphia: WB Saunders Co, 1993: pp 586-682.
6. Zimmermann G. Über die Dura Mater Encephali und die Sinus der Schädelhöhle des Hundes. *Z Anat Entw Gesch* 1936;106:107-137.
7. Seiferle E. Hüllen des Zentralnervensystems, Meninges. Gefassversorgung von Rückenmarck und Gehirn. In: Nickel R, Schummer A, Seiferle E (eds.), *Lehrbuch der Anatomie der Haustiere. Nervensystem, Sinnesorgane, Endokrine Drüsen*. Berlin: Verlag Paul Parey 1975: pp166-188.
8. Habermehl KH. Zur Topographie der Gehirngefäße des Hundes. *Anat Histol Embryol* 1973;2:327-353.
9. De la Torre E, Mitchell OC, Netsky MG. Anatomic and angiographic study of the vertebral-basilar arterial system in the dog. *Am J Anatomy* 1962;110:187-197.
10. Page RB. Pituitary blood flow. *Am J Physiol* 1982;243:E427-E442.
11. Bergland RM, Page RB. Can the pituitary secrete directly to the brain? (affirmative anatomical evidence). *Endocrinol* 1978;102:1325-1238.
12. Capen CC, Martin SL. Animal model: Hyperadrenocorticism (Cushing's-like syndrome and disease in dogs). *Am J Pathol* 1975;81:459-462.
13. Feldman EC, Nelson RW. Comparative aspects of Cushing's syndrome in dogs and cats. *Endocrinol Metab Clin North Am* 1994;23:671-691.
14. Rijnberk A. Clinical endocrinology of dogs and cats. Kluwer, Dordrecht 1996 pp 11-34.
15. Galac S, Kooistra HS, Voorhout G, van den Ingh TSGAM, Mol JA, van den Berg G, Meij BP. Hyperadrenocorticism in a dog due to ectopic secretion of adrenocorticotrophic hormone. *Domest Anim Endocrinol* 2005;28:338-348.

16. Reusch CE. New treatment options in Canine Cushing's syndrome. Proceedings WSAVA congress 2002.
17. Kintzer PP, Peterson ME. Mitotane (o,p'-ddd) treatment of 200 dogs with pituitary-dependent hyperadrenocorticism. *J Vet Int Med* 1991;5:182-190.
18. Nelson RW, Ihle SL, Feldman EC. Pituitary macroadenomas and macroadenocarcinomas in dogs treated with mitotane for pituitary-dependent hyperadrenocorticism: 13 cases (1981-1986). *J Am Vet Med Assoc* 1989;194:1612-1617.
19. Sarfaty D, Carillo M, Peterson ME. Neurologic, endocrinologic, and pathologic findings associated with large pituitary tumors in dogs: eight cases (1976-1984). *J Am Vet Med Assoc* 1988;193:854-856.
20. Nichols R. Problems associated with medical therapy of canine hyperadrenocorticism. *Problems in Veterinary Medicine* 1990;2:551-556.
21. Duesberg CA, Feldman EC, Nelson RW, Bertoy EH, Dublin AB, Reid MH. Magnetic resonance imaging for diagnosis of pituitary macrotumors in dogs. *J Am Vet Med Assoc* 1995;206:657-662.
22. Meij BP, Voorhout G, Van den Ingh TSGAM, Hazewinkel HAW, Teske E, Rijnberk A. Results of transsphenoidal hypophysectomy in 52 dogs with pituitary-dependent hyperadrenocorticism. *Vet Surg* 1998;27:246-261.
23. Meij BP. Hypophysectomy as a treatment for canine and feline Cushing's disease. *Vet Clin North Am (Small Anim Pract)* 2001;31:2015-2041.
24. Dijkshoorn NA, Rijnberk A. Detection of brain tumors by scintigraphy. *J Am Vet Radiol Soc* 1977;18:147-152.
25. Clarkson TB, Netsky MG, De la Torre E. Chromophobe adenoma in a dog: Angiographic and anatomic study. *J Neuropathol Exp Neurol* 1959;18:559-562.
26. Lee R, Griffiths IR. A comparison of cerebral angiography and cavernous sinus venography in the dog. *J Small Anim Pract* 1972;13:225-238.
27. Chastain CB, Riedesel DH, Graham CL. Secondary hypothyroidism in a dog. *Canine Practice* 1979;6:59-64.
28. Barr SC. Pituitary tumour causing multiple endocrinopathies in a dog. *Austr Vet J* 1985;62:127-129.
29. Voorhout G. Cisternography combined with linear tomography for visualization of the pituitary gland in healthy dogs. A comparison with computed tomography. *Vet Radiol* 1990;31:68-73.
30. Kooistra HS, Voorhout G, Mol JA, Rijnberk A. Correlation between

- impairment of glucocorticoid feedback and the size of the pituitary gland in dogs with pituitary-dependent hyperadrenocorticism. *J Endocrinol* 1997;152:387-394.
31. Voorhout G, Rijnberk A. Cisternography combined with linear tomography for visualization of pituitary lesions in dogs with pituitary-dependent hyperadrenocorticism. *Vet Radiol* 1990;31:74-78.
  32. Gardeur D, Naidich TP, Metzger J. CT analysis of intrasellar pituitary adenomas with emphasis on patterns of contrast enhancement. *Neuroradiol* 1987;20:241-247.
  33. Hasegawa T, Ito H, Shoin K, Kogure I, Kubota T, Yamamoto S. Diagnosis of an "isodense" pituitary microadenoma by dynamic CT scanning. *J Neurosurg* 1984;60:424-427.
  34. Bonneville JF, Cattin F, Moussa-Bacha K, Portha C. Dynamic computed tomography of the pituitary gland: the 'tuft sign'. *Radiology* 1983;149:145-148.
  35. Elster AD. Modern imaging of the pituitary. *Radiology* 1993;187:1-14.
  36. Hemminghytt S, Kalkhoff RK, Daniels DL, Williams AL, Grogan JP, Haughton VM. Computed tomographic study of hormone-secreting microadenomas. *Radiology* 1983;146:65-69.
  37. Bonneville JF, Cattin F, Dietemann JL. Pituitary adenomas with suprasellar extension. In: Bonneville JF, Cattin F, Dietemann JL (eds.), *Computed Tomography of the Pituitary Gland*. Berlin: Springer Verlag 1986: pp 47-51.
  38. Heiken JP, Brink JA, Vannier MW. Spiral (helical) computed tomography. *Radiology* 1993;189:647-656.
  39. Meij BP, Voorhout G, Van den Ingh TSGAM, Hazewinkel HAW, Van 't Verlaat JW. Transsphenoidal hypophysectomy in beagle dogs: evaluation of a microsurgical technique. *Vet Surg* 1997;26:295-309.
  40. Kippenes H, Gavin PR, Kraft SL, Sande RD, Tucker RL. Mensuration of the normal pituitary gland from magnetic resonance images in 96 dogs. *Vet Radiol Ultrasound* 2001;42:130-133.
  41. Shores A. Magnetic resonance imaging. *Vet Clin North Am (Small Anim Pract)* 1993;23:437-459.
  42. Meij BP. Transsphenoidal hypophysectomy for treatment of pituitary-dependent hyperadrenocorticism in dogs. Thesis. Utrecht University, 1997.

# CHAPTER 2

## **Intraobserver and interobserver agreement, reproducibility, and accuracy of computed tomographic measurements of pituitary gland dimensions in healthy dogs**

Roselinda H. van der Vlugt-Meijer, DVM, MVR; Björn P. Meij, DVM, PhD;  
George Voorhout, DVM, PhD

**American Journal of Veterinary Research: accepted 2006**

From the Division of Diagnostic Imaging (van der Vlugt-Meijer, Voorhout) and Department of Clinical Sciences of Companion Animals (Meij), Faculty of Veterinary Medicine, Utrecht University, The Netherlands

## Summary

**Objective** - To determine the reproducibility and accuracy of computed tomographic (CT) measurements of pituitary gland dimensions in healthy dogs.

**Animals** - 35 healthy sexually intact adult dogs.

**Procedures** - 2 observers independently viewed CT images of the skull in 35 dogs twice. Pituitary gland height, width, length, volume, and pituitary gland height to brain area ratio (P:B ratio) were measured or calculated. Intraobserver and interobserver agreement indexes (AIs) were calculated for pituitary gland dimensions. Computed tomography was performed also on 5 phantoms and both observers measured phantom dimensions twice. True-value AIs were calculated for the phantom study.

**Results** - The mean  $\pm$  SD interobserver AI between observer 1 and 2, for pituitary gland height and the P:B ratio, was  $0.90 \pm 0.07$ . The intraobserver AI for pituitary gland height and the P:B ratio was  $0.97 \pm 0.04$  for observer 1 and  $0.94 \pm 0.04$  for observer 2. The intra- and interobserver AIs for the other dimensions were lower than those for pituitary gland height and the P:B ratio. All phantom dimensions on CT images were underestimated significantly, compared with their true values.

**Conclusions and Clinical Relevance** - The intra- and interobserver AIs for pituitary gland dimension measurements on CT images was high. However, the same observer preferably should perform serial measurements. Window settings influence pituitary gland dimension measurements and predetermined window settings are recommended to make comparisons among dogs. Pituitary gland dimension measurements made from CT images in our study underestimated the true values.

## Introduction

Computed tomography has been used to examine pituitary glands in healthy dogs<sup>1-4</sup>, dogs with PDH<sup>5-7</sup>, and dogs with congenital growth hormone deficiency.<sup>8</sup> Pituitary gland dimensions are measured when pituitary adenomas are suspected or when transsphenoidal hypophysectomy is considered.<sup>6,7,9,10</sup> In healthy dogs, the pituitary gland measures approximately 10 mm in length, 7 mm in width, and 5 mm in height,<sup>11</sup> but the size of the pituitary gland varies among breeds of dogs and among individuals. With increasing body size an absolute increase in pituitary gland size is found, but a relative decrease in proportion to BW.<sup>11</sup> The pituitary gland height, width, and length have been described in dogs with PDH.<sup>1,5-7,12</sup> In a study<sup>5</sup> on the relation between impairment of glucocorticoid feedback and the size of the pituitary gland in dogs with PDH, the P:B ratio was assessed. Pituitary glands were judged visually to be enlarged or nonenlarged. Pituitary gland height (in mm) and brain area (mm<sup>2</sup>) were measured on the image that (visually) contained the largest cross-section of the pituitary gland and the P:B ratio was calculated as follows:

$$\text{P:B ratio} = \frac{\text{pituitary gland height (mm)}}{\text{brain area (mm}^2\text{)}} \times 100$$

Results of the study<sup>5</sup> revealed that visually nonenlarged pituitary glands had a P:B ratio of  $\leq 0.31 \text{ mm}^{-1}$  whereas visually enlarged pituitary glands had a P:B ratio of  $> 0.31 \text{ mm}^{-1}$ . Therefore use of the P:B ratio allowed distinction of enlarged from nonenlarged pituitary glands.<sup>5</sup> Computed tomography dimensions of the pituitary gland in healthy dogs and dogs with pituitary disease have been reported, but little information exists on the agreement within and between observers on CT measurements of the pituitary gland. Also, to our knowledge the accuracy of pituitary gland dimension measurements determined by use of CT has not been reported. The aims of the study reported here were to assess the reproducibility of the pituitary gland dimension measurements obtained by use of CT and determine the accuracy of CT measurements by use of a phantom study.

## Materials and Methods

### Animals

Computed tomography of the pituitary gland was performed in 35 healthy sexually intact adult dogs (29 Beagles and 6 cross-breed dogs). The dogs (16 males and 19 females) ranged in age from 1 to 10 years (mean, 4 years old) and in BW from 11.6 to 18.1 kg (mean, 15.1 kg). Dogs were obtained from the Department of Clinical Sciences of Companion Animals of the Utrecht University. The dogs were used for teaching students in clinical diagnostics and for minor noninvasive studies. Other dogs were part of terminal experiments of other investigators within the department. All dogs received a good standard of care. The Ethical Committee of the Utrecht University approved the experimental protocols.

Six of 35 dogs had normal adrenocortical function as evidenced by morning urinary corticosteroid to creatinine ratios of  $< 10 \times 10^{-6}$  on 2 consecutive days.<sup>13</sup> In 20 of 35 dogs pituitary function was confirmed as normal by anterior pituitary hormone responses to the IV injection of 4 hypothalamic releasing hormones as was described previously.<sup>14</sup> Nine of 35 dogs were euthanatized (by rapid intravenous injection with an overdose of sodium pentobarbital) 1 week after the CT examination for reasons unrelated to the present study and the pituitary glands of these dogs were normal on histologic examination but no pituitary gland dimensions were determined.

Food was withheld from all dogs for 18 hours prior to CT examination. Following premedication with medetomidine<sup>a</sup> (50  $\mu\text{g}/\text{kg}$ , IV), anesthesia was induced by administration of propofol<sup>b</sup> (1 to 2  $\text{mg}/\text{kg}$ , IV) and maintained by inhalation of isoflurane<sup>c</sup> or halothane<sup>d</sup>, nitrous oxide, and oxygen.

### Phantom design

Phantoms were designed with density values comparable with a contrast-enhanced pituitary gland surrounded by unenhanced brain tissue. Density of the normal contrast-enhanced pituitary gland varies between 80 and 120 HU, density of brain tissue is 40 HU. After thorough examination of a number of available materials, cheese (density 100 HU) and buttermilk (density 45 HU) were considered comparable with a contrast-enhanced pituitary gland surrounded by brain tissue.

The cheese was cut with a No. 10 scalpel blade. The 5 oval to spheroid phantoms differed slightly in size, shape, and volume. The width, height, and

length of the phantoms were measured with a Vernier caliper with a scale that was accurate to 0.1 mm. The measurements were repeated 3 times and the mean value represented the true value for each dimension of each phantom. The volume of each phantom was determined by measurement of water displacement caused by the phantom in a calibrated pycnometer and was accurate to 0.1 mm<sup>3</sup>. The 5 phantoms were, 1 at the time, placed in the pituitary fossa of the skull base of a mesocephalic dog and surrounded by buttermilk. Each phantom underwent CT as described for the live dogs.

## **CT**

Computed tomography was performed with a third generation CT scanner<sup>c</sup>. With the dogs in sternal recumbency transverse scans of the pituitary fossa were made perpendicular to the skull base, following an IV bolus of 2 mL of contrast medium<sup>f</sup>/kg. Computed tomography scans were made with a 9 second scanning time at 120 kV and 220 mA and a 22 second interslice delay for tube cooling. Transverse 2-mm-thick contiguous slices were acquired in 19 dogs and transverse 2-mm-thick 1-mm overlapping slices in the other 16 dogs. In addition, sagittal scans of the pituitary fossa were made in 14 of 35 dogs. With the dogs in left lateral recumbency, the head was lifted on a holder and sagittal slices were made with a 9 second scanning time at 120 kV and 220 mA. Sagittal 2-mm-thick contiguous slices were acquired in 8 dogs and sagittal 2-mm-thick 1-mm overlapping slices in 6 other dogs.

The skull base with the phantom was placed parallel to the scanner table and 2-mm-thick contiguous transverse slices were made of the pituitary fossa with a 9 second scanning time at 120 kV and 220 mA. Next, the skull base with the phantom was placed perpendicular to the scanner table (lined up with the gantry) to acquire 2-mm-thick contiguous sagittal slices with the same settings. A soft tissue algorithm was used to reconstruct the images. Measurements were performed on the display monitor with a trackball-driven cursor and CT computer software,<sup>c</sup> with all images displayed at preset WW of 250 HU and WL of 80 HU.

## **Measurements and calculations**

Two observers performed the same set of measurements on the CT images of each dog and each phantom twice, with 5 to 7 days between measurements. The CT images of the dogs and phantoms were viewed and measured in a random order that differed between first and second measurements. The

observers viewed the CT images and selected the slices for their measurements independent from each other. The observers were unaware of the true dimensions of the phantoms.

Each observer selected the transverse image of the largest cross-section (central image) of the pituitary gland (Figure 1) or phantom (Figure 2) for measurement height and width. On the central image of the pituitary gland, the edges of the brain were also traced and the enclosed area (brain area) was calculated by the computer. On every image of the pituitary gland or phantom, the edge of the pituitary gland or phantom was traced and the enclosed area was calculated by the computer. In dogs from which sagittal scans were available and in the phantoms, the mid-sagittal scan was selected and on this image the length of the pituitary gland or phantom was measured (sagittal length). The length of the pituitary gland or phantom was derived indirectly from the position number of the first and the last transverse CT scans that included pituitary gland or phantom (transverse length). The volume was calculated by taking the sum of the pituitary gland or phantom areas on the transverse images, and the sum was multiplied by 2 for the 2-mm-thick contiguous slices, and by 1 for the 1-mm-overlapping 2-mm-thick slices. The length of pituitary gland or phantom and



**Figure 1.** Measurements of pituitary gland height (A to B) and width (C to D) in millimeters on a transverse contrast-enhanced CT image of the skull of an 8-year-old female Beagle.

L = Left. C = Contrast

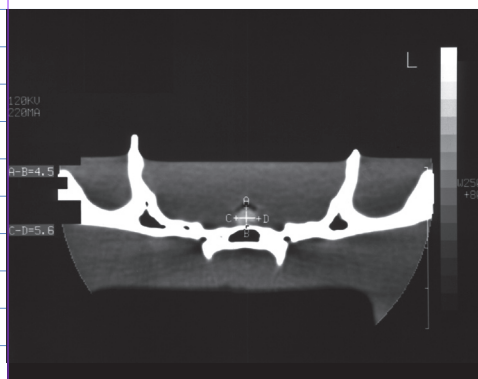


**Figure 2.** Measurement of pituitary phantom height (A to B) and width (C to D) in millimeters on a transverse CT image of a cheese phantom surrounded by buttermilk in a skull base.

L = Left

the volume of the pituitary gland were calculated on the assumption that the most rostral and caudal image contained pituitary gland or phantom for only half of the slice. For the phantoms the volume was calculated twice, first on the assumption that the most rostral and caudal images contained phantom for only half of the slice and, second, on the assumption that those images contained phantom for the whole slice. The P:B ratio was calculated for each dog as was described previously.<sup>4</sup>

### Statistical analysis

The relation between the age of the dogs and pituitary gland height, volume, and the P:B ratio was assessed by use of a correlation analysis. Also, in the group of female dogs versus male dogs, the mean  $\pm$  SD was calculated for age of the dogs and for pituitary gland height, volume, and the P:B ratio. The Student *t* test for unpaired samples was used to compare the mean values between female and male dogs. A value of  $P < 0.05$  was considered significant.

The mean  $\pm$  SD of each pituitary gland dimension (height, width, volume, transverse length, sagittal length, and P:B ratio) was calculated per observer for the dogs and the phantoms. The values in both trials of measurements were used for these calculations. The Student *t* test for paired samples was used 1) to compare the mean values of pituitary gland dimensions measured by the 2 observers in the dog study, and 2) to compare the mean true value and the mean value measured by the observers in the phantom study.

The intra- and interobserver AIs were calculated for the clinical study and true value AIs were calculated for the phantom study. The following AI equation was used<sup>15,16</sup>:

$$AI = 1 - \frac{|X_a - X_b|}{(X_a + X_b)/2}$$

For interobserver calculations,  $X_a$  was the measurement obtained by observer 1 and  $X_b$  the measurement obtained by observer 2. Both first and second measurements were used for the calculations of interobserver AIs. For the intraobserver AIs,  $X_a$  was the first measurement and  $X_b$  the second measurement obtained by the same observer for each dimension. For the true value AIs,  $X_a$  was the measurement obtained by observer 1 or 2 and  $X_b$  the true value. The mean  $\pm$  SD was calculated for the intraobserver, the interobserver, and the true value AIs. The Student *t* test for paired samples was used to compare the mean AI values. A value of  $P < 0.05$  was considered significant.

Dogs			
Variables	Males (n = 16)	Females (n = 19)	P values
Age (y)	3.1 ± 2.5	4.5 ± 2.4	0.10
Body weight (kg)	15.5 ± 1.3	14.7 ± 1.7	0.19
Pituitary gland height (mm)	4.5 ± 0.4	4.3 ± 0.5	0.54
Pituitary volume (mm <sup>3</sup> )	90.1 ± 22.3	83.2 ± 24.2	0.61
P:B ratio (mm-l)	0.28 ± 0.03	0.27 ± 0.03	0.38

**Table 1.** Mean ± SD values of age, BW, and pituitary gland dimensions for male and female dogs.

Observer				
Pituitary gland dimensions	N	1	2	P value*
Height (mm)	70	4.2 ± 0.6	4.6 ± 0.5	< 0.001
Width (mm)	70	5.9 ± 0.7	6.2 ± 0.8	< 0.001
Volume (mm <sup>3</sup> )	70	79.7 ± 24.8	93.1 ± 25.0	< 0.001
Sagittal length (mm)†	28	5.2 ± 0.9	6.2 ± 0.8	< 0.001
Transverse length (mm)	70	4.7 ± 1.1	5.3 ± 1.0	< 0.001
P:B ratio (mm-l)	70	0.27 ± 0.04	0.29 ± 0.03	< 0.001

**Table 2.** Mean ± SD values of pituitary gland dimensions that were measured twice by 2 independent observers (1 and 2) on CT images of 35 healthy dogs.

\*P < 0.05 indicates significantly different mean values between observers 1 and 2. †Sagittal length measurements were only available in 14 dogs. N = Number of measurements.

Intraobserver AI							
Pituitary gland imensions	Interobserver AI	N	Observer 1	N	Observer 2	N	P values*
Height	0.90 ± 0.07	70	0.97 ± 0.04	35	0.94 ± 0.04	35	0.001
Width	0.90 ± 0.08	70	0.94 ± 0.08	35	0.91 ± 0.07	35	0.013
Volume	0.80 ± 0.16	70	0.90 ± 0.14	35	0.89 ± 0.10	35	0.65
Sagittal length†	0.80 ± 0.16	28	0.87 ± 0.10	14	0.88 ± 0.11	14	0.75
Transverse length	0.81 ± 0.22	70	0.90 ± 0.17	35	0.93 ± 0.11	35	0.30
P:B ratio	0.90 ± 0.07	70	0.96 ± 0.04	35	0.94 ± 0.03	35	0.003

**Table 3.** Mean ± SD values of inter- and intraobserver AIs for pituitary gland dimension measurements that were obtained twice by 2 independent observers (1 and 2) on CT images of 35 healthy dogs. See Table 2 for key.

## Results

### Dog study

No correlation was found between the age of dogs and pituitary gland height, volume, or P:B ratio. No significant differences were found between male and female dogs for pituitary gland height, volume, and P:B ratio.

Observer 1 chose the same central transverse slice through the pituitary gland in both sessions for 31 of 35 dogs. Observer 2 chose the same transverse central slice in both sessions for 25 of 35 dogs. The observers differed in choosing the central slice for 8 dogs in the first and second session. Furthermore, observer 1 chose the same central sagittal slice in both sessions for 8 of 14 dogs, whereas observer 2 chose the same sagittal slice in both sessions for 11 of 14 dogs. The observers differed in choosing the same sagittal central slice in 7 dogs for the first measurement and in 6 dogs for the second measurement.

Observer 2 measured significantly higher values for all pituitary gland dimensions than observer 1 (Table 2). Observer 1 had a significantly higher intraobserver AI than observer 2 for measurement of pituitary gland height, width, and the P:B ratio when first and second measurement were compared (Table 3). Interobserver AIs were the highest for measurement of pituitary gland height, width, and P:B ratio (Table 3).

### Phantom study

Both observers measured significantly lower values on the CT images, compared with the true phantom values for phantom height and length, and in the case of observer 2 also for phantom width (Table 4). Both observers measured a significantly lower phantom volume on the CT images than the true value when it was assumed that the most rostral and the most caudal slice contained phantom for half of the slice thickness.

Mean AIs between true phantom values and measured values of phantom dimensions on CT images by the observers had considerable variation that were highest for phantom width and lowest for transverse length (Table 5). Observer 2 was more accurate than observer 1 in measurement of phantom height and transverse length, whereas observer 1 was more accurate than observer 2 in measurement of phantom width. Both observers were significantly more accurate (ie, closer to the true value) when volume was measured assuming that the most rostral and caudal image contained phantom for the entire slice thickness than when they contained phantom for half of the slice thickness.

Phantom CT images									
Phantom dimension	True dimensions	Observer 1				Observer 2			
		Series 1	P value*	Series 2	P value*	Series 1	P value*	Series 2	P value*
Height (mm)	4.8 ± 0.4 (4.2-5.3)	3.9 ± 0.6	0.003	3.8 ± 0.6	0.005	4.4 ± 0.8	0.21	4.1 ± 0.8	0.03
Width (mm)	6.3 ± 0.5 (5.5-6.9)	6.0 ± 0.6	0.36	5.8 ± 0.4	0.10	5.6 ± 0.4	0.04	5.4 ± 0.4	0.01
Sagittal length (mm)	8.3 ± 0.5 (7.8-9.1)	6.6 ± 0.6	0.002	6.6 ± 0.3	0.001	6.4 ± 0.3	< 0.001	6.5 ± 0.9	0.01
Transverse length (mm)	8.3 ± 0.5 (7.8-9.1)	4.4 ± 0.9	< 0.001	ND	NA	5.6 ± 0.9	0.002	ND	NA
Volume 1 (cm3)†	0.1275±0.0224 (0.0944-0.1493)	0.09 ± 0.02	0.004	0.09 ± 0.02	< 0.001	0.09 ± 0.02	0.003	0.09 ± 0.02	0.003
Volume 2 (cm3)‡	0.1275±0.0224 (0.0944-0.1493)	0.13 ± 0.03	0.90	0.12 ± 0.02	0.30	0.11 ± 0.03	0.14	0.11 ± 0.02	0.03

**Table 4.** Mean ± SD (range) values for true dimensions of 5 phantoms and mean phantom dimensions as measured on phantom CT images by 2 observers in a first and a second series of measurements.

\*P < 0.05 indicates significantly lower CT measurements, compared with true dimensions. †Volume 1 was calculated by assuming that the most rostral and the most caudal image contained phantom for half of the CT slice thickness. ‡Volume 2 was calculated by assuming that images contained phantom for the entire slice thickness. ND = Not determined. NA = Not applicable

True vs CT image dimensions			
Phantom dimension	AIs of observer 1	AIs of observer 2	P value*
Height	0.78 ± 0.09	0.84 ± 0.11	0.007
Width	0.92 ± 0.07	0.87 ± 0.07	0.001
Sagittal length	0.76 ± 0.07	0.74 ± 0.09	0.43
Transverse length	0.37 ± 0.11	0.60 ± 0.15	0.005
Volume 1†§	0.64 ± 0.12	0.66 ± 0.11	0.66
Volume 2‡§	0.90 ± 0.06	0.84 ± 0.09	0.08

**Table 5.** Mean ± SD values of AIs between true values and measurements of phantom dimensions on CT images, measured by 2 independent observers in 5 phantoms.

\*P < 0.05 indicates significantly different mean values between observers 1 and 2. §Significant (P < 0.05) difference between mean AIs for volume 1 and volume 2.

See Table 4 for remainder of key.

## Discussion

Results of our study indicate that excellent intra- and interobserver agreement exists in measuring various pituitary gland dimensions, especially for pituitary gland height and the P:B ratio. Results of the phantom study reveal that pituitary gland dimensions on CT images made with the window settings used in our study are systematically underestimated.

The slice containing the largest cross section of the pituitary gland, the so-called central image, was chosen by visual assessment. The difference between consecutive slices is smaller in 1-mm-overlapping slices and more scans are needed to cover the same object length, compared with contiguous 2-mm-thick slices. This may well explain the higher number of noncorresponding\ central images within and between the observers when 1-mm-overlapping 2-mm slices were evaluated, compared with the contiguous 2-mm-thick slices.

Systematic bias can be detected by comparing differences in absolute values.<sup>15,17</sup> Observer 2 measured significantly higher values for all pituitary gland dimensions than observer 1. Apparently, observer 1 and 2 systematically differed in the judgement of the pituitary gland margins and the cursor placement for measurements. Such differences will probably decrease when protocols about cursor placement and definition of pituitary margins are developed and used. However, these observer-related differences are likely to remain and have some influence on measurements.<sup>18</sup> Another factor that may have influenced pituitary gland dimension measurements in a systematic manner is the accuracy of the measurement tool.

Pituitary gland dimensions are usually judged subjectively when CT images are assessed visually for the first time. To compare different patients or different examinations of the same patient it would be preferable to use a more objective standard. Pituitary gland tumors in dogs first increase in height before they extend rostrally or caudally.<sup>5</sup> Because the skull shape and size varies considerably among breeds of dogs and among individual dogs,<sup>11</sup> the P:B ratio was introduced.<sup>5</sup> The P:B ratio can be used for interpatient comparisons because it relates pituitary gland height to a skull measurement (ie, brain area), whereas the pituitary gland height in the P:B ratio allows for inpatient comparisons. Results of our study reveal that pituitary gland height and the P:B ratio have

excellent intra- and interobserver AIs. Differences in intraobserver agreement between the 2 observers could be explained by experience; the more experienced observer had a slightly better intraobserver AI.

In our study pituitary gland height and width were slightly smaller than those found in a MRI study.<sup>12</sup> In our study no correlation was found between age of dogs and pituitary gland height, volume, and P:B ratio. Also, pituitary gland dimensions were not different between male and female dogs. The relationship between BW and pituitary gland dimensions was not investigated in our study because of the small range of BW in the studied population. In the MRI study, pituitary glands were measured by use of gadolinium enhanced MRI in 96 healthy dogs (BW, 13 to 45 kg).<sup>12</sup> Pituitary gland height ranged from 3.1 to 7.5 mm (mean, 5.1 mm) and pituitary gland width ranged from 4.0 to 9.0 mm (mean, 6.4 mm).<sup>12</sup> In the MRI study dogs had a wider range in BW than in our study; as in our study, no significant correlation was found between BW and pituitary gland dimensions.<sup>12</sup>

Both observers significantly underestimated the dimensions of the cheese phantom in the skull specimen on the CT images, compared with the true phantom dimensions. From our phantom study it may be concluded that all pituitary gland dimensions measured on the CT images in our dog study, under the same conditions with the same window settings (WW, 250 HU; WL, 80 HU), were also underestimated. If pituitary gland surgery is considered for the treatment of dogs with PDH<sup>6,9</sup>, and total hypophysectomy is the goal of the surgical treatment, the surgeon must be aware of this underestimation of pituitary gland size. Especially in dogs with large pituitary adenomas this may result in pituitary remnants after incomplete hypophysectomy.

Observer 2 had significantly more accurate measurements of phantom height on CT images than observer 1, which is reflected in a significantly higher AI for observer 2 between true value and measured phantom height value. For phantom width this was the opposite and observer 1 scored better than observer 2. This difference may be explained by the variation caused by the interface between phantom (or pituitary) and its surroundings (ie, bone and buttermilk or bone and brain). Indeed, proper window settings are more important for cursor placement than observer ability.<sup>19-21</sup> The object size that is measured on CT images is highly dependent on the WL and the WW that are used to display

images. Fine level adjustment may be necessary from dog to dog to optimize differentiation of the soft tissue interfaces. The greatest source of error in mensuration may occur at the sella turcica (bone)-pituitary gland interface. The window settings used make accurate placement of the bone-soft tissue interface difficult. The WL of 80 HU used in our study was the best window setting for cursor placement on the border between the pituitary gland and the brain but this level is too low, according to the full-width-at-half-maximum rule, when the cursor is placed on the border between pituitary gland and the bone of the sella turcica.<sup>20</sup> Further research with different window settings will be required to investigate the most proper window settings for visual assessment of the pituitary gland edges and measuring pituitary gland dimensions.

To correct for the fact that the most rostral and most caudal slice through the pituitary gland would not contain pituitary gland tissue for the full slice thickness (partial volume effect),<sup>22</sup> these slices were counted for only half of their slice thickness in the calculation of transverse length and volume of the pituitary. With this method, results of the phantom study revealed that both observers significantly underestimated transverse length and volume dimensions. Therefore it is concluded that the most rostral and the most caudal scan that contain pituitary gland do so for more than half their slice thickness, and that it is more accurate to count both slices as full thickness slices for transverse length and volume calculations as was shown by the second method of phantom volume calculation.

In summary, the inter- and intraobserver agreement in measuring various pituitary gland dimensions was excellent, especially for measurement of pituitary gland height and the P:B ratio. However, because of small systematic interobserver differences it is preferred to perform intra- and interpatient comparisons by the same observer. Also, it must be realized that pituitary gland dimensions on CT images with the window settings used in our study are underestimated. Further research is warranted to investigate the influence of the window and level settings on the pituitary gland dimensions and the pituitary-bone interface, to maximize tissue differentiation and obtain a more accurate assessment of all aspects of pituitary gland size.

- a. Domitor, Smith Kline Beecham Animal Health B.V., Zoetermeer, the Netherlands
- b. Diprivan-10, Zeneca B.V., Ridderkerk, the Netherlands
- c. Forene, Abbot Laboratories Ltd, Queenborough, Kent, UK
- d. Halothan, Albic B.V., Maassluis, the Netherlands
- e. Philips Tomoscan CX/S, Philips NV, Eindhoven, the Netherlands
- f. Telebrix 38, sodium and meglumine ioxothalamate containing 380 mg iodine/mL, Guerbet Nederland BV, Gorinchem, the Netherlands

## References

1. Voorhout G, Cn PR, Kraft SL, Sande RD, Tucker RL. Mensuration of the normal pituitary gland from magnetic resonance images in 96 dogs. *Vet internography combined with linear tomography for visualisation of the pituitary gland in healthy dogs: a comparison with computed tomography.* *Vet Radiol* 1990;31:68-73.
2. Meij BP, Voorhout G, van den Ingh TSGAM, et al. Transsphenoidal hypophysectomy in beagle dogs: evaluation of a microsurgical technique. *Vet Surg* 1997;126: 295-309.
3. Van der Vlugt-Meijer RH, Meij BP, Voorhout G. Dynamic computed tomographic evaluation of the pituitary gland in healthy dogs. *Am J Vet Res* 2004;65:1518-1524.
4. Love NE, Fisher P, Hudson L. The computed tomographic enhancement pattern of the normal canine pituitary gland. *Vet Radiol Ultrasound* 2000;41:507-510.
5. Kooistra HS, Voorhout G, Mol JA, et al. Correlation between impairment of glucocorticoid feedback and the size of the pituitary gland in dogs with pituitary-dependent hyperadrenocorticism. *J Endocrinol* 1997;152: 387-394.
6. Meij BP, Voorhout G, van den Ingh TSGAM, et al. Results of transsphenoidal hypophysectomy in 52 dogs with pituitary-dependent hyperadrenocorticism. *Vet Surg* 1998;27: 246-261.
7. Van der Vlugt-Meijer RH, Meij BP, van den Ingh TSGAM, et al. Dynamic computed tomography of the pituitary gland in dogs with pituitary-dependent hyperadrenocorticism. *J Vet Intern Med* 2003;17:773-780.
8. Kooistra HS, Voorhout G, Selman PJ, et al. Progesterin-induced GH-production in treatment of dogs with congenital GH-deficiency. *Domest Anim Endocrinol* 1998;15:93-102.
9. Meij BP, Voorhout G, Rijnberk A. Progress in transsphenoidal hypophysectomy for treatment of pituitary-dependent hyperadrenocorticism in dogs and cats. *Mol Cell Endocrinol* 2002;197:89-96.
10. Van der Vlugt-Meijer RH, Voorhout G, Meij BP. Imaging of the pituitary gland in dogs with with pituitary-dependent hyperadrenocorticism. *Mol Cell Endocrinol* 2002;197:81-87.
11. Hullinger RL. The endocrine system. In: Evans HE, ed. *Millers anatomy of the dog*. 3rd ed. Philadelphia: WB Saunders Co, 1993:559-585.

12. Kippenes H, GaviRadiol Ultrasound 2001;42:130-133.
13. Rijnberk A, van Wees A, Mol JA. Assessment of two tests for the diagnosis of canine hyperadrenocorticism. *Vet Rec* 1988;122:178-180.
14. Meij BP, Mol JA, Hazewinkel HAW, et al. Assessment of a combined anterior pituitary function test in beagle dogs: rapid sequential intravenous administration of four hypothalamic releasing hormones. *Domest Anim Endocrinol* 1996;13:161-170.
15. Bland JM, Altman DG. Statistical methods for assessing agreement between 2 methods of clinical measurement. *Lancet* 1986;8:307-310.
16. Filippi M, Horsfield MA, Bressi S, et al. Intra- and inter-observer agreement of brain MRI lesion volume measurements in multiple sclerosis: a comparison of techniques. *Brain* 1995;118:1593-1600.
17. Joe BN, Fukui MB, Cidis Meltzer C, et al. Brain tumor volume measurement: comparison of manual and semiautomated methods. *Radiology* 1999; 13:161-170.
18. Breiman RS, Beck JW, Korobkin M, et al. Volume determinations using computed tomography. *Am J Radiol* 1982;138:329-333.
19. Hoe van L, Haven F, Bellon E, et al. Factors influencing the accuracy of volume measurements in spiral CT: a phantom study. *J Comp Assist Tomogr* 1997;21:332-338.
20. Baxter BS, Sorenson JA. Factors affecting the measurement of size and CT number in computed tomography. *Invest Radiol* 1980;16:337-341.
21. Koehler PR, Anderson RE, Baxter B. The effect of computed tomography viewer controls on anatomical measurements. *Radiology* 1979;130:189-194.
22. Hathcock JT, Stickle RL. Principles and concepts of computed tomography. *Vet Clin North Am (Small Anim)* 1993;23:399-415.

# CHAPTER 3

## **Dynamic computed tomographic evaluation of the pituitary gland in healthy dogs**

Roselinda H. van der Vlugt-Meijer, DVM, MVR; Björn P. Meij, DVM, PhD;  
George Voorhout, DVM, PhD

**American Journal of Veterinary Research 2004;65:1518-1524**

From the Division of Diagnostic Imaging (van der Vlugt-Meijer, Voorhout)  
and Department of Clinical Sciences of Companion Animals (Meij), Faculty of  
Veterinary Medicine, Utrecht University, The Netherlands

## Summary

**Objective** - To determine the contrast enhancement pattern of the pituitary gland in healthy dogs via dynamic computed tomography (CT).

**Animals** - 17 dogs.

**Procedure** - With each dog in sternal recumbency, transverse CT scans were made perpendicular to the skull base, from the rostral clinoid processes to the dorsum sellae. At the position of the image that contained the largest cross-section of the pituitary gland, a series of 9 to 11 scans was made during and after IV injection of contrast medium (dynamic CT scans). The contrast enhancement pattern of the pituitary gland and surrounding arteries was assessed visually and by use of time-density curves.

**Results** - After strong enhancement of the maxillary arteries, the intracavernous parts of the internal carotid arteries, and the communicating arteries of the arterial cerebral circle, there was a strong enhancement of the central part of the pituitary gland followed by enhancement of its peripheral part. On the last images of the dynamic series of the pituitary gland, the central part was hypodense, compared with the peripheral part. Time-density curves confirmed an early, strong enhancement of the central part and a delayed, less strong enhancement of the peripheral part of the gland.

**Conclusions and Clinical Relevance** - The difference in enhancement between the central and peripheral parts of the pituitary gland was attributable to a difference in vascularization of the neurohypophysis and adenohypophysis, respectively. Distortion or disappearance of the strong central enhancement (pituitary flush) may be used for the detection and localization of pituitary abnormalities in the adenohypophysis.

## Introduction

Naturally occurring pituitary-dependent hyperadrenocorticism (PDH) is one of the most frequently occurring endocrinopathies in dogs.<sup>1</sup> The characteristics of PDH in dogs are similar to those of PDH (Cushing's disease) in humans, but this form of hyperadrenocorticism is much more common in dogs than it is in humans.<sup>2,3</sup> In dogs, treatment for PDH can be medical (eg, administration of an adrenocorticolytic agent such as mitotane) or surgical (eg, via bilateral adrenalectomy or transsphenoidal hypophysectomy).<sup>1,4,5</sup> For hypophysectomy, detailed information about the size of the pituitary gland and its exact location in relation to the surgical landmarks is required.<sup>4,5</sup> Information regarding the size and expansion of pituitary lesions also has prognostic implications. Therefore, PDH is the most frequent indication for evaluation of the pituitary gland in dogs by use of advanced imaging techniques.<sup>1,5</sup>

Contrast-enhanced computed tomography (CT) is used in humans and dogs to evaluate pituitary tumors.<sup>5-9</sup> Large pituitary tumors with suprasellar expansion are readily diagnosed.<sup>5,6,8,10</sup> However, microadenomas that do not affect the size and shape of the pituitary gland may not be detected because of isoattenuation of the adenoma tissue and the surrounding unaffected pituitary tissue.<sup>11-14</sup>

In humans, microadenomas have been identified by use of dynamic CT.<sup>7,15,16</sup> Dynamic contrast-enhanced CT includes a series of scans of identical slice thickness, at the same slice position through the center of the pituitary gland, during and after IV injection of a bolus of contrast medium.<sup>6,7,15</sup> During dynamic CT in humans, enhancement of the internal carotid artery is observed followed by enhancement of the central part of the secondary capillary bed of the adenohypophysis, which has been called the pituitary tuft.<sup>6,15</sup> Finally, there is a centrifugal enhancement of the pars distalis of the adenohypophysis. Microadenomas may cause a deviation or distortion of the secondary capillary bed (the so-called tuft sign).<sup>15</sup>

There are important anatomical differences between human and canine pituitary glands. In humans, the axis of the pituitary gland is vertical,<sup>17,18</sup> whereas in dogs, the axis of the pituitary gland is more horizontal.<sup>19,20</sup> In humans, a transverse CT imaging section includes either the anterior lobe or the posterior lobe; in dogs, both parts of the pituitary gland are visible in a transverse section, in which the neurohypophysis appears in the center, partly enveloped by the adenohypophysis. Therefore, the enhancement patterns obtained via transverse

dynamic CT of the pituitary glands of dogs and humans may be different.

The enhancement pattern of the normal canine pituitary gland during dynamic CT has been reported.<sup>21</sup> In 3 of the 4 dogs of that study, an early intense enhancement of the central portion of the pituitary gland was observed which was followed by a peripheral rim enhancement. However, a time-density curve for the complete pituitary gland was plotted in that particular study<sup>21</sup> and therefore, differences in enhancement pattern between the central and the peripheral part of the pituitary gland were not specified. The purpose of the study reported here was to determine the dynamic CT enhancement pattern of the pituitary gland in healthy dogs. Changes in the enhancement pattern within the contours of the pituitary gland were monitored by use of separate time-density curves.

## Materials and Methods

### Dogs

Seventeen clinically healthy dogs (12 Beagles and 5 crossbreed dogs) were included in the study. The dogs were 2 to 10 years of age (median age, 4 years) and body weights ranged from 11.5 to 18.1 kg (median weight, 15 kg). Normal pituitary function was confirmed in all dogs on the basis of results of a pituitary function test that consisted of a combined IV injection of 4 hypothalamic hormones (corticotropin-releasing hormone, growth hormone-releasing hormone, gonadotropin-releasing hormone, and thyrotropin-releasing hormone) and measurements of plasma adrenocorticotropin, cortisol, growth hormone, luteinizing hormone, and prolactin concentrations, as described.<sup>22</sup> The experimental protocol was approved by the Ethical Committee of the Utrecht University.

### Anesthesia

Food was withheld from all dogs for 18 hours prior to CT evaluation. After premedication with medetomidine<sup>a</sup> (50 µg/kg, IV), anesthesia was induced by IV administration of propofol<sup>b</sup> (1 to 2 mg/kg). The trachea was intubated and inhalation anesthesia was maintained in a semi-closed system with a mixture of isoflurane,<sup>c</sup> nitrous oxide, and oxygen. Continuous monitoring during anesthesia consisted of electrocardiography, capnography, and pulse oxymetry and a stable plane of anesthesia was maintained during CT examination and injection of the contrast medium.

### Computed tomography

Evaluation via CT was performed by use of a third-generation CT scanner.<sup>d</sup> With each dog in sternal recumbency, transverse scans of the skull were made (perpendicular to the skull base) from the rostral clinoid processes to the dorsum sellae. By use of a 9-second scanning time and a 22-second interslice delay, 2-mm-thick contiguous slices were made with 120 kV and 220 mA. The image that contained the largest cross-section of the pituitary gland (usually the most caudal image just rostral to the dorsum sellae) was selected and at the position of this image, a series of 9 to 11 scans was made with 120 kV and 220 mA (dynamic series of scans). One scan was made before (unenhanced scan) and 8 to 10 scans during and following the rapid IV bolus injection of an iodine-containing contrast medium (sodium and meglumine ioxithalamate<sup>e</sup> containing 380 mg of iodine/mL). The contrast medium was injected through an 18-gauge IV catheter

placed in the cranial branch of the lateral saphenous vein of the hind limb. All contrast material was injected by hand by an experienced anesthesia technician and injection was completed within 12 seconds. Because of a preparation delay inherent to the scanner used, the start of the first of the 8 to 10 scans was 5 seconds after the start of the injection. Three scanning protocols were used: in 3 dogs, the dynamic series of scans was made with a 2.8-second scanning time and an interscan time of 11.2 seconds (380 mg of iodine/kg was administered); in 6 dogs, the dynamic series of scans was made with a 2.8-second scanning time and an interscan time of 11.2 seconds (760 mg of iodine/kg was administered); and in 8 dogs, the dynamic series of scans was made with a 4.5-second scanning time and an interscan time of 9.5 seconds (760 mg of iodine/kg was administered).

After completion of the dynamic series of scans, the region from the rostral clinoid processes to the dorsum sellae was rescanned (spatial series of scans) by use of the same protocol (9-seconds scanning time and 22-seconds interslice delay) as that used for the pre-contrast series of scans. The dogs that underwent the first and

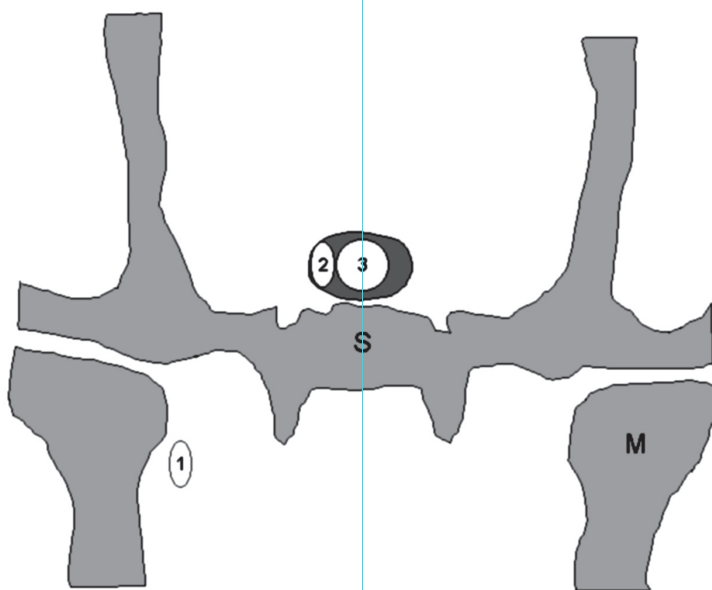


**Figure 1** - Schematic presentation of the regions of interest for density measurements on a transverse scan obtained during dynamic computed tomography (CT) of the pituitary gland in a healthy Beagle. 1 = Maxillary artery. 2 = Peripheral part of the pituitary gland. 3 = Central part of the pituitary gland. S = Sphenoid bone. M = Mandible.

third scanning protocols received an additional dose of 380 mg of iodine/kg. The dogs that underwent the second scanning protocol received no additional contrast medium. The spatial series of scans was performed to obtain a contrast-enhanced complete view of the pituitary gland from the rostral to caudal extents, and to identify its exact location and relation to the bony landmarks of the skull base.

### **Image analysis**

For all dogs, the enhancement patterns of the arteries and the pituitary gland on the dynamic series of scans were assessed visually by the same observer (RvdV-M). The computer software used enabled different settings of window width (contrast) and window level (brightness), and image subtraction to identify the borders of the pituitary gland and outline the difference in enhancement between the central and peripheral parts of the pituitary gland in 1 CT image. Unsynchronized density measurements were made of 1 of the maxillary arteries and of the central and peripheral part of the pituitary gland. Densities were measured in Hounsfield units (HUs) on all images in the same regions of interest (Figure 1). The location of the regions of interest was set to be a reliable representation of the structures to be measured. In each dog, the moment of maximum enhancement of the maxillary artery was the moment after the contrast medium injection (in the series of dynamic scans) at which the highest density of the maxillary artery was measured. This moment was designated as time 0 (synchronization). Synchronized density measurements of the central and peripheral part of the pituitary gland were made on the unenhanced image at the moment of maximum enhancement of the maxillary artery (time 0), and on the subsequent images of the dynamic series. Mean and SD values of density were calculated and time-mean density curves were calculated for the maxillary artery and for the central and peripheral part of the pituitary gland for the different groups of dogs.

With the images of the spatial series of scans displayed at the same window settings (window width, 250; window length, +80), the shape and enhancement of the pituitary gland were assessed visually. The height of the pituitary gland was measured from the image that contained the largest cross-section of the pituitary gland. On the same image, the edges of the brain were traced and the enclosed area was calculated by the computer. The ratio of the pituitary height (mm) to brain area ( $\text{mm}^2$ )  $\times 100$  was calculated (designated the P:B ratio), as described.<sup>8</sup> All measurements were performed by use of a trackball-driven cursor and CT computer software.

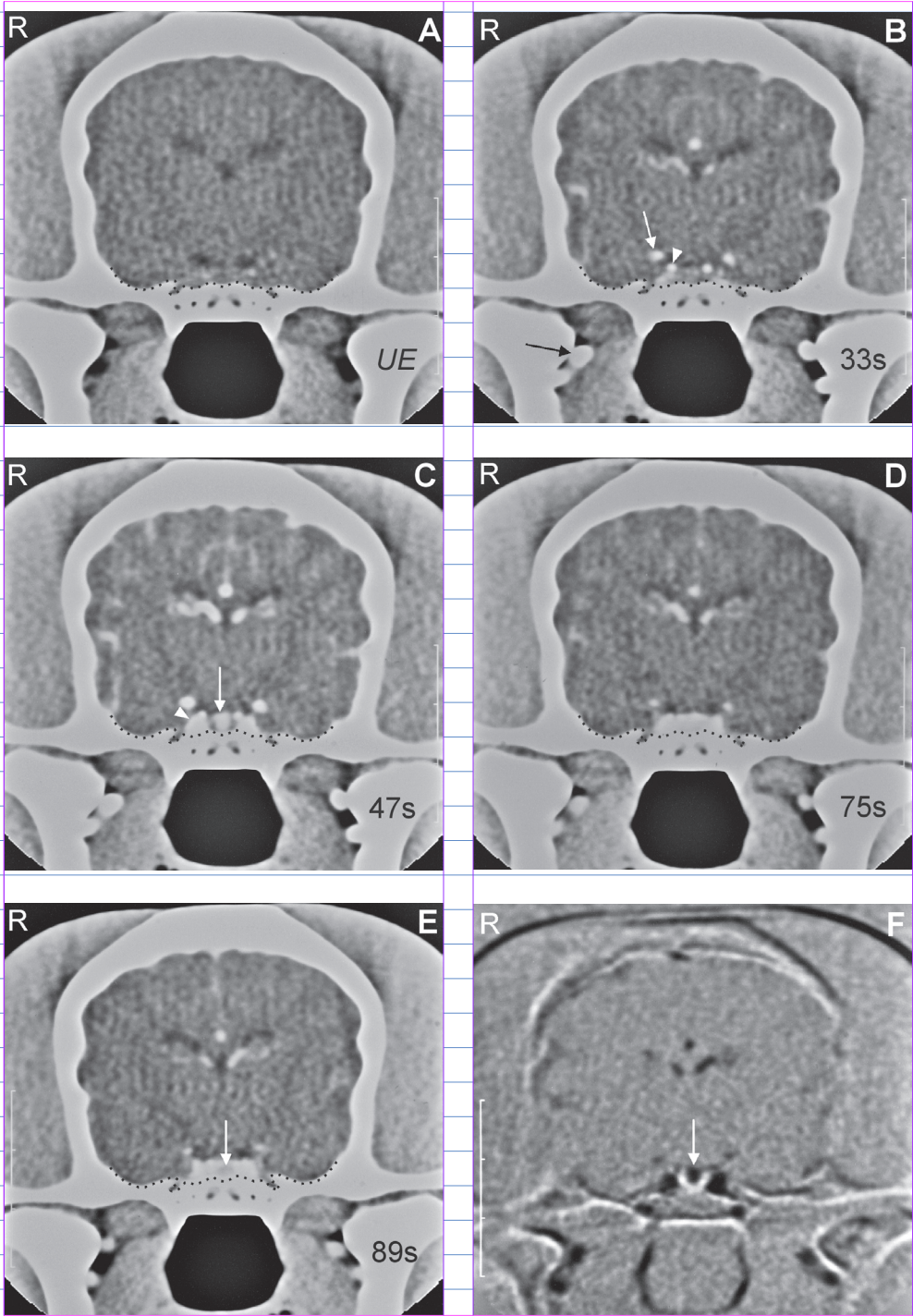


**Figure 2** - Representative transverse dynamic CT images through the pituitary fossa in a healthy Beagle. The dotted line delineates the brain and pituitary gland from the bone of the skull base.

A - Unenhanced (UE) image.

B - Image obtained at 33 seconds (synchronized as time 0 [sec]) after IV injection of contrast medium illustrating the arterial phase, including contrast enhancement of the maxillary artery (black arrow), the intracavernous part of the internal carotid artery (arrowhead), and the arterial cerebral circle (white arrow).

C - Image obtained at 47 seconds (synchronized time, 14 seconds) after IV injection of contrast medium. Notice the contrast enhancement of the central part of the pituitary gland (ie, the neurohypophysis [arrow]) and of the remaining parts of the cavernous sinuses (arrowhead).

D - Image obtained at 75 seconds (synchronized time, 42 seconds) after IV injection of contrast medium. Notice the homogeneous enhancement of the pituitary gland as a result of decreased enhancement of the central part (neurohypophysis) and increased enhancement of the peripheral part (ie, the adenohypophysis).

E - Image obtained at 89 seconds (synchronized time, 56 seconds) after contrast medium injection. Notice the hypodense appearance of the central part of the pituitary gland (arrow), compared with the appearance of the peripheral part of the pituitary gland.

F - Subtraction image derived from images in panel C and E. Notice the difference in enhancement between the central (arrow) and peripheral part (white rim) of the pituitary gland. In all panels, R represents the right side of the dog.

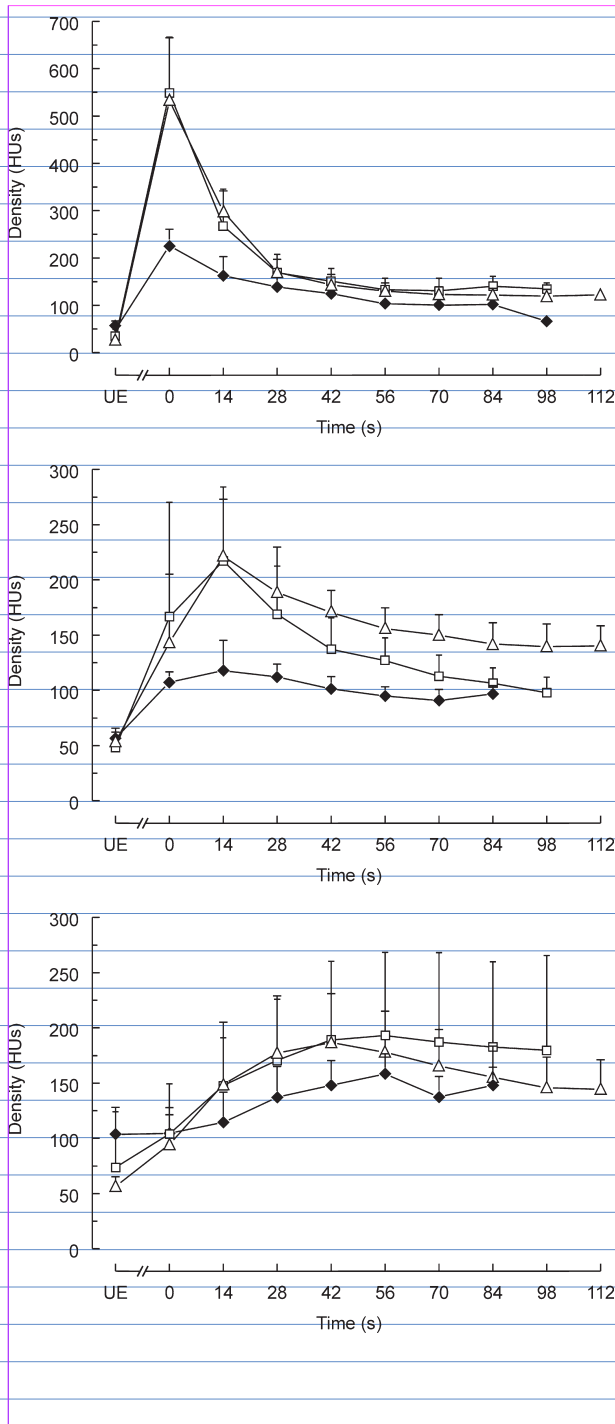


**Figure 3** - Time-mean density curves obtained during dynamic CT imaging of the maxillary artery (A) and the central (B) and peripheral (C) parts of the pituitary glands of 17 healthy dogs receiving 1 of 3 imaging protocols. Protocols used to complete the dynamic series included IV administration of contrast medium equivalent to a dose of 380 mg of iodinelkg after which scans were made with scanning time of 2.8 seconds and interscan time of 11.2 seconds (3 dogs; black diamond); IV administration of contrast medium equivalent to a dose of 760 mg of iodinelkg after which scans were made with scanning time of 2.8 seconds and interscan time of 11.2 seconds (6 dogs; open square); or IV administration of contrast medium equivalent to a dose of 760 mg of iodinelkg after which scans were made with scanning time of 4.5 seconds and interscan time of 9.5 seconds (8 dogs; open triangle). HUs = Hounsfield units. UE = Value obtained from unenhanced imaging. Time 0 = Moment of maximum enhancement of the maxillary artery.

## Results

The dynamic series with short scanning time (2.8 seconds) and incomplete rotation of the x-ray tube resulted in poor image quality. A scanning time of 4.5 seconds, coupled to a 360° rotation of the x-ray tube, resulted in a better image quality.

On the subsequent images of the dynamic series of scans, the same enhancement pattern was detected in all dogs (Figure 2). Following strong enhancement of the maxillary arteries, the intracavernous parts of the internal carotid arteries, and the communicating arteries of the arterial cerebral circle, there was strong enhancement of the central part of the pituitary gland, followed by enhancement of the peripheral part of the pituitary gland. On the last images of the dynamic series, the central part of the pituitary was hypodense, compared with the peripheral part of the pituitary gland. Especially during the enhancement phase that followed the pituitary flush, it was difficult to differentiate the homogeneously enhanced pituitary gland from the surrounding bone. To improve the differentiation of the enhanced pituitary gland, the window width and window level were adjusted; subtraction images outlined the difference in enhancement of the central and peripheral part of the pituitary gland and emphasized the enhancement patterns.

The mean  $\pm$  SD moment of maximum enhancement (unsynchronized) of the maxillary artery following the start of the injection of contrast medium was  $35.5 \pm 10.2$  seconds (range, 19 to 61 seconds). The degree of enhancement of the maxillary artery varied among individual dogs and the degree of enhancement achieved with the dose of contrast medium that provided 380 mg of iodine/kg was less than that achieved with the dose of contrast medium that provided 760 mg of iodine/kg ( $226 \pm 34.4$  HUs and  $539.8 \pm 122.0$  HUs, respectively; Figure 3). The mean pre-contrast values for the central and peripheral parts of the pituitary gland were  $52.2 \pm 7.5$  HUs and  $70.9 \pm 34.7$  HUs, respectively. After synchronization of the maximum enhancement of the maxillary artery to time 0, the maximum enhancement of the central part of the pituitary occurred at  $13.2 \pm 6$  seconds (range, 0 to 28 seconds) and the maximum enhancement of the peripheral part of the pituitary gland occurred at  $50.2 \pm 14.9$  seconds (range, 14 to 70 seconds; Figure 4). The mean maximum enhancement for the central and peripheral parts of the pituitary was  $201.7 \pm 65.3$  HUs and  $180.7 \pm 52.4$  HUs, respectively.

The pituitary gland was identified in all dogs on the images of the spatial series of scans. The pituitary had a triangular or round shape on the most rostral image that contained a part of the pituitary gland, and a round or oval shape on the caudal images. The dorsal margin was convex in all dogs. The height of the pituitary gland ranged from 3.7 to 5.5 mm (mean height  $\pm$  SD,  $4.1 \pm 0.5$  mm) and the brain area ranged from 1,368.5 mm<sup>2</sup> to 1,799.2 mm<sup>2</sup> (mean area,  $1,561.5 \pm 148.4$  mm<sup>2</sup>); the P:B ratio ranged from 0.22 to 0.31 (mean value,  $0.26 \pm 0.03$ ). The pituitary was enhanced uniformly on the images of the spatial series in 10 dogs (of which 5 dogs received a total of 760 mg of iodine/kg and 5 dogs received a total of 1,140 mg of iodine/kg). In 7 dogs (of which 4 dogs received a total of 760 mg of iodine/kg and 3 dogs received a total of 1,140 mg of iodine/kg), the central part of the pituitary was somewhat hypodense, compared with the peripheral part of the pituitary gland.

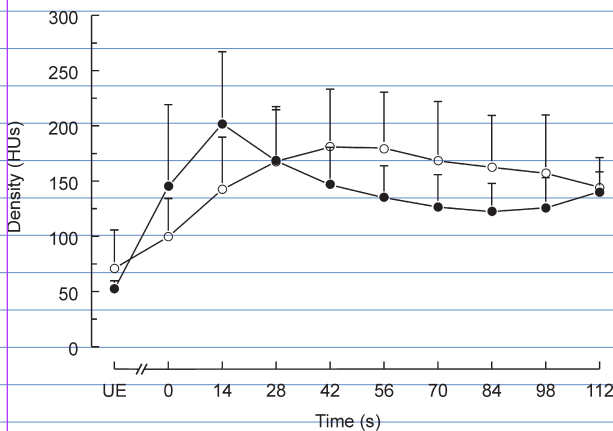


**Figure 4** - Time-mean density curves obtained during dynamic CT imaging of the central (solid circle) and peripheral part (open circle) of the pituitary gland in 17 dogs regardless of imaging protocol. See Figure 3 for key.

## Discussion

In the study reported here, a strong and early enhancement of the central part of the pituitary gland followed by enhancement of the peripheral part of the pituitary gland was observed in all 17 dogs. Similar findings were reported for 3 of 4 dogs included in a study conducted by Love et al.<sup>21</sup> The difference in the timing of enhancement between the central and peripheral parts of the pituitary gland may be explained by a different blood supply of the neurohypophysis and adenohypophysis in dogs. In the caudal distal region where the adenohypophysis does not completely invest the pars distalis neurohypophysis, distinct arterioles termed the caudal hypophyseal arteries (branchings of the caudal intercarotid artery, itself a branch of the internal carotid artery) enter the parenchyma of the pars distalis neurohypophysis and distribute as capillaries.<sup>20</sup> The direct arterial vascularization of the pars distalis neurohypophysis has been confirmed histologically in a Beagle.<sup>23</sup> Through these caudal hypophyseal arteries, the neurohypophysis (central part of the pituitary gland) has a direct arterial blood supply, in contrast with the pars distalis adenohypophysis (peripheral part of the pituitary gland) which receives its blood supply from veins; the latter are the hypophyseal portal vessels that connect the primary capillary network in the median eminence of the hypothalamus (supplied by the rostral hypophyseal arteries) with the secondary blood capillary network that form the sinusoids of the adenohypophysis.<sup>20</sup> In humans, blood reaches the arterioles of the neurohypophysis earlier than it does the sinusoids of the adenohypophysis.<sup>24-29</sup> On transverse dynamic CT images in humans, there is also a strong enhancement in the center of the pituitary gland, but this has been explained by the sudden filling of the secondary capillary bed of the adenohypophysis and not by enhancement of the neurohypophysis.<sup>15</sup> In humans, the strong and early enhancement of the neurohypophysis and its subsequent hypodense appearance, compared with the adenohypophysis, has been detected by use of dynamic CT in an axial scan plane.<sup>30,31</sup> The adenohypophysis (anterior lobe) and neurohypophysis (posterior or neural lobe) in humans cannot be observed in the same transverse slice because the axis of the pituitary gland is vertical, and the adenohypophysis oriented anteriorly and the neurohypophysis oriented posteriorly.<sup>17,18,32</sup> In dogs, the pituitary gland lies in a more horizontal position, with the infundibular process oriented dorsally and the neural lobe embedded in the pars distalis ventrally.<sup>19,20</sup> The enhancement of the secondary capillary bed of the adenohypophysis in transverse CT images in humans has

been called the pituitary tuft, and displacement or distortion of this tuft (called the tuft sign) has been used to identify pituitary microadenomas.<sup>15</sup> To avoid confusion with the term pituitary tuft, the term pituitary flush has been used to describe the enhancement of the neurohypophysis in dogs with PDH.<sup>33</sup> The adenohypophyseal tuft was not detected in dogs, probably because of the smaller dimensions and peripheral distribution of the adenohypophysis and the overwhelming central neurohypophyseal flush.

Because administration of contrast agent to provide a dose of 380 mg of iodine/kg resulted in a weak enhancement of the pituitary gland, the dose was increased to 760 mg of iodine/kg. In the dynamic study, 1 image was made every 14 seconds. In 9 dogs, a scanning time of 2.8 seconds was used, which is the shortest possible scanning time of the scanner used. This scanning time was coupled to an incomplete rotation of the x-ray tube during exposure and an interscan time of 11.2 seconds. The short scanning time and the incomplete rotation of the x-ray tube resulted in poor image quality. A scanning time of 4.5 seconds, coupled to a 360° rotation of the x-ray tube, resulted in a better image quality. Because of the shorter interscan time (9.5 seconds), this did not increase the total time between scans. In a dynamic CT study of 55 dogs with PDH,<sup>33</sup> the protocol involving the higher dose of contrast medium (760 mg of iodine/kg) was used; in those dogs, distortion or displacement of the central flush and also absence of a pituitary flush with a diffusely abnormal contrast enhancement of the gland indicated the presence of an adenoma.<sup>33</sup> In the study of this report, administration of 380 mg of iodine/kg to healthy dogs resulted in a weak central flush of the pituitary gland and therefore, in clinically affected dogs, the conclusion that a pituitary flush is absent (indirectly indicating the presence of an adenoma) may only be drawn when a higher dose (760 mg of iodine/kg) of contrast medium is used.

The variation in moment and degree of maximum enhancement of the maxillary artery among the dogs in our study may be explained by differences in injection volume, rate of contrast medium injection, body weight, blood viscosity, blood pressure, cardiac output, PCO<sub>2</sub>, and heart rate.<sup>34-37</sup> To get a better overview of the enhancement pattern of the canine pituitary gland the maximum enhancement of the maxillary artery was synchronized in all dogs. The shape of the time-density curve of the complete pituitary gland as reported by Love et al<sup>21</sup> is mainly influenced by the early and strong enhancement of the central neurohypophysis and resembles the arterial time-density curves of other organs.<sup>38-40</sup> In our study in dogs, the separate time-density curves of the central and peripheral parts of the pituitary gland illustrated the difference in blood supply of the neurohypophysis

and adenohypophysis, respectively. The curves resembled the time-density curves of the posterior lobe and anterior lobe of the pituitary gland in humans.<sup>6,41</sup>

Computed tomographic imaging of the pituitary gland in dogs with PDH that may undergo hypophysectomy should include a conventional contrast-enhanced series of scans, which enables assessment of the size of the pituitary tumor and its precise localization of the pituitary tumor in relation to the surgical landmarks.<sup>5</sup> Single slice dynamic CT imaging of the pituitary gland provides useful additional information. The displacement or distortion of the pituitary flush (ie, the neurohypophysis) has been reported in dogs with PDH,<sup>33</sup> and was used to detect microadenomas of the adenohypophysis in the same way as the tuft sign has been used in humans.<sup>15</sup> Dynamic CT was performed in 55 dogs with PDH that underwent hypophysectomy and in 36 of those dogs a distinct contrast enhancement of the neurohypophysis was detected. In 24 of the 36 dogs, the pituitary flush was displaced, which indicated the presence of an adenoma; in 18 of those 24 dogs, this diagnosis was confirmed grossly during surgery and histologically.<sup>33</sup> In the 19 dogs in which no pituitary flush was detected, the contrast-enhancement pattern was diffusely abnormal and diffusely abnormal tissue was confirmed histologically in all 19 dogs.<sup>33</sup> It was concluded that the use of dynamic CT imaging in dogs with PDH provided useful additional information, such as the identification of an adenoma (pituitary flush displaced) or a diffusely abnormal pituitary gland (no pituitary flush).<sup>33</sup> Single slice dynamic CT may give indirect evidence of the presence of a microadenoma when it is captured within the scan slice volume and when the adenoma is of sufficient size to displace or distort the neurohypophysis. Dynamic CT examination of the total volume of the pituitary gland (eg, with the use of spiral CT) may generate a 3-dimensional pituitary flush that enables localization of microadenomas in the complete pituitary gland in a single session.<sup>42</sup>

In adult humans, the upper aspect of the normal pituitary gland appears most often flat or concave,<sup>6,7,43</sup> whereas the dorsal margin of the pituitary gland in healthy dogs is convex.<sup>20,44</sup> In healthy dogs, the size of the pituitary gland varies among different breeds and among individual dogs of the same breed. With an increase of body weight, there is an absolute increase in pituitary size but a decrease in proportion to body weight.<sup>20</sup> In a study on the relation between impairment of glucocorticoid feedback and the size of the pituitary gland in dogs with PDH, the ratio between the height of the pituitary gland and the area of the brain appeared to provide good discrimination between enlarged and non-enlarged pituitary glands.<sup>8</sup> The P:B ratio in dogs with non-enlarged

pituitary glands is  $\leq 0.31$  and the P:B ratio in dogs with enlarged pituitaries is  $> 0.31$ . In the dogs of our study, the shapes, heights, and P:B ratios indicated that the pituitary glands were not enlarged.<sup>20,44</sup>

Evaluation of our study reveals certain weaknesses and strengths. The use of hand-injection rather than pressure injection may have introduced variability in the contrast enhancement pattern among dogs. Furthermore, variation in arterial blood CO<sub>2</sub> concentration and peripheral blood pressure may also have provided additional sources of variability. However, all contrast medium injections were completed within 12 seconds and density measurements for the pituitary gland were synchronized to the maximal enhancement of the maxillary artery. Also, if there were additional sources of variability, then these were similar for all dogs. All examinations, assessments, and measurements were performed by 1 observer. The major strength of our study was that we demonstrated the separate assessment of the adenohypophysis and neurohypophysis with a simple single slice CT scanner. The direct arterial vascularization of the neurohypophysis (which explains the pituitary flush during dynamic CT) has been confirmed by findings of histologic examination of normal canine pituitary gland, reported previously by 1 of the authors.<sup>23</sup>

Our data have indicated that the difference in timing of enhancement between the central and peripheral parts of the pituitary gland is a consequence of a difference in vascularization of the neurohypophysis and the adenohypophysis, respectively. For dynamic CT imaging of the pituitary gland of dogs, it is recommended to make a series of 2-mm-thick scans with a scanning time of 4.5 seconds and an interscan time of 9.5 seconds after IV injection of contrast medium to provide a dose of 760 mg of iodine/kg. Displacement, distortion, or disappearance of the strong central enhancement (pituitary flush) may be used for the detection and localization of pituitary abnormalities in the adenohypophysis such as microadenomas in dogs with PDH.

<sup>a</sup> Domitor, SmithKline Beecham Animal Health BV, Zoetermeer, The Netherlands.

<sup>b</sup> Diprivan-10, Zenaca BV, Ridderkerk, The Netherlands.

<sup>c</sup> Forene, Abbot Laboratories BV, Maarsse, The Netherlands.

<sup>d</sup> Tomoscan CX/S, Philips NV, Eindhoven, The Netherlands.

<sup>e</sup> Telebrix 38, Guerbet Nederland BV, Gorinchem, The Netherlands.

## References

1. Rijnberk A. Hypothalamus-pituitary system. In: Rijnberk A, ed. *Clinical endocrinology of dogs and cats*. Dordrecht/Boston: Kluwer Academic Publishers, 1996;11–34.
2. Kempainen RJ, Peterson ME. Animal models of Cushing's disease. *Trends Endocrinol Metabol* 1994;5:21–28.
3. Feldman EC, Nelson RW. Comparative aspects of Cushing's syndrome in dogs and cats. *Endocrinol Metab Clin North Am* 1994;23:671–691.
4. Meij BP, Voorhout G, Van den Ingh TSGAM, et al. Transsphenoidal hypophysectomy in beagle dogs: evaluation of a microsurgical technique. *Vet Surg* 1997;26:295–309.
5. Meij BP, Voorhout G, Van den Ingh TSGAM, et al. Results of transsphenoidal hypophysectomy in 52 dogs with pituitary-dependent hyperadrenocorticism. *Vet Surg* 1998;7:246–261.
6. Bonneville JF, Cattin F, Dietemann JL. Pituitary adenomas with suprasellar extension. In: Bonneville JF, Cattin F, Dietemann JL, eds. *Computed tomography of the pituitary gland*. Berlin: Springer Verlag, 1986;47–51.
7. Elster AD. Modern imaging of the pituitary. *Radiology* 1993;187:1–14.
8. Kooistra HS, Voorhout G, Mol JA, Rijnberk A. Correlation between impairment of glucocorticoid feedback and the size of the pituitary gland in dogs with pituitary-dependent hyperadrenocorticism. *J Endocrinol* 1997;152:387–394.
9. Voorhout G, Stolp R, Lubberink AAME, et al. Computed tomography in the diagnosis of canine hyperadrenocorticism not suppressible by dexamethasone. *J Am Vet Med Assoc* 1988;192:641–666.
10. Nelson RW, Ihle SL, Feldman EC. Pituitary macroadenomas and macroadenocarcinomas in dogs treated with mitotane for pituitary-dependent hyperadrenocorticism: 13 cases (1981-1986). *J Am Vet Med Assoc* 1989;194:1612–1617.
11. Davis PC, Hoffman JC, Tindall GT, et al. CT-surgical correlation in pituitary adenomas: evaluation in 113 patients. *Am J Neuroradiol* 1985;6:711–716.
12. Davis PC, Hoffman JC, Spencer T, et al. MR imaging of pituitary microadenomas: CT, clinical and surgical correlation. *Am J Neuroradiol* 1987;8:107–112.
13. Gardeur D, Naidich TP, Metzger J. CT analysis of intrasellar pituitary adenomas with emphasis on patterns of contrast enhancement.

- Neuroradiology 1981;20:241–247.
14. Hasegawa T, Ito H, Shoin K, et al. Diagnosis of an isodense pituitary microadenoma by dynamic CT scanning. *J Neurosurg* 1984;60:424–427.
  15. Bonneville JF, Cattin F, Moussa-Bacha K, et al. Dynamic computed tomography of the pituitary gland: the ‘tuft sign’. *Radiology* 1983;149:145–148.
  16. Hemminghytt S, Kalkhoff RK, Daniels DL, et al. Computed tomographic study of hormone-secreting microadenomas. *Radiology* 1983;146:65–69.
  17. Daniel PM, Pritchard MML. Studies of the hypothalamus and the pituitary gland. *Acta Endocrinol* 1975;80:S27–S63.
  18. Roppolo HMN, Latchaw RE, Meyer JD, et al. Normal pituitary gland: 1. Macroscopic anatomy-CT correlation. *Am J Neuroradiol* 1983;4:927–935.
  19. Eigenmann JE, Lubberink AAME. The pituitary. In: Slatter DH, ed. *Textbook of small animal surgery*. Philadelphia: WB Saunders Co, 1985;1840–1848.
  20. Hullinger RL. The endocrine system. In: Evans HE, ed. *Miller’s anatomy of the dog*. 3rd ed. Philadelphia: WB Saunders Co, 1993;559–585.
  21. Love NE, Fisher P, Hudson L. The computed tomographic enhancement pattern of the normal canine pituitary gland. *Vet Radiol Ultrasound* 2000;41:507–510.
  22. Meij BP, Mol JA, Hazewinkel HAW, et al. Assessment of a combined anterior pituitary function test in beagle dogs: rapid sequential intravenous administration of four hypothalamic releasing hormones. *Domest Anim Endocrinol* 1996;13:161–170.
  23. Meij BP, Van den Ingh TSGAM, Mol JA, et al. Immunohistochemical staining for adrenocorticotropin, melanotropin, growth hormone, prolactin, and thyrotropin in a median sagittal section of the pituitary gland in beagle dogs. In: Meij BP, ed. *Transsphenoidal hypophysectomy for treatment of pituitary-dependent hyperadrenocorticism in dogs*. Hooglanderveen, The Netherlands: Trepico, 1997:125–141.
  24. Gorczyca W, Hardy J. Arterial supply of the human anterior pituitary gland. *Neurosurgery* 1987;20:369–378.
  25. Green JD. The comparative anatomy of the portal vascular system and of the innervation of the hypophysis. In: Harris GW, Donovan BT, eds. *The pituitary gland, volume 1*. London: Butterworths, 1966;127–146.
  26. Lecrecq TA, Grisoli F. Arterial blood supply of the normal human pituitary

- gland. *J Neurosurg* 1983;58:678–681.
27. Page RB. Pituitary blood flow. *Am J Physiol* 1982;243:E427–E442.
  28. Popa G, Fielding U. A portal circulation from the pituitary to the hypothalamic region. *J Anat* 1930;65:88–91.
  29. Szentagothai JB, Flerko B, Mess B, et al. Anatomical considerations. In: Szentagothai JB, Flerko B, Mess B., eds. *Hypothalamic control of the anterior pituitary*. Budapest: Akadémiai Kiadó, 1968;84–95.
  30. Bonneville JF, Cattin F, Portha C, et al. Computed tomographic demonstration of the posterior pituitary. *Am J Neuroradiol* 1985;6:889–892.
  31. Bonneville JF, Cattin F, Dietemann JL. Hypothalamic-pituitary region: computed tomographic imaging. *Ballières Clin Endocrinol Metabol* 1989;3:35–59.
  32. Roppolo HMN, Latchaw RE. Normal pituitary gland: 2. Microscopic anatomy-CT correlation. *Am J Neuroradiol* 1983;4:937–944.
  33. Van der Vlugt-Meijer RH, Meij BP, van den Ingh TSGAM, et al. Dynamic computed tomography of the pituitary gland in dogs with pituitary-dependent hyperadrenocorticism. *J Vet Int Med* 2003;17:773–780.
  34. Claussen CD, Banzer D, Pfretzschner C, et al. Bolus geometry and dynamics after intravenous contrast medium injection. *Radiology* 1984;153:365–368.
  35. Gardeur D, Lautrou J, Millard JC, et al. Pharmacokinetics of contrast media: experimental results in dog and man with CT implications. *J Comput Assist Tomogr* 1980;4:178–185.
  36. Kormano M, Partanen K, Soimakallio S, et al. Dynamic contrast enhancement of the upper abdomen: effect of contrast medium and weight. *Invest Radiol* 1983;18:364–367.
  37. Schad N, Schepke P, Rohde U, et al. Timing of exposure in angiographic computed tomography. *Cardiovasc Intervent Radiol* 1981;4:59–65.
  38. Bader TR, Prokesch RW, Grabenwoger F. Timing of the hepatic arterial phase during contrast-enhanced computed tomography of the liver: assessment of normal values in 25 volunteers. *Invest Radiol* 2000;35:486–492.
  39. Cohen WA, Pinto RS, Kricheff II. Dynamic CT scanning for visualization of the parasellar carotid arteries. *Am J Neuroradiol* 1982;3:185–189.
  40. Jaschke W, Lipton MJ, Boyd D, et al. Dynamic CT scanning of the normal canine liver: interpretation of time-density curves resulting from an intravenous bolus injection of contrast material. *Eur J Radiol* 1985;5:256–

- 260.
41. Turski PA, Watanabe TJ, Chambers EE, Newton TH. Contrast enhancement of the normal and abnormal pituitary gland. Proceedings of the International Workshop on Radiology. Berlin 1981:157–164.
  42. Van der Vlugt-Meijer RH, Voorhout G, Meij BP. Imaging of the pituitary gland in dogs with pituitary-dependent hyperadrenocorticism. *Mol Cell Endocrinol* 2002;197:81–87.
  43. Peyster RG, Hoover ED, Viscarello RR, et al. CT appearance of the adolescent and preadolescent pituitary gland. *Am J Neuroradiol* 1983;4:411–414.
  44. Voorhout G. Cisternography combined with linear tomography for the visualization of the pituitary gland in healthy dogs: a comparison with computed tomography. *Vet Radiol* 1990;31:68–73.

# CHAPTER 4

## **Dynamic computed tomography of the pituitary gland in dogs with pituitary-dependent hyperadrenocorticism**

Roselinda H. van der Vlugt-Meijer, DVM, MVR; Björn P. Meij<sup>1)</sup>, DVM, PhD; Ted S.G.A.M. vanden Ingh<sup>2)</sup>, DVM, PhD; Ad Rijnberk<sup>1)</sup>, DVM, PhD; George Voorhout, DVM, PhD.

**Journal of Veterinary Internal Medicine 2003;17:773-780**

From the Division of Diagnostic Imaging, the Department of Clinical Sciences of Companion Animals<sup>1)</sup>, and the Department of Pathology<sup>2)</sup>, Faculty of Veterinary Medicine, Utrecht University, The Netherlands.

## Abstract

Dynamic computed tomography (CT) of the pituitary gland was performed in 55 dogs with pituitary-dependent hyperadrenocorticism (PDH) that underwent transsphenoidal hypophysectomy. On routine contrast-enhanced CT images, microadenomas of the pituitary gland often are indistinguishable from nontumorous pituitary tissue because of isoattenuation. Dynamic CT may allow visualization of these adenomas. The changes in the contrast enhancement pattern of the pituitary during dynamic CT in 55 dogs with PDH were correlated with surgical and histopathological findings. In 36 dogs, dynamic CT identified distinct contrast enhancement of the neurohypophysis (pituitary flush). In 24 dogs, this pituitary flush was displaced, which indicated the presence of an adenoma. This observation was confirmed surgically and histopathologically in 18 of the 24 dogs. In 19 dogs there was a diffusely abnormal contrast enhancement pattern. CT findings agreed with surgical findings in 13 of these dogs and with histopathological findings in all 19 dogs.

It is concluded that a dynamic series of scans should be included in the CT protocol of the pituitary gland in dogs with PDH because it allows for identification of an adenoma or a diffusely abnormal pituitary gland.

## Introduction

Since the late 1980's consensus has developed with regard to the therapy of pituitary-dependent hyperadrenocorticism (PDH) or Cushing's disease in humans. Microsurgical transsphenoidal pituitary adenomectomy is considered the primary treatment for pituitary adenomas.<sup>1,2</sup> Although the first experiences with pituitary surgery were obtained in dogs,<sup>3-5</sup> so far the use of surgery in the treatment of dogs with PDH has been limited. Only recently, hypophysectomy was revisited in the treatment of PDH in dogs.<sup>6,7</sup>

Detailed imaging of the pituitary gland is a prerequisite for successful outcome in transsphenoidal hypophysectomy in dogs. It allows for accurate preoperative assessment of the size of the pituitary gland as well as for localization of the pituitary gland in relation to the surgical landmarks.<sup>6</sup> Conventional contrast-enhanced computed tomography (CT) includes a series of consecutive scans (spatial series) of the same slice thickness (e.g., 2 mm) from rostral to caudal through the pituitary gland, after the injection of contrast medium. On conventional contrast-enhanced CT images, microadenomas often are indistinguishable from nontumorous pituitary tissue because of isoattenuation.<sup>8-11</sup> Dynamic contrast-enhanced CT includes a series of scans (dynamic series) of identical slice thickness, at the same slice position through the center of the pituitary gland, during and after IV injection of contrast medium. In humans, dynamic CT images of the pituitary gland enable visualization of the sinusoid vessels of the secondary capillary bed of the anterior lobe, which, when displaced or compressed (so-called 'tuft sign'), can be helpful in diagnosing even small intra-hypophyseal lesions.<sup>12</sup>

Conventional CT of the pituitary gland has been evaluated in healthy dogs<sup>6,13</sup> and in dogs with PDH.<sup>7,14</sup> Recently, dynamic CT of the normal pituitary gland in dogs has been described,<sup>15</sup> and the use of dynamic CT in dogs with PDH has been proposed.<sup>16,17</sup> After enhancement of the internal carotid arteries and the arterial cerebral circle, the central part of the pituitary or neurohypophysis enhances maximally.<sup>17</sup> Subsequently, enhancement of the adenohypophysis occurs with a temporary hypodense appearance of the neurohypophysis. Similar to the pituitary tuft sign in humans, displacement, distortion, or disappearance of the pituitary flush in the early phase of the dynamic CT examination may be used to identify and localize microadenomas in dogs.

In this study, we report on dynamic CT of the pituitary gland in dogs with PDH. The aim of the study was to assess the changes in the contrast

enhancement pattern of the pituitary gland on dynamic CT and to correlate the observations with the findings at transsphenoidal hypophysectomy and on histopathological examination of the surgical specimens.

## Materials and methods

### Animals

The group of dogs with PDH (n=55; median age 10 years; range 4 - 14 years) comprised 32 females (17 ovariectomized) and 23 males (4 castrated). In 43 of these 55 dogs, pituitary dimensions (height, width, length, and volume), as measured on contrast enhanced CT images, have been described previously.<sup>7</sup> The preliminary diagnosis of hyperadrenocorticism was based on characteristic signs such as polyuria, polydipsia, truncal obesity, cutaneous atrophy, muscular weakness, and increased corticoid/creatinine (C/C) ratios in 2 consecutive morning urine samples collected at home.<sup>18,19</sup> Immediately after collection of the second sample, the dogs received 3 oral doses of 0.1 mg dexamethasone per kg of body weight at 8-h intervals and the next morning a third urine sample was collected. By expressing the C/C ratio of the third sample as a percentage of the mean of the first two samples, a measure of dexamethasone resistance was obtained. If suppression was more than 50% PDH, was diagnosed.<sup>18</sup> In animals with < 50 % suppression of the C/C ratio, the diagnosis of PDH was made by measurements of basal plasma ACTH.<sup>20</sup>

### Computed tomography

Food was withheld from the dogs for 18 hours before CT. After premedication with medetomidine<sup>1</sup> (50 µg/kg, IV), anesthesia was induced by IV administration of propofol<sup>2</sup> (1-2 mg/kg). The trachea was intubated and inhalation anesthesia was maintained in a semi-closed system with a mixture of isoflurane<sup>3</sup>, nitrous oxide and oxygen.

CT was performed with a third generation CT scanner<sup>4</sup>. With the dogs in sternal recumbency, transverse scans of the skull base were made, from the rostral clinoid processes to the dorsum sellae, using 9 s scanning time with 120 kV, 220 mA and 2-mm-thick consecutive slices. The most caudal image completely rostral to the dorsum sellae, usually containing the largest cross-section of the pituitary gland, was selected and at this position a series of 2-mm-thick scans was made using 4.5 s scanning time with 9.5 s interscan time. One scan was made

before contrast medium injection and then a series of 8 to 10 scans (dynamic series of scans) was made during and after the IV bolus injection of sodium and meglumine ioxotalamate (Telebrix 350<sup>5</sup>, containing 350 mg iodine/ml, 2 ml/kg of body weight, with a maximum of 60 ml). Due to a 5 sec standby delay before the start of a series of scans, inherent to the scanner used, the first scan of this series was started 5 s after the start of the contrast medium injection. After the dynamic series of scans, an additional bolus injection of sodium and meglumine ioxotalamate (Telebrix 350; 1 ml/kg of body weight, with a maximum of 30 ml) was given and immediately after the completion of the injection a spatial series of scans was made consisting of 2-mm-thick consecutive scans from the rostral clinoid processes to the dorsum sellae.

Dimensions and densities were measured from the display monitor using a trackball-driven cursor and CT computer software, with all images displayed at the same window settings (WW 250, WL +80).

In each dog, the height of the pituitary was measured from the image of the spatial series that contained the largest cross-section of the pituitary gland. On the same image, the edges of the brain were traced and the enclosed area was calculated by the computer. From the height of the pituitary (mm) x 100 and the area of the brain (mm<sup>2</sup>), the pituitary height/brain area (P/B) ratio was calculated. Pituitary glands with P/B ratio  $\leq 0.31$  were considered normal in size and pituitary glands with P/B ratio  $> 0.31$  were considered enlarged.<sup>21</sup> Only dogs in which the height of the pituitary was  $\leq 10$  mm were included in this study.

On the last image of the dynamic series, a region of interest (ROI) containing the pituitary and a ROI containing brain, was selected. Using these ROI's, density measurements of the pituitary gland and brain tissue were made and expressed in Hounsfield Units (HU). Density measurements of the pituitary gland were made on the unenhanced image at the moment of maximal enhancement of the cerebral arterial circle, and on the subsequent images of the dynamic series. Density measurements of the brain were made on the unenhanced image at the moment of maximal enhancement of the cerebral arterial circle, and on the image 14 s thereafter.

The contrast enhancement pattern of the pituitary glands was assessed visually on the images of both the dynamic series and the spatial series, using different window settings. Dynamic images were viewed for presence and localization of an early, strong enhancement of the neurohypophysis (pituitary flush).<sup>17</sup> Spatial images were viewed for homogeneity or inhomogeneity of contrast enhancement of the pituitary gland.

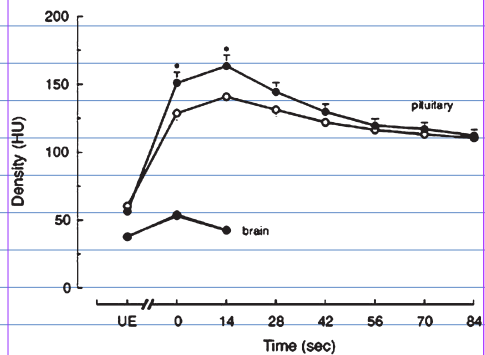
## Hypophysectomy and histopathology

Transsphenoidal hypophysectomy was performed according to a microsurgical technique and standardized peri- and postoperative treatment protocols as described previously.<sup>6,7</sup> In the event that during surgery normal and abnormal pituitary tissue could be distinguished, an attempt was made to collect separate samples for histopathology. When this was not possible, pituitary tissue was collected as a single sample for histopathological examination. Subsequently, histopathological examination was performed according to histological techniques described previously.<sup>6,7,22</sup>

## Statistical analysis

Results are expressed as means  $\pm$  SD or as median values (with ranges) where appropriate. After division of the dogs into 2 groups on the basis of pituitary size or the presence of a pituitary flush, results were statistically evaluated using Student's t-test for independent samples (two-tailed). After division of the dogs in 4 groups, differences were first analyzed by the Kruskal-Wallis one-way ANOVA, and when significant differences were found, these were further analyzed by the Mann-Whitney U-Wilcoxon rank sum test.  $P < 0.05$  was considered significant.

**Figure 1.** Time-density (mean  $\pm$  sd) curve for the pituitary gland and brain in 28 dogs with normal-sized pituitary glands (●) and 27 dogs with enlarged pituitary glands (○). Y axis is labelled in Hounsfield Units (HU). At maximal contrast enhancement of the arterial cerebral circle (time 0) and 14 s thereafter, the normal-sized pituitary glands were significantly more contrast-enhanced than the enlarged pituitary glands (\* $P < 0.05$ ). UE = unenhanced.



## Results

In 27 of 55 dogs, the pituitary gland was enlarged, and P/B ratios ranged from 0.32 to 0.67 (median, 0.43). In 28 of 55 dogs, the pituitary gland was not enlarged, and P/B ratios ranged from 0.16 to 0.31 (median, 0.25).

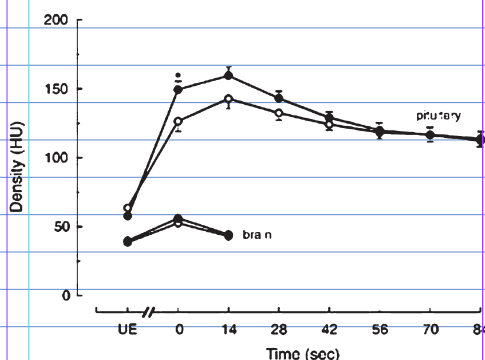
### Dynamic CT findings

Maximal enhancement of the arterial cerebral circle occurred 5 to 61 sec (median, 33 sec) after the start of the injection of contrast medium. On dynamic images, an early and strong enhancement of the neurohypophysis (pituitary flush) occurred in 36 dogs whereas no pituitary flush was visible in the remaining 19 dogs.

At the moment of maximal enhancement of the cerebral arterial circle (time 0) and 14 sec thereafter, the contrast enhancement in the normal-sized pituitary glands was significantly greater than in the enlarged pituitary glands (Fig. 1). No difference in brain enhancement was observed between the 2 groups (Fig. 1). At the moment of maximal contrast enhancement of the cerebral arterial circle (time 0), the pituitary glands showing a pituitary flush were significantly more contrast-enhanced than the pituitary glands in which no flush was seen (Fig. 2). There was no difference in brain enhancement between the 2 groups (Fig. 2).

On the basis of pituitary size (enlarged or not enlarged) and the occurrence or absence of a pituitary flush, the dogs were divided in 4 groups (Table 1): (1) 10 dogs with an enlarged pituitary gland and pituitary flush (Fig. 3); (2) 17 dogs with an enlarged pituitary gland and no pituitary flush (Fig. 4); (3) 26 dogs without pituitary gland enlargement and with pituitary flush (Fig.

**Figure 2.** Time-density (mean  $\pm$  sd) curve for the pituitary gland and brain in 36 dogs with a distinct pituitary flush ( $\bullet$ ) and 19 dogs without a distinct pituitary flush ( $\circ$ ). Y axis is labelled in Hounsfield Units (HU). At maximal contrast enhancement of the arterial cerebral circle (time = 0), the pituitary glands with a pituitary flush were significantly more contrast enhanced than the pituitary glands in which no flush was seen ( $*P < 0.05$ ). UE = unenhanced.



5a and 5b); and (4) 2 dogs without pituitary gland enlargement and no pituitary flush (Fig. 6). At the moment of maximal contrast enhancement of the arterial cerebral circle (time 0), pituitary gland enhancement was significantly greater in dogs with normal pituitary gland size and pituitary flush than in the dogs with an enlarged pituitary gland and no pituitary flush (Fig. 7). No difference in brain enhancement was observed between the groups (Fig. 7).

## Relation between dynamic CT findings and surgical and histopathological findings

### Discernible pituitary flush

In 36 of 55 dogs a distinct pituitary flush allowed identification of the neurohypophysis (Table 1). In 24 of these dogs, the pituitary flush was displaced and displacement was dorsal in 7, right-dorsal in 8, right in 3, ventral in 3, left-ventral in 2, and left in 1 dog. The displacement of the flush indicated the presence of an adenoma in the part of the gland away from the flush. This group of 24 dogs included 15 dogs with normal-sized pituitary glands and 9 dogs with moderately enlarged (P/B ratios ranging from 0.32 to 0.55) pituitary glands.

In 18 of these 24 dogs, the CT findings corresponded with the surgical

	Pituitary not enlarged	Pituitary enlarged	Total
Pituitary flush	26	10	36
No pituitary flush	2	17	19
Total	28	27	55

**Table 1.** Subdivision of 55 dogs with pituitary dependent-hyperadrenocorticism in 4 groups based on dynamic computed tomography findings (pituitary size and pituitary flush sign)

	Pituitary not enlarged	Pituitary enlarged	Total
Uniform enhancement	20	16	36
Diffuse irregular enhancement	4	3	7
Localized hypoattenuation	4	8	12
Total	28	27	55

**Table 2.** Subdivision of 55 dogs with pituitary dependent-hyperadrenocorticism in 6 groups based on spatial computed tomography findings (pituitary size and enhancement pattern).

findings (i.e. during hypophysectomy abnormal pituitary tissue was recognized in a location corresponding to the location of the adenoma on the dynamic CT images). In 9 of these 18 dogs, the adenoma was isolated and collected separately from the remainder of the pituitary gland. On histological examination, the part of the gland that was judged to be pituitary tumor during surgery and that corresponded to the location of the adenoma on dynamic CT images contained adenomatous adeno-hypophyseal tissue in all 9 dogs. The other part, judged to be unaffected pituitary tissue during surgery and corresponding to the displaced pituitary flush on the CT images, contained neurohypophyseal tissue (4 dogs), neurohypophyseal tissue together with unaffected adeno-hypophyseal tissue (4 dogs), or neurohypophyseal tissue together with adenomatous adeno-hypophyseal tissue (1 dog). In the other 9 of the 18 dogs, abnormal pituitary tissue encountered during surgery and corresponding to the location of the adenoma on CT images was collected together with the part of the pituitary gland that corresponded to the displaced pituitary flush. Histologic examination identified adenomatous adeno-hypophyseal tissue in 8 dogs and additional neurohypophyseal tissue in 7 dogs. In one of the 9 dogs, the specimen was too small for a histological diagnosis.

In 6 of the 24 dogs with a displaced pituitary flush, no correlation was found between the dynamic CT and the surgical findings with respect to the location of the adenoma. In 5 of these dogs, abnormal adeno-hypophyseal tissue was seen during surgery in a location that did not correlate with the dynamic CT findings, and in 1 dog the pituitary gland was macroscopically judged to be normal. In all 6 dogs, adenomatous adeno-hypophyseal tissue as well as neurohypophyseal tissue, pars intermedia, and adeno-hypophyseal tissue was found in the pituitary fragments submitted for histological examination.

In 10 dogs with a pituitary glands of normal size, a normal pituitary flush was observed. In 7 of these dogs, macroscopically normal adeno-hypophyseal tissue was encountered during surgery. Histological examination identified adenomatous adeno-hypophyseal tissue in 6 dogs but no tumor could be identified in the other dog. In 3 dogs, abnormal adeno-hypophyseal tissue was found during surgery and was identified on histological examination as adenoma in 1 dog but no tumor tissue was found in the other 2 dogs.

In 9 of 10 dogs with a normal pituitary flush on the CT images, a well-circumscribed neurointermediate lobe came into view after removal of the adeno-hypophyseal tissue. Manipulation of the neurointermediate lobe usually resulted in a small hemorrhage from the caudal hypophyseal artery.

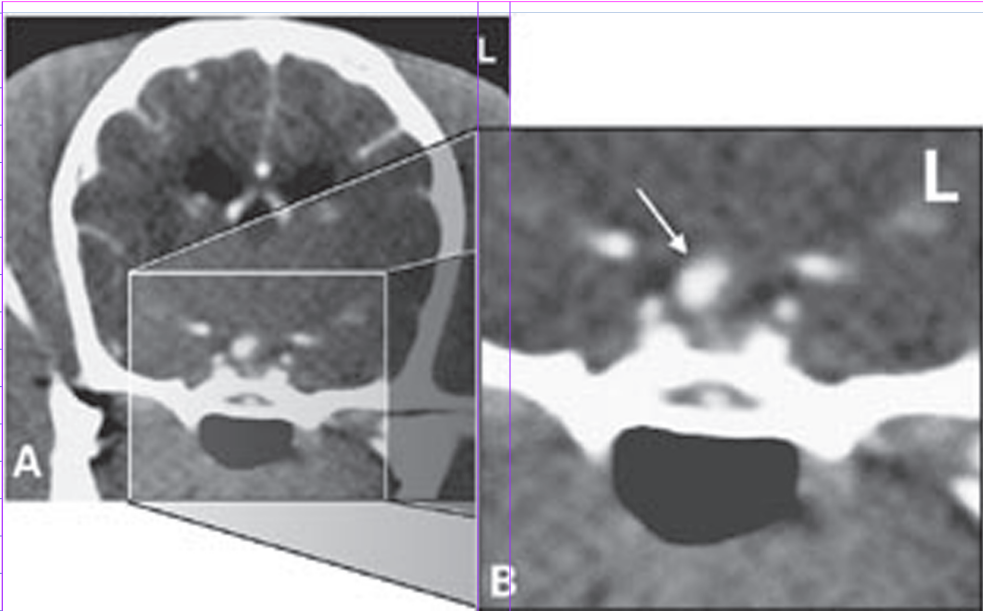


**Figure 3.** Transverse dynamic CT image through the pituitary fossa at the moment of maximal contrast enhancement of the arterial cerebral circle in an 8-year-old Yorkshire terrier with PDH. The pituitary gland is enlarged (P/B ratio 0.43) and there is a distinct pituitary flush (arrow) which is displaced dorsally and to the right. (A) overview of the cranium and (B) close-up view of the pituitary gland.

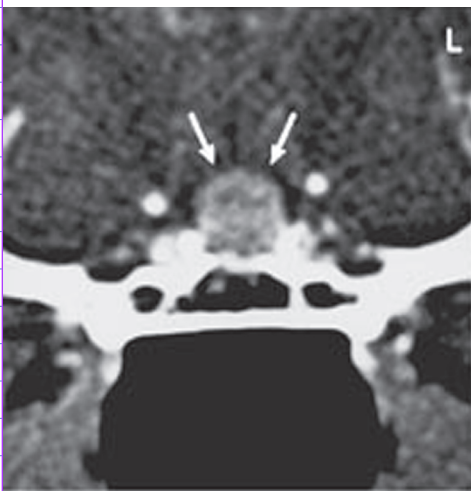


**Figure 4.** Transverse dynamic CT image through the pituitary fossa at the moment of maximal contrast enhancement of the arterial cerebral circle in a 10-year-old Doberman pinscher with PDH. The pituitary gland (arrows) is enlarged (P/B ratio 0.42) and no pituitary flush is discernible.

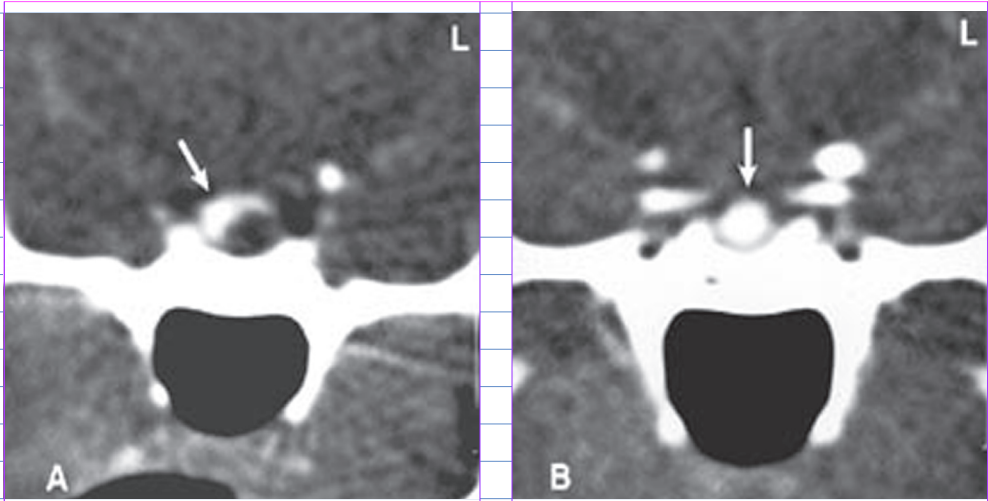


**Figure 5.** Transverse dynamic CT image through the pituitary fossa at the moment of maximal contrast enhancement of the arterial cerebral circle in a 6-year-old Yorkshire terrier (A) and a 7-year-old Maltese dog (B) with PDH. (A) The pituitary gland is not enlarged (P/B ratio 0.29) and the pituitary flush (arrow) is displaced dorsally and to the right, indicating an adenoma ventrally and to the left. (B) The pituitary gland is not enlarged (P/B ratio 0.27) and the pituitary flush (arrow) is not displaced.

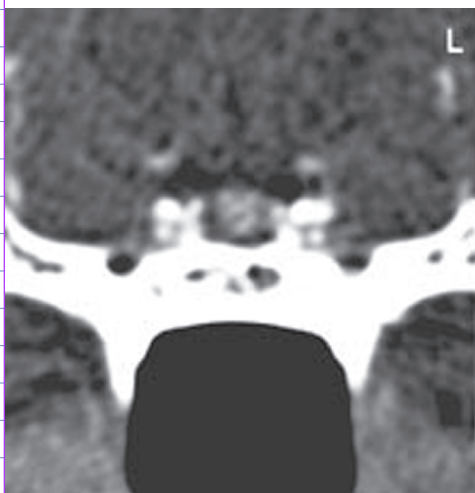


**Figure 6.** Transverse dynamic CT image through the pituitary fossa at the moment of maximal contrast enhancement of the arterial cerebral circle in an 8-year-old Rottweiler with PDH. The pituitary gland is not enlarged (P/B ratio 0.26) and there is no pituitary flush.

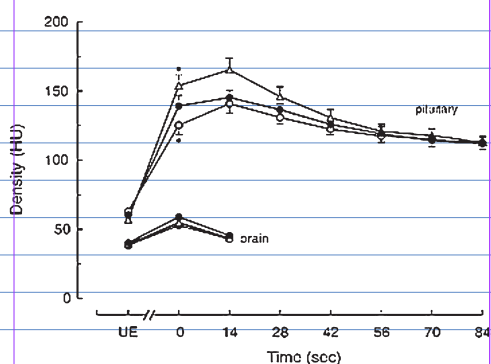
The neurointermediate lobe was situated caudally in the surgical field, close to the dorsum sellae. In 5 of these 9 dogs, small neurointermediate lobe samples were collected separately from the adenohypophyseal tissue and histological examination confirmed that this material was neurohypophyseal tissue in all cases.

In 2 dogs, the pituitary flush could not be categorized as either displaced or normal. One of these dogs had an enlarged pituitary gland and an early left- and right-dorsal pituitary flush was observed followed by a ventral flush. In the center, a hypodense area remained, which indicated the presence of an adenoma. At surgery, an abnormal pituitary gland was removed and histopathological examination identified neurohypophyseal tissue, pars intermedia, and adenohypophyseal tissue as well as cysts and adenomatous adenohypophyseal tissue. The other dog had a normal-sized pituitary gland, and the pituitary flush was difficult to discern due to simultaneous enhancement of the arteries of the cerebral circle. Cystic adenohypophyseal tissue and a well circumscribed neurointermediate lobe were removed separately. Histopathological examination identified adenomatous adenohypophyseal tissue in the former sample and neurohypophyseal tissue in the latter sample.

### No pituitary flush discernible

In 19 of 55 dogs, no pituitary flush was discernible (Table 1). In 17 of these 19 dogs, the pituitary gland was enlarged (P/B ratios ranging from 0.32 to

**Figure 7.** Time-density (mean  $\pm$  sd) curve for the pituitary gland and brain in 10 dogs with an enlarged pituitary gland and a pituitary flush ( $\bullet$ ), 17 dogs with an enlarged pituitary gland and no pituitary flush ( $\circ$ ), and 26 dogs with a normal-sized pituitary gland and a pituitary flush ( $\Delta$ ). Y axis is labelled in Hounsfield Units (HU). At maximal contrast enhancement of the arterial cerebral circle (time 0), the normal-sized pituitary glands with a pituitary flush were significantly more contrast enhanced than the enlarged pituitary glands without a flush ( $*p < 0.05$  between group ( $\Delta$ ) and ( $\circ$ ). UE = unenhanced.



0.67) and in 2 dogs no pituitary enlargement was observed.

In 13 of the 19 dogs, CT findings agreed with surgical findings and in these dogs variable amounts of mucoïd greyish pituitary tissue was encountered during surgery. Histological examination identified adenomatous adenohypophyseal tissue together with unaffected adenohypophysis, pars intermedia, and neurohypophysis. In 6 of these 13 dogs, small pieces of white tissue, resembling normal adenohypophyseal tissue, were collected separately but histological examination disclosed adenomatous adenohypophyseal tissue. In 1 of the 13 dogs, a solid mass was found in addition to the mucoïd adenoma. This mass was histopathologically diagnosed as cystadenomatous hyperplasia of the craniopharyngeal duct.

In 6 of the 19 dogs, the CT findings agreed less well with the surgical findings. Before removal of the adenoma in 3 dogs, a small, white, rather consistent part of the ventral anterior pituitary gland was encountered. On histological examination, this material proved to be unaffected adenohypophyseal tissue. After removal of the adenoma in the other 3 dogs, a well-circumscribed neurointermediate lobe came into view and small samples taken from this lobe were found on histological examination to contain neurohypophyseal tissue. Neither the location of the unaffected anterior pituitary gland nor the neurointermediate lobe had been visualized on dynamic CT images in these dogs.

### **Relation between CT findings on the spatial series and the dynamic series of scans**

In the 28 dogs with normal sized pituitary glands, the pituitary glands were uniformly enhanced on images of the spatial series of scans in 20 dogs, diffusely but irregularly enhanced in 4 dogs, and in 4 dogs a poorly defined localized area of hypoattenuation was present within the enhanced pituitary gland (Table 2). In 2 of these last 4 dogs, the area of hypoattenuation corresponded to the area of an adenoma on the dynamic images.

In 27 dogs with an enlarged pituitary gland, the pituitary gland was uniformly enhanced on images of the spatial series of scans in 16 dogs, diffusely but irregularly enhanced in 3 dogs, and in 8 dogs a poorly defined localized area of hypoattenuation was present within the enhanced pituitary gland (Table 2). In 4 of these last 8 dogs, the area of hypoattenuation corresponded to the results of dynamic scans, but only in 2 dogs did the area of hypoattenuation corresponded to the area of an adenoma.

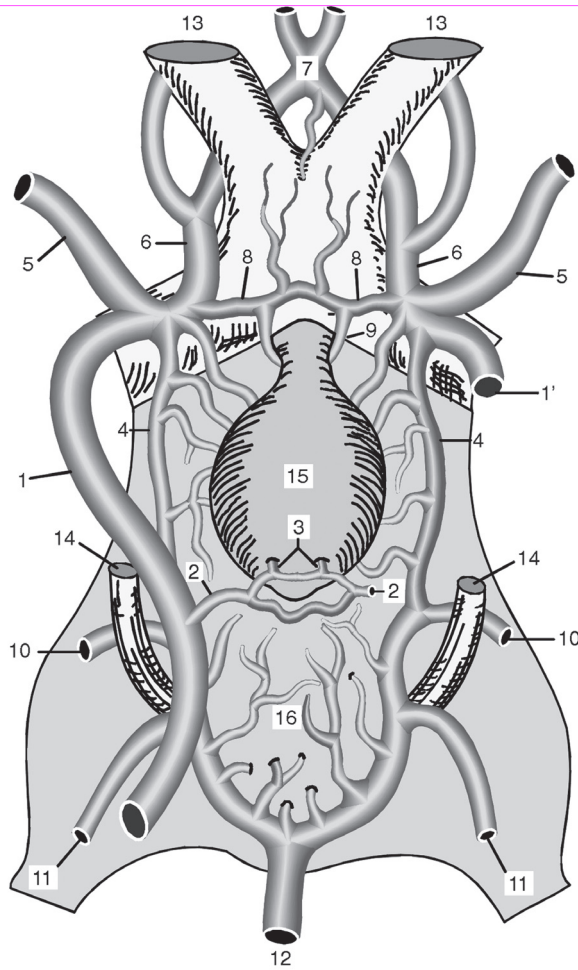


**Figure 8.** Ventral view of the arterial vascularization of the canine pituitary gland after complete removal of the dura mater (16).

1 = Right internal carotid a. in cavernous sinus (not shown)

1' = Left internal carotid a.

2 = Caudal intercarotid a.

3 = Caudal hypophyseal a.

4 = Caudal communicating a.

5 = Middle cerebral a.

6 = Rostral cerebral a.

7 = Rostral communicating a.

8 = Rostral intercarotid a.

9 = Rostral hypophyseal a.

10 = Caudal cerebral a.

11 = Rostral cerebellar a.

12 = Basilar a.

13 = Optic nerve

14 = Oculomotor nerve

15 = Pituitary gland

16 = Position of dorsum sellae (not shown)

## Discussion

CT has been used in normal dogs<sup>6,13</sup> and in dogs with PDH<sup>7,21</sup> to assess the size of the pituitary gland. An increase in the height of the pituitary gland (i.e. a dorsal extension into the suprasellar region) is the first sign of pituitary enlargement due to corticotropic tumor.<sup>21</sup> The size of the pituitary glands of normal dogs varies among different breeds and among individual dogs of the same breed, but varies less than the body weight.<sup>23</sup> Therefore, pituitary height was not related to body size but to the size of the cranium. The P/B ratio provides a valuable tool for the distinction between enlarged and normal sized pituitary glands.<sup>21</sup> The large percentage of enlarged pituitary glands in our dogs (53 %) seems to disagree with the findings of others that PDH in dogs most often is caused by a microadenoma.<sup>24,25</sup> Also, in humans the majority of ACTH-producing pituitary adenomas are microadenomas.<sup>26</sup> It may merely be a matter of definition. Both in humans<sup>26,27</sup> and dogs,<sup>28,29</sup> adenomas 10 mm in diameter have been designated microadenomas and adenomas >10 mm in diameter have been called macroadenomas. Because maximal height of the pituitary glands in our dogs was 10 mm (used as an inclusion criterium), all adenomas would have been classified microadenomas by definition. In dogs however, the P/B ratio allows for detection of even the smallest increase in height of the pituitary gland<sup>21</sup> and therefore it seems appropriate for dogs to adjust the definition of microadenomas to adenomas that do not affect the size or shape of the pituitary gland.

In humans, the results of conventional, contrast-enhanced CT of the pituitary gland for the detection of ACTH-producing tumors has been disappointing with a diagnostic accuracy varying between 39% and 63% in different reports.<sup>26,27</sup> Better results have been obtained with dynamic CT. Displacement or compression of the early enhanced secondary hypophyseal capillary bed (so called 'tuft sign') is considered an important feature in the diagnosis of pituitary microadenomas.<sup>12,30</sup>

In dogs, the pituitary gland has a more horizontal position than in humans, and its long axis is almost parallel to the ventral surface of the brain. The adenohypophysis (which consists of the pars tuberalis, the pars intermedia, and the pars distalis) extends as a collar around the neurohypophysis (which consists of the infundibulum and the lobus nervosus).<sup>23,31</sup> The vasculature of the canine pituitary gland is illustrated in Figure 8. The neurohypophysis receives direct arterial blood supply from the internal carotid artery, when still

in the cavernous sinus, by way of the caudal intercarotid artery and the caudal hypophyseal artery. The adenohypophysis is provided with blood from the portal vessels that originate from the primary blood capillary network in the median eminence. The primary blood capillary network is supplied by the mantle plexus and the rostral hypophyseal artery. The rostral hypophyseal artery is a branch from the rostral intercarotid artery which in turn branches off the internal carotid artery after its point of exit from the cavernous sinus. Thus, blood in the internal carotid artery reaches the hypophysis by 2 routes, by a short arterial route connecting directly with the neurohypophyseal capillary bed and by a longer route over the hypothalamus (the primary blood capillary network) and the portal vessels connecting with the secondary blood capillary network in the pars distalis of the adenohypophysis.<sup>23,32-37</sup> These separate blood flows explain the strong and early enhancement of the neurohypophysis and the subsequent centrifugal enhancement of the adenohypophysis during dynamic CT.<sup>15,17</sup> The early, strong enhancement of the neurohypophysis visible on a dynamic slice reflects an arterial phase whereas the slow, weak enhancement pattern visible during conventional CT enhancement reflects the secondary capillary phase. Although this 'pituitary flush' is a completely different phenomenon than the 'pituitary tuft' in humans, the diagnostic implications of absence, displacement or compression of the 'flush' may be similar.

It was found in the present study that normal-sized pituitary glands enhance more than enlarged pituitary glands. Also, the pituitary glands that show the flush sign enhance more than those that do not show the flush sign. The flush sign was more frequently present in normal-sized pituitary glands (26 of 28 dogs) than in enlarged pituitary glands (10 of 27 dogs). These findings may be explained by several factors. After the injection of contrast medium, the neurohypophysis displays an early and strong enhancement. In enlarged pituitary glands that showed a flush sign, the flush sign itself (i.e., the neurohypophysis) was not larger than the flush sign in normal-sized pituitary glands. The region of interest for density measurements was chosen by drawing a line around the pituitary borders. In enlarged pituitary glands, the same volume of contrast medium per kg body weight is distributed over more pituitary tissue volume than in normal-sized pituitary glands. Also, increased compression of the neurohypophysis by pituitary adenomatous tissue may result in displacement of the neurohypophysis or reduction of its volume. Consequently, the flush sign may be distorted, displaced, smaller or absent. These factors may contribute to a lower enhancement in enlarged pituitary glands than in normal-sized pituitary

glands and more enhancement in the pituitary glands that show the flush sign than in those without the flush sign.

In some dogs, dynamic CT findings did not correspond to surgical findings, histological findings or both. In dynamic CT, only one single 2-mm thick slice was examined and therefore small adenomas may have been outside the scan plane. In 9 dogs with normal-appearing pituitary glands on dynamic CT, the neurohypophysis came into view during surgery after removal of the adenohypophysis. The neurointermediate lobe was found to be positioned close to the dorsum sellae. This observation indicates that in these dogs during dynamic CT the neurohypophysis was probably in the scan slice, which usually was the most caudal slice just rostral to the dorsum sellae. Therefore it seems advisable that if the pituitary flush is present and not displaced, the dynamic CT examination should be repeated more rostrally because this part of the pituitary gland may contain a microadenoma.

In 6 of 24 dogs with a displaced pituitary flush, the suspicion of a localized adenoma by dynamic CT could not be confirmed during surgery. This finding indicates that for selective adenomectomy careful presurgical localization of the adenoma is not the only prerequisite. For selective adenomectomy to be successful, the adenoma site found by dynamic CT also must be recognized during surgery, as was the case in 18 dogs in the present study. The adenoma must then be isolated from the remainder of the pituitary gland, which was only possible in 9 of these 18 dogs. In the other 9 dogs it was not possible to differentiate between the adenoma and the unaffected adenohypophyseal tissue during surgery. Finally, selective adenomectomy is successful if the remainder of the pituitary gland consists of unaffected adenohypophyseal tissue. However, this was only the case in 4 dogs. On the basis of these observations, it appears that currently selective adenomectomy is only rarely an option in transsphenoidal surgery in dogs with PDH.

If separate removal of the adenohypophysis had been the aim of transsphenoidal surgery in this study, it would have been possible in 24 of the 55 dogs on the basis of the CT findings. However, in only 18 dogs did the CT findings agree with the surgical findings. In addition, in only 8 of the 18 dogs the remainder of the pituitary gland, corresponding to the pituitary flush, was free of adenomatous tissue. Thus, separate removal of the adenohypophysis also seems to be restricted to a small number of dogs with PDH.

In the dogs of this study, conventional contrast-enhanced CT of the pituitary gland was abnormal in 29 of 55 cases. The pituitary gland was enlarged

in 27 dogs and in 2 dogs with normal-sized pituitary glands a poorly defined local area of hypoattenuation was observed that corresponded to the area of an adenoma on dynamic CT, which was confirmed by the findings of surgery and histological examination.

In this study, in 45 of 55 dogs (82%) with PDH the pituitary gland appeared to be abnormal using dynamic CT. In 10 of 55 dogs (18%) the finding of a normal-sized pituitary gland coincided with the finding of a non-displaced pituitary flush and these dogs could not be distinguished from normal dogs on the basis of the CT findings. Nevertheless, the dynamic CT results in dogs seem to be slightly better than the results of dynamic CT in humans, in which the pituitary gland appeared to be normal in 39 of 85 patients (46%) with microadenomas.<sup>12</sup>

It is concluded that when a displaced pituitary flush is observed during dynamic CT separate removal of the adenohypophysis is an option if the neurointermediate lobe can be identified during surgery, but even then adenomatous tissue may be left behind. In dogs with a displaced pituitary flush but no definable neurointermediate lobe during surgery, as well as in dogs with a normal pituitary flush pattern or no pituitary flush at all, the results of this study indicate that hypophysectomy should be performed.

The results of this study demonstrate that dynamic CT provides very useful information in addition to conventional contrast-enhanced CT. CT of the pituitary gland in dogs with PDH should include a spatial and a dynamic series of scans. The spatial series allows for precise localization of the pituitary gland in relation to the surgical landmarks<sup>6</sup> and assessment of the size of the pituitary gland whereas the dynamic series allows identification of an adenoma (pituitary flush displaced) or a diffusely abnormal pituitary gland (no pituitary flush).

1 Domitor, Smith KlineBeecham Animal Health BV, Zoetermeer The Netherlands

2 Diprivan-10, Zeneca BV, Ridderkerk, The Netherlands

3 Forene, Abbott Laboratories BV, Maarssen, The Netherlands

4 Tomoscan CX/S, Philips NV, Eindhoven, The Netherlands

5 Telebrix 350, Guerbet Nederland BV, Gorinchem, The Netherlands

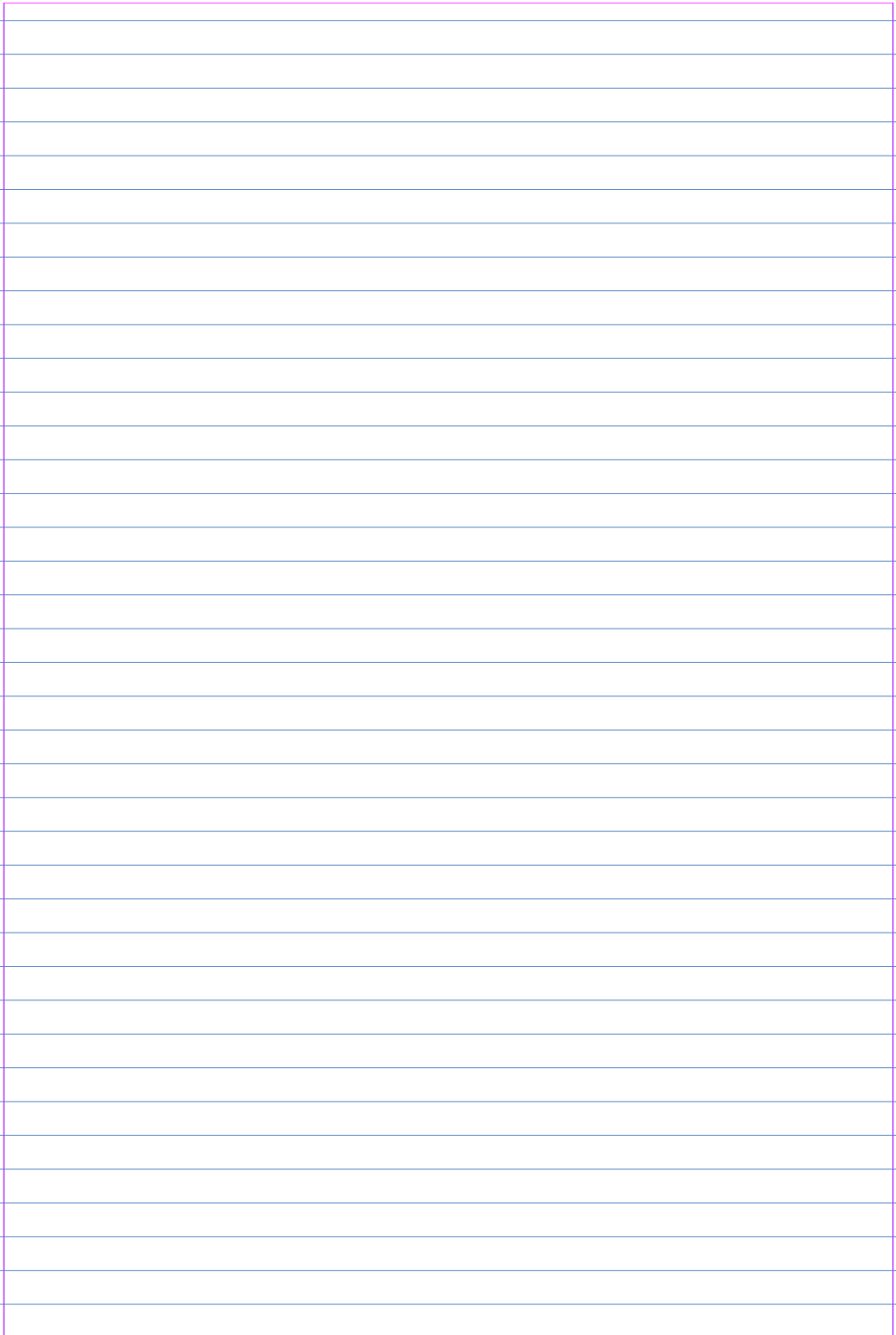
## References

1. Melby JC. Therapy of Cushing disease: a consensus for pituitary microsurgery. *Annals Int Med* 1988;109:445-446.
2. Thorner MO, Vance ML, Horvath E, Kovacs K. Dynamic tests of pituitary function. In: Wilson JD, Foster DW, eds. *Williams Textbook of Endocrinology*. Philadelphia: WB Saunders Co, 1992:246-260.
3. Horsley V. Functional nervous disorders due to loss of thyroid gland and pituitary body. *The Lancet* 1886;1:5.
4. Crowe SJ, Cushing H, Homans J. Experimental hypophysectomy. *Bull Johns Hopkins Hosp* 1910;21:127-169.
5. Aschner B. Über die Funktion der Hypophyse. *Pflüger's Archiv für die Gesamte Physiologie des Menschen und der Tiere* 1912;146:1-146.
6. Meij BP, Voorhout G, Van den Ingh TSGAM, Hazewinkel HAW, Van 't Verlaat JW. Transsphenoidal hypophysectomy in beagle dogs: evaluation of a microsurgical technique. *Vet Surg* 1997;26:295-309.
7. Meij BP, Voorhout G, Van den Ingh TSGAM, Hazewinkel HAW, Teske E, Rijnberk A. Results of transsphenoidal hypophysectomy in 52 dogs with pituitary-dependent hyperadrenocorticism. *Vet Surg* 1998;27:246-261.
8. Davis PC, Hoffman JC, Tindall GT, Braun IE. CT-surgical correlation in pituitary adenomas: evaluation in 113 patients. *Am J Neuroradiol* 1985;6:711-716.
9. Davis PC, Hoffman JC, Spencer T, Tindall GT, Braun IE. MR imaging of pituitary microadenomas: CT, clinical and surgical correlation. *Am J Neuroradiol* 1987;8:107-112.
10. Gardeur D, Naidich TP, Metzger J. CT analysis of intrasellar pituitary adenomas with emphasis on patterns of contrast enhancement. *Neuroradiol* 1981;20:241-247.
11. Hasegawa T, Ito H, Shoin K, Kogure Y, Kubota T, Yamamoto S. Diagnosis of an 'isodense' pituitary microadenoma by dynamic CT scanning. *J Neurosurg* 1984;60:424-427.
12. Bonneville JF, Cattin F, Moussa-Bacha K, Portha C. Dynamic computed tomography of the pituitary gland: the 'tuft sign'. *Radiology* 1983;149:145-148.
13. Voorhout G. Cisternography combined with linear tomography for the visualization of the pituitary gland in healthy dogs: a comparison with computed tomography. *Vet Radiol* 1990;31:68-73.

14. Voorhout G, Stolp R, Lubberink AAME, Van Waes PFGM. Computed tomography in the diagnosis of canine hyperadrenocorticism not suppressible by dexamethasone. *J Am vet Med Assoc* 1988;192:641-646.
15. Love NE, Fisher P, Hudson L. The computed tomographic enhancement pattern of the normal canine pituitary gland. *Vet Radiol US* 2000; 41:507-510.
16. Meij BP. Hypophysectomy as a treatment for canine and feline Cushing's disease. *Vet Clin North Am Small Anim Pract* 2001;31:1015-1041.
17. Van der Vlugt-Meijer RH, Voorhout G, Meij BP. Imaging of the pituitary gland in dogs with pituitary-dependent hyperadrenocorticism. *Mol Cell Endocrinol* 2002;197:81-87.
18. Rijnberk A, Van Wees A, Mol JA. Assessment of two tests for the diagnosis of canine hyperadrenocorticism. *Vet Rec* 1988;122:178-180.
19. Stolp R, Rijnberk A, Meijer JC, Croughs RJM. Urinary corticoids in the diagnosis of canine hyperadrenocorticism. *Res Vet Sci* 1983;34:141-144.
20. Rijnberk A. Clinical endocrinology of dogs and cats. Dordrecht/Boston: Kluwer Academic Publishers; 1996;11-34.
21. Kooistra HS, Voorhout G, Mol JA, Rijnberk A. Correlation between impairment of glucocorticoid feedback and the size of the pituitary gland in dogs with pituitary-dependent hyperadrenocorticism. *J Endocrinol* 1997;152:387-394.
22. Meij BP, Mol JA, van den Ingh TSGAM, Bevers MM, Hazewinkel HAW, Rijnberk A. Assessment of pituitary function after transsphenoidal hypophysectomy in beagle dogs. *Domest Anim Endocrinol* 1997;14:81-97.
23. Hullinger RL. The endocrine system. In: Evans HE, ed. *Miller's anatomy of the dog*. 3rd ed. Philadelphia: WB Saunders Co; 1993;559-585.
24. Peterson ME, Orth DN, Halmi NS, Zielinski AC, Davis DR, Chavez FT, Drucker WD. Plasma immunoreactive proopiomelanocortin peptides and cortisol in normal dogs and dogs with Addison's disease and Cushing's syndrome: basal concentrations. *Endocrinol* 1986;119:720-730.
25. Mauldin GN, Burke RL. The use of diagnostic computerized tomography and radiation therapy in canine and feline hyperadrenocorticism. *Problems in Veterinary Medicine* 1990;2:557-564.
26. Saris SC, Patronas NJ, Doppman JL, Loriaux DL, Cutler Jr GB, Nieman LK, Chrousos GP, Oldfield EH. Cushing syndrome: pituitary CT scanning. *Radiology* 1987;162:775-777.

27. Marcovitz S, Wee R, Chan J, Hardy J. The diagnostic accuracy of preoperative CT scanning in the evaluation of pituitary ACTH-secreting adenomas. *Am J Neuroradiol* 1987;8:641-644.
28. Nelson RW, Ihle SL, Feldman EC. Pituitary macroadenomas and macroadenocarcinomas in dogs treated with mitotane for pituitary-dependent hyperadrenocorticism: 13 cases (1981-1986). *J Am Vet Med Assoc* 1989;194:1612-1617.
29. Bertoy EH, Feldman EC, Nelson RW, Dublin AB, Reid MH, Feldman MS. One-year follow-up evaluation of magnetic resonance imaging of the brain in dogs with pituitary-dependent hyperadrenocorticism. *J Am Vet Med Assoc* 1996;208:1268-1273.
30. Bonneville JF, Cattin F, Dietemann JL. Dynamic CT of the pituitary gland. In: *Computed tomography of the pituitary gland*. Berlin: Springer Verlag; 1986;33-46.
31. Eigenmann JE, Lubberink AAME. The pituitary. In: Slatter DH, ed. *Textbook of Small Animal Surgery*. Philadelphia: WB Saunders Co; 1985;1840-1851.
32. Dandy WE, Goetsch E. The blood supply of the pituitary body. *Am J Anat* 1911;11:137-150.
33. Green JD. The comparative anatomy of the portal vascular system and of the innervation of the hypophysis. In: Harris GW, Donovan BT, eds. *The Pituitary Gland*, volume 1. London: Butterworths; 1966;127-146.
34. Lecrecq TA, Grisoli F. Arterial blood supply of the normal human pituitary gland. *J Neurosurg* 1983;58:678-681.
35. Page RB. Pituitary blood flow. *Am J Physiol* 1982;243:E427-E442.
36. Gorczyca W, Hardy J. Arterial supply of the human anterior pituitary gland. *Neurosurgery* 1987;20:369-378.
37. Szentagothai JB, Flerko B, Mess B, Halasz B. Hypothalamic control of the anterior pituitary. Budapest: Akadémiai Kiadó; 1968;86-95.

## DIAGNOSTIC IMAGING OF THE PITUITARY GLAND IN DOGS



A large, empty rectangular box with a purple border, occupying the majority of the page below the title. This box is likely intended for a student to draw a diagram or insert an image related to the diagnostic imaging of the pituitary gland in dogs.

# CHAPTER 5

## **Dynamic helical computed tomography of the pituitary gland in healthy dogs**

Roselinda H. van der Vlugt-Meijer<sup>1</sup>, Björn P. Meij<sup>2</sup>, George Voorhout<sup>1</sup>.

**Veterinary Radiology and Ultrasound, accepted 2006**

Division of Diagnostic Imaging<sup>1</sup> and Department of Clinical Sciences of Companion Animals<sup>2</sup>, Faculty of Veterinary Medicine, Utrecht University, The Netherlands

## Abstract

Dynamic helical CT of the pituitary gland can be used to image the three-dimensional shape and dimensions of abnormalities within the pituitary gland. The aim of this study was to develop a protocol for dynamic helical CT of the pituitary gland in healthy dogs as a future reference study for patients with pituitary disease.

Dynamic helical series of 9 scans of the pituitary gland during and following contrast medium injection were performed in 6 healthy dogs using the following protocols: a series with 1 mm collimation and a table feed per x-ray tube rotation of 2 mm (pitch of 2) in 6 dogs, a series with 2 mm collimation and pitch of 2 in 3 dogs, and a series with 1 mm collimation and pitch of 1 in 3 other dogs. Multiplanar reconstructions of the images were made using a reconstruction index of 0.5. Images of all series were assessed visually for enhancement of the arteries, the neurohypophysis, and the adenohypophysis. The enhancement pattern of the neurohypophysis was distinguished adequately from that of the adenohypophysis in 5 dogs that were scanned with 1 mm collimation and pitch of 2, but the difference was less discernable when the other protocols were used. The carotid artery, its trifurcation, and the arterial cerebral circle were best visualized in dorsal reconstructions. Dynamic helical CT of the pituitary gland in healthy dogs can be performed with 1 mm collimation and pitch of 2, and a scan length that includes the entire pituitary region. Using this protocol, with the specific scanner used, the neurohypophysis, the adenohypophysis, and the surrounding vascular structures are adequately visualised.

## Introduction

Computed tomography (CT) is a valuable tool to visualize the pituitary gland in dogs, and to assess the size of the gland in normal dogs and dogs with pituitary-dependent hyperadrenocorticism (PDH).<sup>1-3</sup> In addition, CT enables accurate assessment of the position of the pituitary gland relative to surgical landmarks when transsphenoidal hypophysectomy is performed in dogs with PDH.<sup>4,5</sup>

In approximately 40% of dogs with PDH, the size and shape of the pituitary gland is not changed.<sup>1</sup> Usually conventional contrast enhanced CT of the pituitary gland is normal in these dogs since microadenomas may go undetected due to isoattenuation.<sup>1,6</sup> With dynamic CT of the pituitary gland, however, the neurohypophysis can be differentiated from the adenohypophysis due to early arterial, enhancement.<sup>7,8</sup> Displacement or distortion of this neurohypophyseal flush may be useful for indirect assessment of the location of the microadenoma.<sup>6,9</sup>

Dynamic CT findings may not always correlate with surgical and/or histologic findings in dogs with PDH that underwent transsphenoidal hypophysectomy.<sup>9</sup> Dynamic CT using a conventional CT scanner only allows for one single slice through the pituitary gland. Therefore, in dogs with a normal dynamic CT examination, the microadenoma may have been outside the scan plane. If a neurohypophyseal flush was not detected, the neurohypophysis may have been displaced rostral or caudal to the scan plane, or the neurohypophysis may have been too small to detect. When the adenoma was detected in the scan plane no information was available about the rostral or caudal extension of the adenoma. From our previous studies it was concluded that for accurate pre-surgical localization of the adenoma, a dynamic CT examination of the entire pituitary gland should be performed.<sup>6,9</sup>

Since the introduction of the slip-ring interfaces in gantry constructions, interscan intervals have decreased and volume-acquisition scanning is possible.<sup>10-13</sup> Helical CT enables scanning of a complete organ during the time of maximal enhancement after intravenous administration of contrast medium.<sup>10,12-14</sup> Furthermore, the volume of CT data can be reprocessed with different slice positions and indices (distance between the slices).<sup>15</sup>

The aim of the present study was 1) to develop a protocol for dynamic helical CT examination of the pituitary gland in healthy dogs as a reference for studies in patients with pituitary disease and, 2) to assess the enhancement pattern of the pituitary gland and the surrounding vasculature during dynamic helical CT.

## Materials and Methods

### Dogs

Six healthy dogs (3 intact males, 1 neutered male, and 2 intact females) were studied. Dogs were obtained from the Department of Clinical Sciences of Companion Animals of the Utrecht University. The dogs were used for teaching students in clinical diagnostics and for minor non-invasive studies. The experimental protocols were approved by the Ethical Committee of the Utrecht University. The dogs (3 Beagles and 3 crossbreed dogs) were 1.9 to 8.3 years old (mean 5.4 years). Body weight (BW) varied from 11 to 24 kg (mean 17 kg). Pituitary function was normal as determined by pituitary hormone responses of plasma adrenocorticotropin, growth hormone, luteinizing hormone and prolactin to the combined intravenous injection of corticotropin-releasing hormone, growth hormone-releasing hormone, gonadotropin-releasing hormone and thyrotropin-releasing hormone, respectively.<sup>16</sup>

### Anesthesia

CT examinations were performed under anesthesia. Food was withheld from the dogs for 18 hours prior to CT. Following intravenous premedication with medetomidine (50 µg/kg BW; Domitor, SmithKline Beecham Animal Health BV, Zoetermeer, The Netherlands), anesthesia was induced and maintained by the intravenous administration of propofol (1-2 mg/kg BW; Diprivan-10, Zenaca BV, Ridderkerk, The Netherlands) while the dogs were breathing spontaneously.

Dog	CT series 1			CT series 2		
	Length (mm)	Collimation (mm)	Pitch	Length (mm)	Collimation (mm)	Pitch
1	10	1	2	16	2	2
2	10	1	2	16	2	2
3	10	1	2	16	2	2
4	10	1	2	6	1	1
5	10	1	2	6	1	1
6	10	1	2	6	1	1

**Table 1.** Dynamic helical CT protocols in 6 healthy dogs.

## Computed Tomography

CT was performed with a single slice helical CT-scanner (Somatom AR star, Siemens AG, Germany). While in sternal recumbency, transverse helical scans of the brain were performed over a length of 60 mm, perpendicular to the skull base, using 63 mA, 110 kV, and 1.9 sec scanning time per rotation. The helical scan was performed with a collimation (slice thickness) of 3 mm and a table feed of 3 mm for each x-ray tube rotation (pitch of 1). Images were reconstructed with a reconstruction index of 1 (3 mm thick consecutive slices) and a 90 mm field of view. From these images the rostral end (tuberculum sellae) and the caudal end (dorsum sellae) of the pituitary fossa were identified. Two series of nine dynamic helical scans were performed in each dog (Table 1): one scan before and eight scans during and following the intravenous bolus injection of 2 ml of contrast medium per kg of body weight (Telebrix 350, sodium and meglumine ioxothalamate containing 350 mg iodine/ml, Guerbet Nederland BV, Gorinchem, The Netherlands). Series were performed with 110 kV, 63 mA and 1.5 sec scanning time per rotation. Mean interscan interval ranged from 16-26 sec. The first dynamic helical series of scans, covering 10 mm length of the pituitary region, was performed using a collimation of 1 mm and a table feed of 2 mm for each x-ray tube rotation (pitch of 2). In 3 dogs, the second dynamic helical series of scans was performed with a collimation of 2 mm and a table feed of 4 mm for each x-ray tube rotation (pitch of 2) over a length of 16 mm, including the pituitary gland and the vasculature surrounding the pituitary gland. In the other 3 dogs, the second dynamic helical series of scans was performed with a collimation of 1 mm and a table feed of 1 mm for each x-ray tube rotation (pitch of 1) over a length of 6 mm including the pituitary gland. All helical scans were made from rostral to caudal. The images that were generated from the dynamic helical series were reconstructed with a reconstruction index of 0.5 (0.5 or 1 mm overlapping 1- or 2-mm-thick slices) and a 90 mm field of view. In addition, sagittal and dorsal multiplanar reconstructions were created.

## Analysis

The helical CT images of the pituitary gland were assessed by one observer. The observer was aware of the imaging protocol. The contrast enhancement pattern of the pituitary on the dynamic series was assessed visually using different window settings. The images were initially assessed at window level of 80 HU and window width of 250 HU and were then adjusted to enhance the structures of interest.

Image quality was assessed subjectively as follows: 1) based upon the delineation of the structures of interest, i.e., the pituitary gland and the bony landmarks, and 2) based upon the enhancement of the arteries, the neurohypophysis and the adenohypophysis. Enhancement was subjectively categorized as strong, weak, or no enhancement (Table 2). The image quality was considered good if there was distinct and separate enhancement of the arteries, the neurohypophysis, and the adenohypophysis. For all series in all dogs x-ray attenuation was measured within a region of interest surrounding the entire pituitary gland on a transverse image containing the largest cross-section of the pituitary gland at the time of maximum enhancement of the neurohypophysis and at a time point two series later. Mean enhancement per time per imaging protocol was calculated and displayed in a graph.

The dynamic transverse and reconstructed dorsal and sagittal images were viewed for the location and shape of the neurohypophyseal flush and for the difference in time between enhancement of the neurohypophysis and adenohypophysis.<sup>7</sup>

The transverse and reconstructed dorsal images were assessed for the presence and shape of the arteries of the arterial cerebral circle and surrounding vessels. Sketches of the enhanced arteries were derived from several dorsal reconstructed images per series. After that, arteries were identified according to these sketches.

## Results

The enhancement of the arterial cerebral circle and the neurohypophysis, when visible, was weak in 2, and strong in 4 of the 6 dynamic helical series with 1 mm collimation and pitch of 2 (Table 2). The neurohypophyseal flush was identified from rostral to caudal allowing differentiation between the enhancement pattern of the neurohypophysis (Figure 1) and the adenohypophysis (Figure 2) in 5 dogs. In the sixth dog the center of the pituitary was hypoattenuating and no neurohypophyseal flush was seen (Figure 3).

In the second dynamic series there was more intense enhancement of the pituitary gland than in the first dynamic series in all 6 dogs (Figure 4). However, the distinction between enhancement of the neurohypophysis and adenohypophysis was less clear on the dynamic series with 2 mm collimation and pitch of 2 than on the first dynamic series with 1 mm collimation and pitch of 2 (Table 2). Enhancement was less conspicuous on the second dynamic series with 1 mm collimation and pitch of 1. Also, the rostral part of the arterial cerebral circle and the pituitary stalk were not visualised on the dynamic series with 1 mm collimation and pitch of 1.

The arterial cerebral circle was best visualized on the dorsal reconstructed images (Figure 5) as compared to the transverse images, but not all arteries that branch from the arterial cerebral circle were identified in every dog (Table 3). The caudal communicating arteries were usually easily identified, but the rostral and caudal intercarotid arteries were more difficult to detect. In dorsal reconstructions the internal carotid artery and its trifurcation were visible in all dogs. In 2 dogs, an additional vessel was identified on transverse images, located between the caudal communicating artery and the intracavernous part of the carotid artery (Figure 6). On dorsal MPRs this vessel seemed to branch from the carotid artery ventral to the trifurcation.

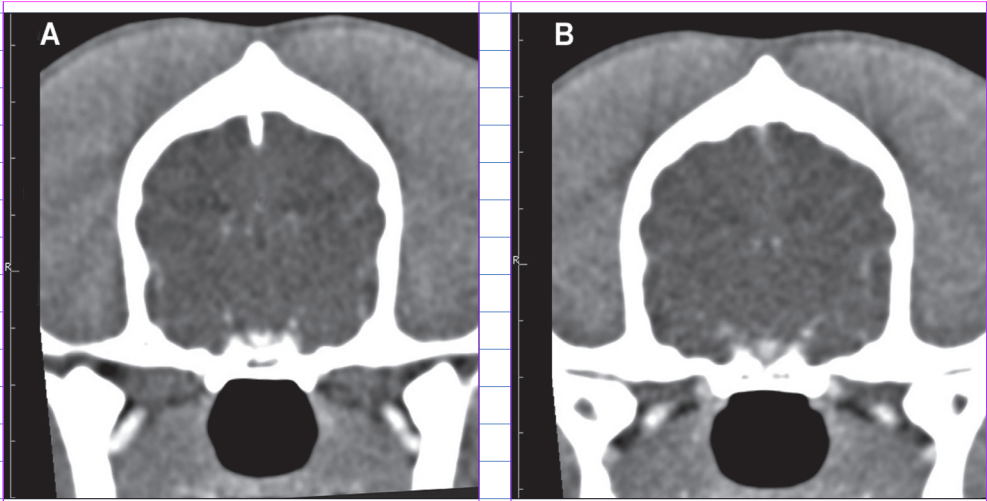


**Figure 1.** 1-mm-thick transverse dynamic (7 sec time frame) helical CT images of the pituitary gland in a healthy 8-year-old crossbreed dog. Note the enhancement of the neurohypophysis rostrally (A) and centrally (B). The neurohypophyseal flush is visible around the infundibular process at the rostral image (A) and is triangular shaped in the center of the pituitary (B).

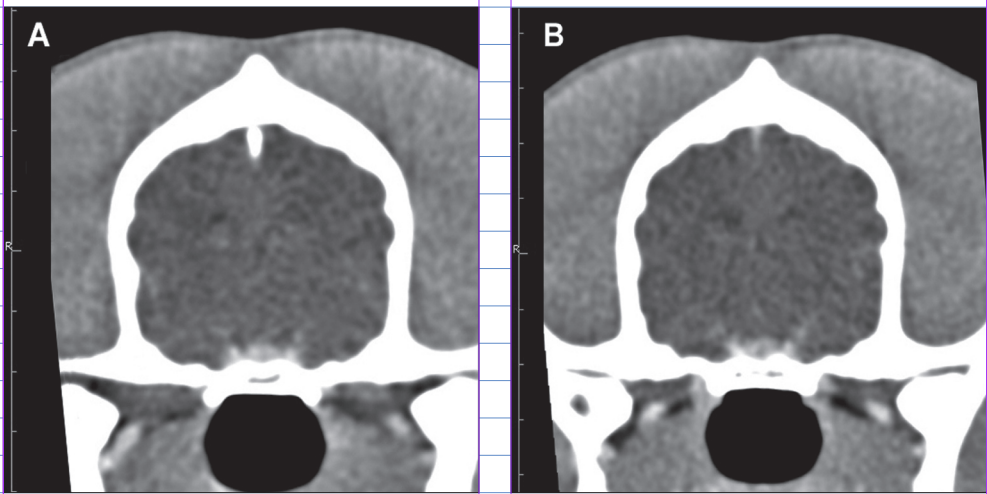


**Figure 2.** 1-mm-thick transverse dynamic helical CT images of the pituitary gland in the same dog as in Figure 1. Note the enhancement of the adenohypophysis rostrally (A) and centrally (B).

CT series	Structure	Enhancement #					
		Dog 1	Dog 2	Dog 3	Dog 4	Dog 5	Dog 6
Collimation 1 Pitch 2	Arteries	+	+	±	±	+	+
	Neurohypophysis	+	+	±	±	+	-
	Adenohypophysis	+	+	+	±	+	±
Collimation 2 Pitch 2	Pituitary gland	+	+	+	±	+	+
	Arteries	-	+	+			
	Neurohypophysis	±	±	±			
Collimation 1 Pitch 1	Adenohypophysis	±	±	±			
	Pituitary gland	+	+	+			
	Arteries				+	+	+
Collimation 1 Pitch 1	Neurohypophysis				±	±	-
	Adenohypophysis				±	±	±
	Pituitary gland				+	+	+

**Table 2.** Assessment of the enhancement of the pituitary gland and arteries during dynamic helical CT in 6 healthy dogs.

#Enhancement: + = strong and separate enhancement; ± = weak enhancement, not separate from the enhancement of other structures; - = no separate enhancement.

Vascular structure	Visualization*					
	Dog 1	Dog 2	Dog 3	Dog 4	Dog 5	Dog 6
Carotid artery	+	+	+	+	+	+
Trifurcation	+	+	+	+	+	+
Right caudal communicating artery	+	-	+	+	+	+
Left caudal communicating artery	+	+	+	+	+	+
Rostral intercarotid artery	+	±	-	-	-	+
Caudal intercarotid artery	-	+	-	±	-	-
Additional vessel	+	+	-	-	-	-

**Table 3.** Visualization of the arteries with dynamic helical CT in 6 healthy dogs. The arteries were identified on sketches of the dorsal reconstructed images, except for the additional vessel which was identified on the transverse reconstructed images.

\*Visualization: + = completely visualised; ± = partially visualised; - = not visualised.

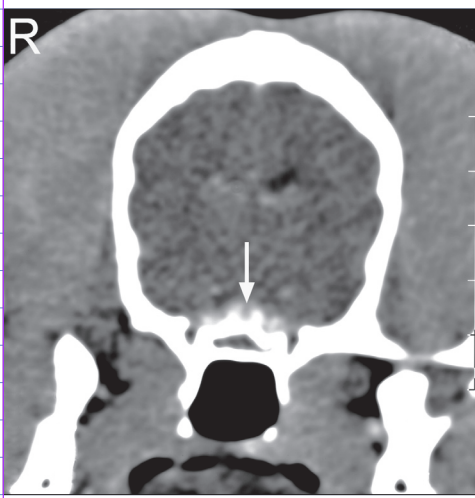


**Figure 3.** 1-mm-thick transverse dynamic helical CT image of the pituitary gland in a healthy 3-year-old female crossbreed dog. Note the hypodense central region (arrow) in the pituitary gland.

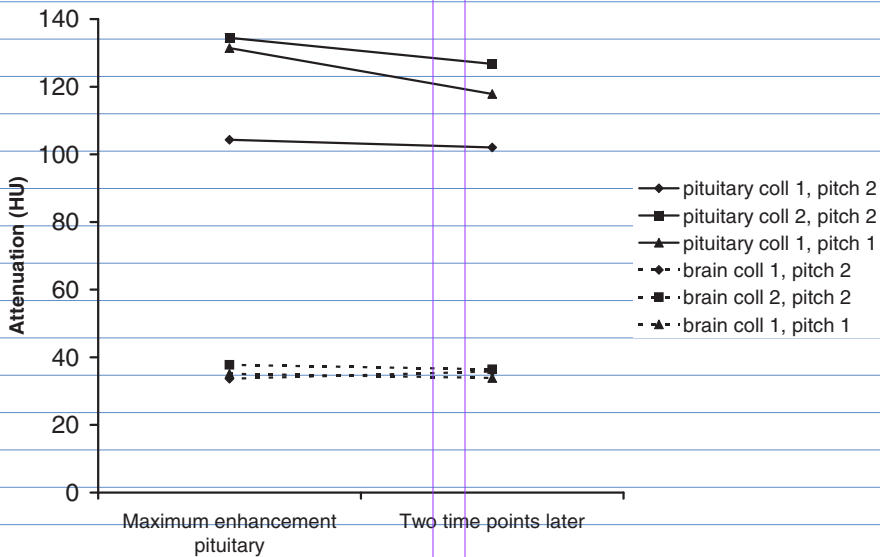


**Figure 4.** Mean attenuation of the pituitary gland and brain per dynamic helical CT protocol at the time point of maximum enhancement of the pituitary gland (1) and at a time point two series later

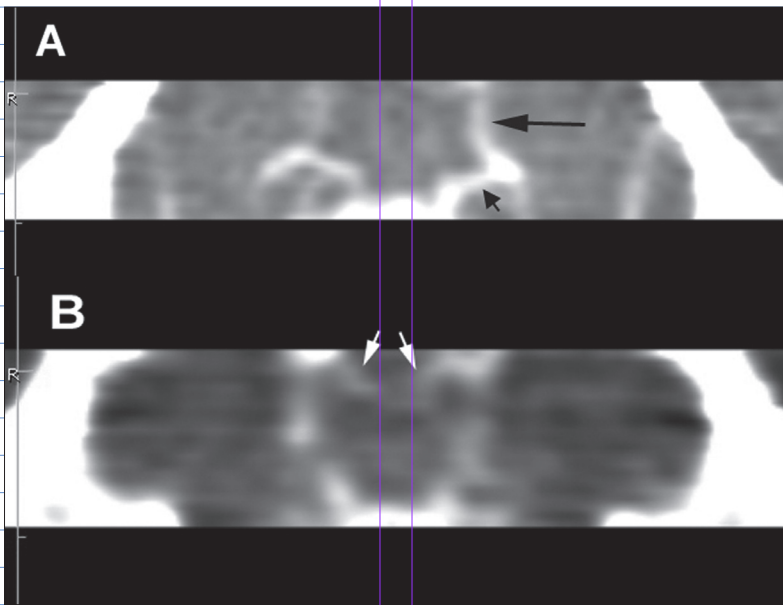


**Figure 5.** Dorsal reconstruction of transverse CT images of the skull at the level of the arterial cerebral circle on the dorsal margin of the pituitary gland in a healthy 8-year-old crossbreed dog (A) and a healthy 8-year-old Beagle (B). In figure A note the caudal communicating artery (large arrow), and the caudal cerebral artery (small arrow). In figure B note the left and right cranial intercarotid arteries (arrows) that give rise to the rostral hypophyseal arteries.

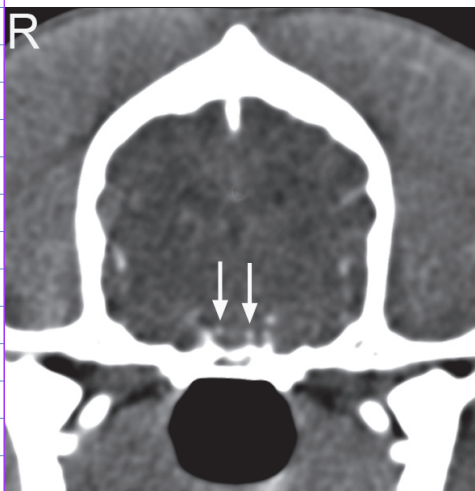


**Figure 6.** 1-mm-thick transverse dynamic helical CT image of the pituitary gland in a healthy 8-year-old crossbreed dog. Note the enhancement of the arteries. An additional vessel (arrows) is visible located between the caudal communicating artery and the intracavernous part of the carotid artery.

## Discussion

Performing dynamic CT of the entire pituitary gland with conventional single-slice dynamic CT is too time-consuming and would require excessive contrast medium. Dynamic helical CT of the entire pituitary gland can be performed in 7 sec with a mean interscan interval of 18 sec. In this study the protocol with a collimation of 1 mm and a table feed of 2 mm per x-ray tube rotation (pitch of 2) resulted in adequate visualization of the neurohypophysis, the adenohypophysis, and the surrounding vasculature of the pituitary gland.

In 5 of 6 dogs, a similar enhancement pattern was observed with dynamic helical CT as with single-slice dynamic CT that was used in previous studies.<sup>7,8</sup> In the dog in which no distinction between the early-enhancing neurohypophysis and the later-enhancing adenohypophysis was observed, a hypoattenuating area was present in the center of the pituitary gland which obscured the difference in enhancement between the neurohypophysis and adenohypophysis. This region may be caused by a deeply invaginating infundibular recess.

During the second dynamic series the pituitary gland seemed to enhance more than during the first dynamic series but the difference between the enhancement of the neurohypophysis and adenohypophysis was smaller. This may be explained by the cumulative effect of the contrast medium in the second dynamic series.

Because of the continuous table movement in dynamic helical CT, the real slice-thickness is not equal to the thickness of the x-ray beam (or collimation), but depends on the pitch and the reconstruction algorithms.<sup>17</sup> The choice of collimation for helical scanning is based on the goal of the scan. With single-slice dynamic CT of the canine pituitary gland, the slice-thickness was 2 mm and adenomas outside the scan plane or adenomas smaller than 2 mm may have been missed.<sup>9</sup> The distinction between the enhancement of the neurohypophysis and that of the adenohypophysis was less clear on the dynamic helical series with a collimation of 2 mm than on those with a collimation of 1 mm when the same pitch (pitch of 2) was used. However, as mentioned before, this may be caused by the fact that when a pitch of 1 was used the pituitary gland was already enhanced.

In dynamic helical CT, the speed of the table is an important variable which is represented by the pitch, i.e., the ratio between the table feed per

rotation and the collimation.<sup>10-13,17</sup> When a higher pitch is used, a longer area can be scanned in the same time period, but the effective slice thickness increases and the image quality decreases. The pitch can be increased up to 2 without significantly compromising image quality.<sup>17</sup> In the present study, the images produced with a pitch of 1 were not superior in quality in comparison with the images produced with a pitch of 2.

Using the CT scanner in the present study, the dynamic helical series of scans, covering the entire pituitary region over a length of 10 mm and produced with a collimation of 1 mm and pitch of 2, is a suitable protocol for dynamic imaging of the pituitary gland and its surrounding vasculature. The protocol that is recommended is specific to the scanner that was used. The quality of the images may be further improved by small modifications. For example, the mAs used in this protocol was restricted by the x-ray tube capacity. When the mA was increased, the x-ray tube became overheated and the interscan interval increased rapidly. This can be solved by making fewer scans in the dynamic series. The difference between the enhancement pattern of the neurohypophysis and the adenohypophysis was often observed during the first 6 scans. Therefore, by reducing the number of scans in the dynamic series, the mA can be increased which may improve the resolution of the images.

Helical CT produces high-quality multiplanar reformatted images, especially when overlapping reconstruction indices (of half the slice thickness) and small collimations are used.<sup>10,15,18</sup> The dorsal reconstructed images gave more detail regarding vascular anatomy surrounding the pituitary gland. In this study not all the vessels of the arterial cerebral circle were detected. The caudal communicating arteries were more easily detected than the rostral and caudal intercarotid arteries. A number of factors may influence vessel conspicuity, such as size, flow rate, and the position of the vessel near other highly attenuating structures.<sup>19</sup> In two dogs, an additional vessel was observed between the intracavernous part of the internal carotid artery and the arterial cerebral circle that appeared to branch from the carotid artery just ventral to the trifurcation. This vessel may be the middle hypophyseal artery, which has occasionally been described in humans and is reported to branch from the carotid artery just ventral to the division in the rostral and medial cerebral arteries. The vessel courses closely on the anterior side of the pituitary stalk and in humans the vessel is one of the arteries of the neurohypophysis.<sup>20</sup>

It is concluded that in healthy dogs, using the CT scanner in the present study, the dynamic helical series of scans produced with a collimation of 1 mm and a table feed of 2 mm per x-ray tube rotation (pitch of 2) is the best protocol for dynamic imaging of the pituitary gland and its surrounding vasculature. The quality of the images may be further improved by small modifications. Dynamic helical CT may give information about the rostrocaudal enhancement pattern of the pituitary gland and the surrounding vessels. Considering the size of microadenomas in dogs with PDH that do not change the size or shape of the pituitary gland, dynamic helical CT of the entire pituitary gland could be used for the detection of pituitary microadenomas in dogs. Selective adenomectomy, rather than hypophysectomy, may then be considered in dogs with PDH, when imaging reveals the size and localisation of the adenoma.

### **Acknowledgements**

The authors would like to thank Mr. T. Roding and colleagues for the opportunity to use the helical CT-scanner at the Hogeschool Haarlem. The technical assistance of Mr. G. Haalboom is highly appreciated.

## References

1. Kooistra HS, Voorhout G, Mol JA, Rijnberk A. Correlation between impairment of glucocorticoid feedback and the size of the pituitary gland in dogs with pituitary-dependent hyperadrenocorticism. *J Endocrinol* 1997;152:387-394.
2. Voorhout G. Cisternography combined with linear tomography for the visualization of the pituitary gland in healthy dogs: a comparison with computed tomography. *Vet Radiol* 1990;31:68-73.
3. Van der Vlugt–Meijer RH, Meij BP, Voorhout G. Intraobserver and interobserver agreement, reproducibility, and accuracy of computed tomographic measurements of pituitary gland dimensions in healthy dogs. *Am J Vet Res* 2006 (in press).
4. Rijnberk A. *Clinical endocrinology of dogs and cats*. Dordrecht: Kluwer, 1996;11-34.
5. Hanson JM, van 't Hoofd MM, Voorhout G, Teske E, Kooistra HS, Meij BP. Efficacy of transsphenoidal hypophysectomy in treatment of dogs with pituitary-dependent hyperadrenocorticism. *J Vet Intern Med* 2005;19:687-694.
6. Van der Vlugt-Meijer RH, Voorhout G, Meij BP. Imaging of the pituitary gland in dogs with with pituitary-dependent hyperadrenocorticism. *Mol Cell Endocrinol* 2002;197:81-87.
7. Van der Vlugt-Meijer RH, Meij BP, Voorhout G. Dynamic computed tomographic evaluation of the pituitary gland in healthy dogs. *Am J Vet Res* 2004;65:1518-1524.
8. Love NE, Fisher P, Hudson L. The computed tomographic enhancement pattern of the normal canine pituitary gland. *Vet Radiol Ultrasound* 2000;41:507-510.
9. Van der Vlugt–Meijer RH, Meij BP, van den Ingh TSGAM, Rijnberk A, Voorhout G. Dynamic computed tomography of the pituitary gland in dogs with pituitary-dependent hyperadrenocorticism. *J Vet Intern Med* 2003;17:773-780.
10. Heiken JP, Brink JA, Vannier MW. Spiral (helical) CT. *Radiology* 1993;189:647-656.
11. Kalender WA, Seissler W, Vock P. Single-breath-hold spiral volumetric CT by continuous patient translation and scanner rotation. *Radiology* 1989;173(P):414.

12. Kalender WA, Seissler W, Klotz E, Vock P. Spiral volumetric CT with single-breath-hold technique, continuous transport, and continuous scanner rotation. *Radiology* 1990; 176:181-183.
13. Kalender WA, Vock P, Polacin A, Soucek M. Spiral CT : a new volume scanning technique. *Röntgenpraxis* 1990;43:9.
14. Polacin A, Kalender WA, Marchal G. Evaluation of section sensitivity profiles and image noise in spiral CT. *Radiology* 1992;185:29-35.
15. Kasales CJ, Hopper KD, Ariola DN, et al. Reconstructed helical CT scans : Improvement in z-axis resolution compared with overlapped and nonoverlapped conventional CT scans. *AmJRoentgenology* 1995;164:1281-1284.
16. Meij BP, Mol JA, Hazewinkel HAW, Bevers MM, Rijnberk A. Assessment of a combined anterior pituitary function test in beagle dogs: Rapid sequential intravenous administration of four hypothalamic releasing hormones. *Domest Animal Endocrinol* 1996;13:161-70.
17. Brink JA. Technical aspects of helical (spiral) CT. *Radiol Clin North Am* 1995;33: 825-917.
18. Kalender WA. Thin section three-dimensional spiral CT: Is isotropic imaging possible? *Radiology* 1995;197:578-580.
19. Katz DA, Marks MP, Napel SA, Bracci PM, Roberts SL. Circle of Willis: evaluation with spiral CT Angiography, MR angiography, and conventional angiography. *Radiology* 1995;195:445-449.
20. Leclerq TA, Grisoli F. Arterial blood supply of the normal human pituitary gland. *J Neurosurg* 1983;58:678-681.

# CHAPTER 6

## **Thin-slice 3-dimensional gradient-echo magnetic resonance imaging of the pituitary gland in healthy dogs**

Roselinda H. van der Vlugt-Meijer<sup>1</sup>, Björn P. Meij<sup>2</sup>, George Voorhout<sup>1</sup>.

**American Journal of Veterinary Research: accepted 2006**

Division of Diagnostic Imaging<sup>1</sup> and Department of Clinical Sciences of Companion Animals<sup>2</sup>, Faculty of Veterinary Medicine, Utrecht University, The Netherlands

## Abstract

**Objective** - To evaluate thin-slice 3-dimensional gradient-echo (GE) magnetic resonance imaging (MRI) of the pituitary gland in healthy dogs.

**Animals** - 11 healthy dogs.

**Procedure** - By use of a 0.2 Tesla open magnet, MRI of the skull was performed with T1-weighted GE sequences and various protocols with variations in imaging plane, slice thickness, and flip angle before and after administration of contrast medium; multiplanar reconstructions were made. The pituitary region was subjectively assessed and its dimensions were measured. Image quality was determined by calculation of contrast-to-noise and signal-to-noise ratios.

**Results** - Best-detailed images were obtained with a T1-weighted GE sequence with 1-mm slice thickness and 30° flip-angle, before and after administration of contrast medium. Images with flip angles > 50° were of poor quality. Quality of multiplanar reconstruction images with 1-mm slices was better than with 2 mm slices. The bright signal was best seen without contrast medium. With contrast medium, the dorsal border of the pituitary gland was clearly delineated, but lateral borders were more difficult to discern.

**Conclusions and Clinical Relevance** - MRI of the canine pituitary gland with a 0.2 Tesla open magnet should include a T1-weighted GE sequence with 1-mm slice thickness and flip angle of 30°, before and after administration of contrast medium. The neurohypophysis was best visualized without contrast medium. MRI examination permitted differentiation between the pituitary gland and surrounding structures.

## Introduction

Detailed imaging of the pituitary gland in dogs has diagnostic and therapeutic planning value<sup>1-3</sup>. Several techniques have been described, amongst which CT is most commonly used.<sup>4-6</sup> It gives information about the size of the pituitary gland and the exact location of the pituitary gland in relation to the bony surgical landmarks required for transsphenoidal hypophysectomy in dogs with PDH.<sup>1,2,5,7</sup> In addition, dynamic CT, which comprises a series of transverse scans through the center of the pituitary gland during and after rapid IV injection of contrast medium, may indirectly reveal the site of the microadenoma in dogs with PDH by visualization of the displacement or distortion of the neurohypophyseal flush.<sup>5-6, 8</sup>

The imaging modality of choice for the evaluation of the pituitary gland in humans is MRI.<sup>9-12</sup> It allows for superior differentiation of soft tissue structures in all scan planes.<sup>9-11,13</sup> Furthermore, the pituitary bright signal, a hyperintense signal on T1-weighted images representing the neurohypophysis, can give additional anatomic and functional information.<sup>14-17</sup> In dogs, MRI has been used to diagnose pituitary gland macrotumors<sup>18</sup> and for evaluation of the pituitary gland in dogs with pituitary-dependent hyperadrenocorticism.<sup>19,20</sup> There are two reports on MRI of the pituitary gland in healthy dogs performed with a 1.5 Tesla machine and SE sequences with 3 mm<sup>21</sup> and 5 mm slice thickness.<sup>22</sup> Normal pituitary gland anatomic features, including the appearance of the pituitary bright signal, was described in one report<sup>21</sup>. Furthermore, the contrast enhancement pattern during dynamic MRI has been described<sup>21</sup>. In the other report pituitary gland dimensions were related to the size of the dog.<sup>22</sup>

Microadenomas in dogs with PDH do not change the size or shape of the pituitary gland and may be as small as 1-2 mm in diameter.<sup>25</sup> Therefore pituitary imaging modalities for detection of microadenomas should have a slice thickness of 2 mm or thinner. On images of slices with a thickness of 3 mm or more, pituitary gland changes and lesions may go unnoticed. With 3D GE sequences however, thinner slices can be made and quality may be improved substantially.

The purpose of the study reported here was to determine the best protocol for pituitary gland imaging by use of thin-slice 3D GE MRI with a 0.2 T open magnet, assess quality of the MR images by varying the imaging plane, flip angle, and slice thickness, and determine the effect of administration of contrast medium.

## Materials and Methods

### Dogs

Eleven healthy adult dogs (6 Beagles and 5 crossbreed dogs with comparable skull types) were used. The dogs were 2 to 9 years of age (median 7 years) and body weights ranged from 11 to 24 kg (median 18 kg). The dogs included 9 sexually intact male dogs and 2 sexually intact female dogs that were not in estrus during the study. Dogs were obtained from the Department of Clinical Sciences of Companion Animals of the Utrecht University. The dogs were used for teaching students in clinical diagnostic exercises and for minor non-invasive studies. During their stay in the Department, all dogs received the best standard of care. The experimental protocols were approved by the Ethical Committee (DEC) of the Utrecht University. Normal pituitary function was determined by evaluation of plasma concentrations of adrenocorticotropin, cortisol, growth hormone, luteinizing hormone, and prolactin after IV injection of corticotropin-releasing hormone, growth hormone-releasing hormone, gonadotropin-releasing hormone and thyrotropin-releasing hormone, respectively.<sup>25</sup>

### Anesthesia

Food was withheld from all dogs for 18 hours prior to MRI. Following IV administration of medetomidine<sup>a</sup> (50 µg/kg of body weight), anesthesia was induced by IV administration of propofol<sup>b</sup> (1-2 mg/kg body weight). The trachea was intubated and inhalation anesthesia was maintained in a semi-closed system with a mixture of isoflurane<sup>c</sup>, nitrous oxide, and oxygen.

### MRI

MRI was performed with a 0.2 Tesla open magnet<sup>d</sup> with dogs in sternal recumbency and by use of the small multipurpose coil. In all dogs, 2 series of MRI experiments were performed with a 1 month interval between experiments. Contiguous slices of the pituitary gland were obtained with a T1-weighted 3D GE sequence (flash 3D, time of repetition [TR] 34 milliseconds, time of echo [TE] 12 milliseconds, slab thickness 32 mm, time of acquisition [TA] 22.02 minutes, with a rectangular 140 x 160 mm field of view.

**Experiment 1.** Sequences of transverse (n = 11 dogs), dorsal (11), and sagittal (3) 1-mm-thick slices with a flip angle of 30° were obtained before contrast medium injection. After IV injection of 0.2 mL of contrast medium<sup>e</sup> (containing 377 mg megluminegadoteraat per ml)/kg of bodyweight (BW) ,

sequences of transverse 1-mm ( $n = 10$  dogs) and 2-mm (9) thick slices with a flip angle of  $30^\circ$  were obtained.

**Experiment 2.** Before contrast medium injection, sequences of transverse and dorsal 1-mm-thick slices were obtained. After contrast medium injection sequences of transverse and dorsal 2-mm-thick slices were obtained. Both before and after contrast medium injection, variations in flip angle were studied. Dogs were randomly assigned to the study protocols and no divisions were made on the basis of breed, sex, age or weight. Before contrast medium injection, dogs were studied with a flip angle of  $20^\circ$  (5 dogs),  $50^\circ$  (3 dogs; in 1 dog unintentionally a flip angle of  $30^\circ$  was used instead of a flip angle of  $50^\circ$ , which contributed to the number of measurements in experiment 1),  $70^\circ$  (1 dog), and  $90^\circ$  (1 dog). After IV injection of 0.3 mL of contrast medium/kg, sequences were obtained with the same flip angle as before contrast medium injection, except for the dog that was studied before contrast injection with a flip angle of  $90^\circ$ . In this dog a flip angle of  $70^\circ$  was used after contrast medium injection.

By use of dedicated computer software<sup>f</sup> MPRs were made. Dorsal and sagittal reconstructions were made of the transverse series, transverse and sagittal reconstructions were made of the dorsal series and transverse and dorsal reconstructions were made of the sagittal series.

### **Anatomy and dimensions**

The anatomy and shape of the pituitary gland, the sella turcica, and the vessels surrounding the pituitary gland were assessed on the series and MPRs. The pituitary bright signal was identified and size, shape, and localization was assessed on the imaging series.

The height and width of the pituitary gland were measured on the images of the original transverse series before contrast medium injection. Length was measured on the sagittal MPR series from the original transverse series. On the image of the transverse series that contained the largest cross-section of the pituitary gland, the edges of the brain were traced and the enclosed area was calculated by the computer. The P:B ratio was calculated by dividing the height of the pituitary gland ( $\text{mm} \times 10^2$ ) and the area of the brain ( $\text{mm}^2$ ) as described for CT measurements of the pituitary gland.<sup>7</sup>

The pterygoid hamular processes and the shape of the sphenoid bone from rostral to caudal were assessed on the transverse series. The thickness of the basisphenoid bone was measured on the image of the transverse series

that contained the largest cross-section of the pituitary gland. On the sagittal reconstructed series, the location of the pituitary gland was assessed in relation to the tuberculum sellae, the sphenoid bone, and the dorsum sellae.

### Quality

Quality was assessed subjectively (visually). Subjective assessment of quality was based on correct identification of the anatomic structures of interest (pituitary gland, pituitary bright signal, arteries, cavernous sinuses and the sphenoid bone). A subjective comparison was also made between the series. Subjective quality was assessed as 'good', 'moderate' or 'poor' for the individual series and as 'better' or 'worse' for comparison between the series.

The SNR and CNR were calculated as an objective reflection of the subjective findings and to strengthen the subjective findings. For each dog, SNRs and CNRs for the pituitary gland and the pituitary bright signal were calculated. The SNRs and CNRs were calculated for the transverse series of experiments 1 and 2 and for the dorsal and sagittal series of experiment 1. The SNRs and CNRs were not calculated for the dorsal series of experiment 2. On the image that contained the largest cross section of the pituitary gland, ROIs were selected representing the pituitary gland, the pituitary bright signal, the brain, and the background (i.e., the area around the skull). The size of the ROI of the background and the brain was standardized to 0.2 cm<sup>2</sup>. The sizes of the other ROIs were set to be a reliable representation of the structures to be measured. MRI computer software was used to calculate the mean signal intensity (SI) and the SD of the pixel intensities in the ROIs.

The SNR of the pituitary gland ( $SNR_{\text{pituitary}}$ ), the pituitary bright signal ( $SNR_{\text{pit bright signal}}$ ), the surrounding pituitary tissue ( $SNR_{\text{sur pit tissue}}$ ) and the brain ( $SNR_{\text{brain}}$ ) were calculated as the SI divided by the SD of the background intensity as follows:

$$SNR_{\text{pituitary}} = SI_{\text{pituitary}} / SD_{SI \text{ background}};$$

$$SNR_{\text{pit bright signal}} = SI_{\text{pit bright signal}} / SD_{SI \text{ background}};$$

$$SNR_{\text{sur pit tissue}} = SI_{\text{sur pit tissue}} / SD_{SI \text{ background}};$$

$$SNR_{\text{brain}} = SI_{\text{brain}} / SD_{SI \text{ background}}.$$

The CNR of the pituitary in relation to the brain ( $CNR_{\text{pituitary-brain}}$ ) was calculated by subtraction of the SNR of the brain from the SNR of the pituitary as follows:

$$CNR_{\text{pituitary-brain}} = SNR_{\text{pituitary}} - SNR_{\text{brain}}$$

The CNR of the pituitary bright signal in relation to the surrounding pituitary tissue ( $CNR_{\text{pit-bright-signal-sur-pit-tissue}}$ ) was calculated by subtraction of the SNR of the surrounding pituitary tissue from the SNR of the pituitary bright signal as follows:

$$CNR_{\text{pit-bright-signal-sur-pit-tissue}} = SNR_{\text{pit-bright-signal}} - SNR_{\text{sur-pit-tissue}}$$

### Statistical analysis

In each specific MRI setting, the number of measurements (and not the number of dogs) was used to calculate SNR and CNR values. Results are expressed as mean  $\pm$  SD for SNR and CNR values and as median and ranges for pituitary gland dimensions (height, width, length, and P:B). Results of series with different imaging plane, flip angle, slice-thickness, and with or without contrast medium injection were statistically evaluated by use of the Student *t*-test for paired samples because the groups contained the same dogs. For analysis of groups with different dogs the Student *t*-test for independent samples (2-tailed) was used. A value of  $P \leq 0.05$  was considered significant.

Number of measurements	Imaging plane	Flip angle (degrees)	Slice thickness (mm)	Contrast medium used	SNR <sub>pit</sub>	CNR <sub>pit-brain</sub>
12	Tra	30	1	No	15.30 $\pm$ 2.96	0.18 $\pm$ 1.13
12	Dor	30	1	No	14.76 $\pm$ 1.98	0.81 $\pm$ 1.44
3	Sag	30	1	No	13.83 $\pm$ 2.49	0.33 $\pm$ 0.65
5	Tra	20	1	No	15.23 $\pm$ 3.43	0.45 $\pm$ 1.13
3	Tra	50	1	No	10.06 $\pm$ 1.75	0.26 $\pm$ 0.66
10*	Tra	30	1	Yes	17.85 $\pm$ 3.38	3.75 $\pm$ 1.39
10*	Tra	30	2	Yes	24.50 $\pm$ 3.17	3.45 $\pm$ 1.52

**Table 1.** Mean  $\pm$  SD SNR<sub>pit</sub> and CNR<sub>pit-brain</sub> of various numbers of measurements obtained from T1-weighted GE 3D (flash 3D) MR images in healthy dogs. \* In 1 dog it was not possible to determine a ROI containing only the pituitary gland. Tra = Transverse, Sag = Sagittal, Dor = Dorsal.

## Results

### Anatomy and dimensions

The pituitary gland encompassed the infundibular recess rostrally on the transverse images and became more round to oval towards the caudal aspect (Figure 1). The pituitary gland appeared triangular on dorsal images (Figure 2) and had a protracted bean-shape on the sagittal images with the infundibular recess rostrally (Figure 3). The vessels surrounding the pituitary gland were identified on the transverse and the dorsal images.

The pituitary gland was prominent with slightly irregular borders on the transverse images in 3 dogs. A prominent invaginating infundibular recess was seen in 2 dogs with a caudally located pituitary bright signal. In 1 dog, this infundibular recess divided the pituitary gland in 2 parts on the sagittal view and in another dog the infundibular recess formed the center in a ring-shaped pituitary gland on the transverse images (Figure 4).

The rostral and ventral borders of the sella turcica were identified on transverse and sagittal images (Figures 1, 3 and 4). The caudal border formed by the dorsum sellae was more difficult to identify on the transverse series and in 1 dog it had an asymmetrical appearance.

In all dogs, a pituitary bright signal was detected (Figure 1). The pituitary bright signal was dorsocaudal in 3 dogs, centrodorsal in 4 dogs, central in 2 dogs, and completely caudal in 2 dogs. In 1 dog that had a caudally located bright spot, a small supplemental hyperintense area was seen in the region of the infundibular stalk (Figure 5). The bright signal was prominent and round on the transverse images and triangular on the dorsal images in 7 dogs. In 2 dogs, the bright signal had an asymmetrical appearance; in 1 dog, the signal was a small irregular nodule; and in another dog, the bright signal was U-shaped around the infundibular recess.

Pituitary gland height ranged from 4 to 6 mm (median, 5 mm), width ranged from 5 to 9 mm (median, 6 mm), and length ranged from 7 to 9 mm (median, 8 mm). The P:B ratio ranged from 0.21 to 0.31 (median, 0.26).

The hamular processes were identified on the original transverse images. The hamular processes and the basisphenoid bone were best seen on the images of the 1-mm-thick series with a flip angle of 20° and 30°. Visibility of these structures was highly dependent on the contrast density of the surrounding tissues. The thickness of the basisphenoid bone on the transverse image that contained the largest cross-section of the pituitary gland ranged from 2 to 6 mm (median, 4

mm). The following layers could be identified in the structure of the sphenoid bone (from nasopharynx to neurocranium): mucoperiosteal layer, outer cortex, cancellous bone, and inner cortex (Figures 1 and 3). The inner cortex was bordered by the pituitary gland (Figure 1). The position of the pituitary gland in relation to the tuberculum sellae and the dorsum sellae were best seen on sagittal reconstructed images (Figures 3 and 4).

### Quality

The image quality in the 1-mm-thick transverse and dorsal images with a 30° flip angle was good as assessed subjectively. From these series, high quality MPRs were produced. The pituitary gland and the sellar floor were more difficult to distinguish on the dorsal images than on transverse images. The 1-mm-thick sagittal images with a 30° flip angle were of poor quality as assessed subjectively. There were no significant differences in SNR of the pituitary gland between the dorsal, transverse, and sagittal images (Table 1). The CNR between the pituitary bright signal and the surrounding pituitary tissue was not different between dorsal and transverse images (Table 2).

There was no difference in image quality between the series made with a flip angle of 20° or 30° as assessed subjectively. The images of the series made with a flip angle of 50° were considerably darker and the images of the series made with a flip angle of 70° or 90° were of very poor quality. The SNR of the pituitary gland on the transverse images was significantly higher ( $P < 0.05$ ) when the flip angle was 20° than when the flip angle was 50° (Table 1). The pituitary bright signal was better delineated from the remaining pituitary tissue on the images of the series made with a flip angle of 50° than on the series made with a flip angle of 30° and the ability to subjectively detect the signal became less on the series with a flip angle of 20°. The CNR between the pituitary bright signal and the surrounding pituitary tissue on the images of the series made with a flip angle of 30° was higher than that on the images of the series made with a flip angle with 20° or 50°, however, this difference was not significant (Table 2).

On the basis of subjective assessment, 2-mm-thick transverse images were of moderate quality but had less spatial resolution than 1-mm-thick images. Dorsal images obtained after MPR from 2-mm-thick transverse series revealed considerably less spatial resolution than the dorsal images obtained after MPR of the 1-mm-thick transverse series. The SNR of the pituitary gland was significantly ( $P < 0.005$ ) higher on 2-mm-thick transverse images than on the 1-mm-thick transverse images, both with a 30° flip angle (Table 1).

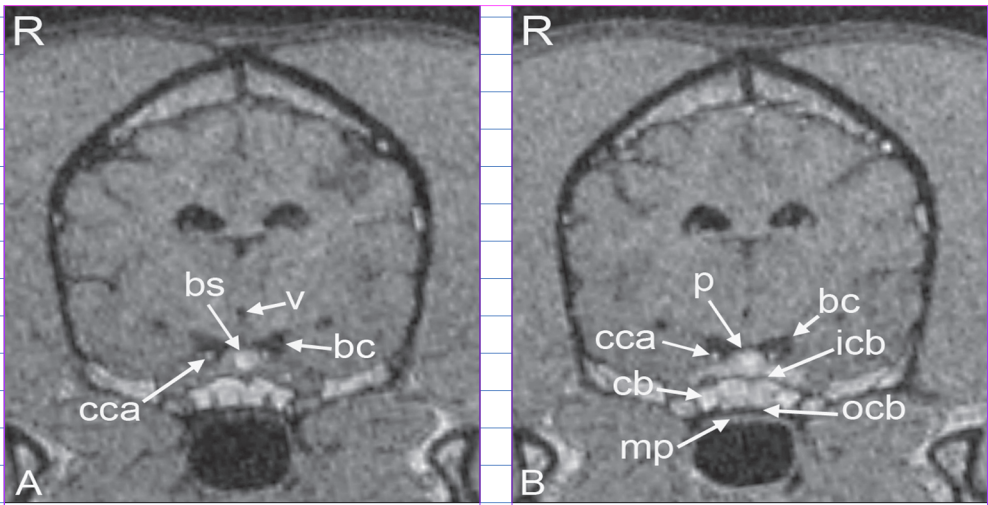


**Figure 1.** Representative transverse MRI of the pituitary gland before (A) and after (B) IV injection of contrast medium in a healthy 2-year-old Beagle. *p* = pituitary gland, *bs* = bright spot, *v* = third ventricle, *cca* = caudal communicating artery, *bc* = basal cistern, *mp* = mucoperiosteal layer of the sphenoid bone, *ocb* = outer cortical bone, *cb* = cancellous bone, *icb* = inner cortical bone, *R* = right.

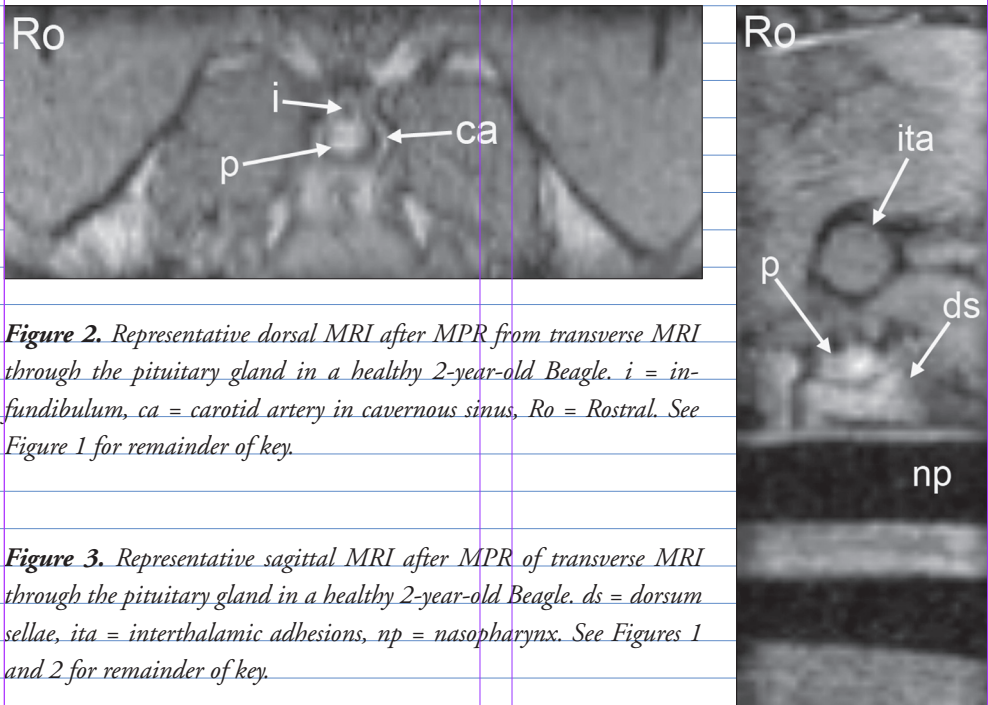


**Figure 2.** Representative dorsal MRI after MPR from transverse MRI through the pituitary gland in a healthy 2-year-old Beagle. *i* = infundibulum, *ca* = carotid artery in cavernous sinus, *Ro* = Rostral. See Figure 1 for remainder of key.

**Figure 3.** Representative sagittal MRI after MPR of transverse MRI through the pituitary gland in a healthy 2-year-old Beagle. *ds* = dorsum sellae, *ita* = interthalamic adhesions, *np* = nasopharynx. See Figures 1 and 2 for remainder of key.

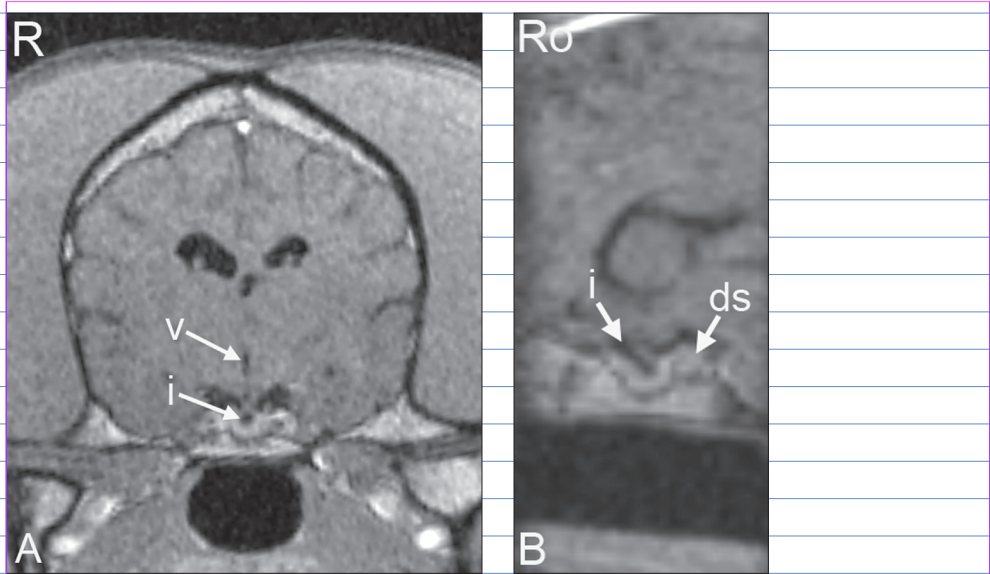


**Figure 4.** Original transverse 1-mm-thick MRI (A) and midsagittal image obtained after MPR (B) of the pituitary gland in a healthy 8-year-old cross-breed dog. The prominent infundibular recess (i) forms the center in a donut-shaped pituitary gland (A) and displaces the pituitary bright signal caudally against the dorsum sellae (B). See Figures 1, 2, and 3 for remainder of key.

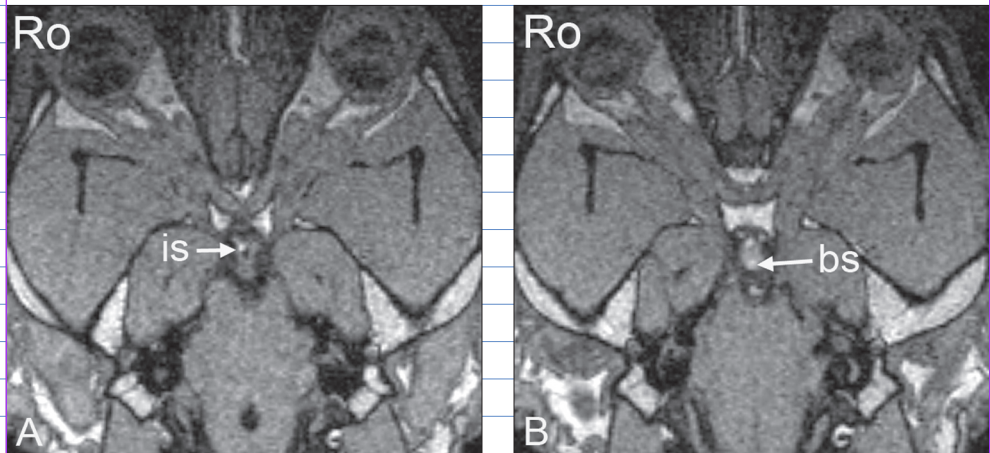


**Figure 5.** Dorsal MRI of 1-mm-thick slices through the pituitary gland in a healthy 5-year-old Beagle. Notice, in the most dorsal slice (A), a hyperintense nodule in the infundibular stalk (is), and 1 slice more ventrally (B), the pituitary bright signal, caudally, representing the neurohypophysis. See Figure 2 for key.

As subjectively assessed, the image of the pituitary gland was strongly enhanced after injection of contrast medium. The dorsal border of the pituitary gland was more demarcated after contrast medium administration, but delineation between the lateral borders of the pituitary gland and the cavernous sinuses was not improved, compared with images obtained before contrast medium administration. The SNR of the pituitary gland was not significantly different between images obtained before versus after contrast medium administration; however, the CNR was significantly ( $P < 0.001$ ) higher on images obtained after administration (Table 1). The delineation between the bright signal and surrounding pituitary tissue became less pronounced after injection of contrast medium.

Number of measurements	Imaging plane	Flip angle (degrees)	Slice thickness (mm)	Contrast medium	CNR
5	Tra	20	1	No	3.02 ± 2.06
12	Tra	30	1	No	5.67 ± 2.42
3	Tra	50	1	No	3.67 ± 0.73
10*	Tra	30	1	Yes	4.00 ± 2.06
10*	Tra	30	2	Yes	4.96 ± 3.84
12	Dor	30	1	No	3.77 ± 2.93

**Table 2.** Mean ± SD  $CNR_{\text{pit bright signal-sur pit tissue}}$  between the pituitary bright signal and the surrounding pituitary gland tissue of the same dogs as in Figure 2.

\*See Table 2 for key.

## Discussion

In the present study, a 0.2 Tesla open MRI scanner was used for pituitary gland imaging in healthy dogs. As subjectively assessed, the optimal quality of the MR images was achieved with a T1-weighted gradient echo (flash 3D) sequence with a slice thickness of 1 mm and a flip-angle of 30°, before and after IV injection of contrast medium. The SNR and CNR values strengthened these subjective findings, but should be interpreted with care because of the variations in number of dogs studied with the different sequences. The superior differentiation of the soft tissues with MRI resulted in detailed images of the pituitary gland, the surrounding structures and vessels. Pituitary gland vascularization on MR images may give valuable information but should be interpreted with care because vessel resolution is influenced by vessel position, size, and flow direction.<sup>26</sup> The infundibular recess invaginates more deeply into the pituitary gland in dogs than in humans.<sup>27</sup> Also, considerable anatomic variation in size and shape of the pituitary gland has been described.<sup>4,28</sup> The deeply invaginating infundibular recess that was seen in 2 dogs in the present study was probably a normal anatomic variation.

In humans, T1-weighted SE sequences are considered the most useful sequences for MRI of the pituitary gland.<sup>9</sup> Three-dimensional GE imaging of the pituitary gland, allowing for thinner slices, has been mentioned as an option for detection of small lesions of the pituitary gland.<sup>9,29,30</sup> In transverse CT of the canine pituitary gland, a slice thickness of 2 mm is used commonly<sup>4,6</sup> whereas with MR SE sequences, the minimum slice thickness is 3 mm. Preliminary examinations with the SE sequences on canine skulls revealed insufficient spatial resolution. Therefore, the 3D GE sequence was chosen instead of the SE technique, to obtain the desired spatial resolution. However, GE images are prone to magnetic susceptibility and motion artifacts.<sup>9,29,30</sup> In our study, there were no obvious artifacts affecting the MR images, which can be explained by the use of a low magnetic field strength, the small size of the canine sphenoid bone containing only little air,<sup>29,31,32</sup> and the use of anesthesia during MRI. However, the acquisition time of GE sequences is considerably longer than that of SE sequences in low- and high-field systems.

T1-weighting in GE sequences is typically manipulated by changing the flip angle.<sup>23,24,33</sup> Contrast is mainly proton-density weighted at low flip-angles (10°) and becomes more T1-weighted for higher flip-angles. However, this effect is accompanied by a loss of signal because of the magnetic field inhomogeneity

effects caused by the missing 180° echopulse used in SE techniques (T2 effects), which greatly affects the GE sequence.<sup>23,24,33</sup> As subjectively assessed, there was no difference in image quality between the images made with a flip angle of 20° and 30°, except for detection of the pituitary bright signal, which was more distinct on the images of the series made with a flip angle of 30°. The images of the series made with a flip angle of 50° already had great signal loss, and the images of the series made with a flip-angle of 70° or 90° were of very poor quality.

The ability to produce MPRs of high quality is a great advantage of thin slice 3D GE imaging and makes supplemental sequences with different imaging planes unnecessary. Similar to helical CT, the quality of the MPR in MRI depends on the slice thickness.<sup>34</sup> In the present study, a slice thickness of 1 mm resulted in high quality MPRs, whereas MPRs from 2-mm-thick slices were of poor quality.

Injection of contrast medium is usually not necessary for detection of lesions of the pituitary gland in humans, but for microadenomas it may give additional information and is therefore recommended.<sup>9,10</sup> In the present study, injection of contrast medium provided images with improved definition of the dorsal border of the pituitary gland, but obscured the pituitary bright signal and the borders between the pituitary gland and the cavernous sinuses. Therefore, a pituitary gland MRI protocol should contain image sequences obtained before and after administration of contrast medium.

In humans, the pituitary bright signal was first thought to be caused by fat within the sella turcica.<sup>35</sup> However, the origin of the pituitary bright signal was later determined to be the neurohypophysis.<sup>14,15</sup> There is considerable variation in the rate of detection of the pituitary bright signal in healthy humans (63%-100%), which is explained by individual variation, differences in age, and different MRI settings.<sup>14,15,17,36-38</sup> There remains some controversy about the exact origin of the high SI, but the intensity appears to depend on the vasopressin concentration in the posterior lobe and the signal is absent in humans with central diabetes insipidus.<sup>14,15,17</sup> Furthermore, the pituitary bright signal is thought to correspond to only a part of the neurohypophysis.<sup>37,39</sup> In the present study, the pituitary bright signal was detected in all dogs, but delineation depended on the imaging protocol. The differences in size, shape, and location of the pituitary bright signal are probably more attributable to physiologic variation than to variation in anatomic features of the neurohypophysis. However, in 2 dogs with a deep infundibular recess, the pituitary bright signal was displaced caudally. There was no explanation for the small hyperintense nodule in the

region of the infundibular stalk in 1 dog, although in a human patient without sellar or parasellar disease it was reported that the pituitary bright signal was located in the area of the median eminence.<sup>37</sup>

In the dogs of the present study, the pituitary height, length, width, and the P:B ratio were comparable to values for healthy dogs in other studies.<sup>6,28,40</sup> With the single slice CT scanner, the distance was measured in tenths of a millimeter.<sup>6</sup> With the software of the MRI machine used in this study, the distance was measured to a resolution of 1 millimeter and accuracy was decreased, compared with the single slice scanner. Therefore measurements had to be done with the greatest care. Furthermore, subjective assessment of the size and shape of the pituitary gland in relation the cavernous sinuses, as described for CT of the pituitary gland in dogs, remains important.<sup>7</sup>

Microsurgical transsphenoidal hypophysectomy is an effective method of treatment for dogs with PDH.<sup>1,2</sup> The position of the pituitary gland in relation to the surgical landmarks, such as the hamular processes, may vary among dogs of different breeds and even among dogs of the same breed.<sup>41</sup> It seems that CT is superior to MRI for accurate preoperative localization of the pituitary gland in relation to the hamular processes and the shape of the outer cortical lamina of the sphenoid bone.<sup>1,2</sup> Although the sphenoid bone itself was visible with MRI, the shape of the outer cortical lamina was difficult to discern on transverse MR images because of insufficient resolution. The hamular processes were visible on the transverse images of MRI series but their detection depended on the imaging protocol and the intensity of the surrounding tissues. The hamular processes could not be identified on the transverse MPRs of the dorsal series of scans because the ventral lining of the slab was positioned dorsally to the nasopharynx and the hamular processes protrude into the nasopharynx. In comparison with CT in dogs,<sup>6</sup> the sagittal MPRs give valuable information on the intracranial relation between the pituitary gland and the bordering bone structures (i.e., the tuberculum sellae and the dorsum sellae).

- a. Domitor, SmithKline Beecham Animal Health BV, Zoetermeer, The Netherlands
- b. Diprivan-10, Zenaca BV, Ridderkerk, The Netherlands
- c. Forene, Abbot Laboratories BV, Maarssen, The Netherlands
- d. Magnetom Open Viva, Siemens AG, Germany
- e. Dotarem, Guerbet Nederland BV, Gorinchem, The Netherlands
- f. Siemens AG, Germany

## References

1. Meij BP, Voorhout G, Van den Ingh TSGAM, et al. Transsphenoidal hypophysectomy in beagle dogs: evaluation of a microsurgical technique. *Vet Surg* 1997;26:295-309.
2. Meij BP, Voorhout G, Van den Ingh TSGAM, et al. Results of transsphenoidal hypophysectomy in 52 dogs with pituitary-dependent hyperadrenocorticism. *Vet Surg* 1998;27:246-261.
3. Rijnberk A. Clinical endocrinology of dogs and cats. Dordrecht/Boston: Kluwer Academic Publishers, 1996;11-34.
4. Van der Vlugt-Meijer RH, Voorhout G, Meij BP. Imaging of the pituitary gland in dogs with pituitary-dependent hyperadrenocorticism. *Mol Cell Endocrinol* 2002;197:81-87.
5. Van der Vlugt-Meijer RH, Meij BP, Van den Ingh TSGAM, et al. Dynamic computed tomography of the pituitary gland in dogs with pituitary-dependent hyperadrenocorticism. *J Vet Int Med* 2003;17:773-780.
6. Van der Vlugt-Meijer RH, Meij BP, Voorhout G. Dynamic computed tomography of the pituitary gland in healthy dogs. *Am J Vet Res* 2004;65(11):1518-1524.
7. Kooistra HS, Voorhout G, Mol JA, et al. Correlation between impairment of glucocorticoid feedback and the size of the pituitary gland in dogs with pituitary-dependent hyperadrenocorticism. *J Endocrinol* 1997;152:387-394.
8. Love NE, Fisher P, Hudson L. The computed tomographic enhancement pattern of the normal canine pituitary gland. *Vet Radiol Ultrasound* 2000;41:507-510.
9. Chong BW, Newton TH. Hypothalamic and pituitary pathology. *Radiol Clin N-Am* 1993;31:1147-1183.
10. Elster AD. Modern imaging of the pituitary. *Radiology* 1993;187:1-14.
11. Escourelle H, Abecassis JP, Betagna X, et al. Comparison of computerized tomography and magnetic resonance imaging for the examination of the pituitary gland in patients with Cushing's disease. *Clin Endocrinol* 1993;39:307-313.
12. Fitzpatrick M, Tartaglino LM, Hollander MD, et al. Imaging of sellar and parasellar pathology. *Radiol Clin N-Am* 1999;37:101-121.
13. Lee BCP, Deck MDF. Sellar and juxtaseilar lesion detection with MR. *Radiology* 1985;157:143-147.

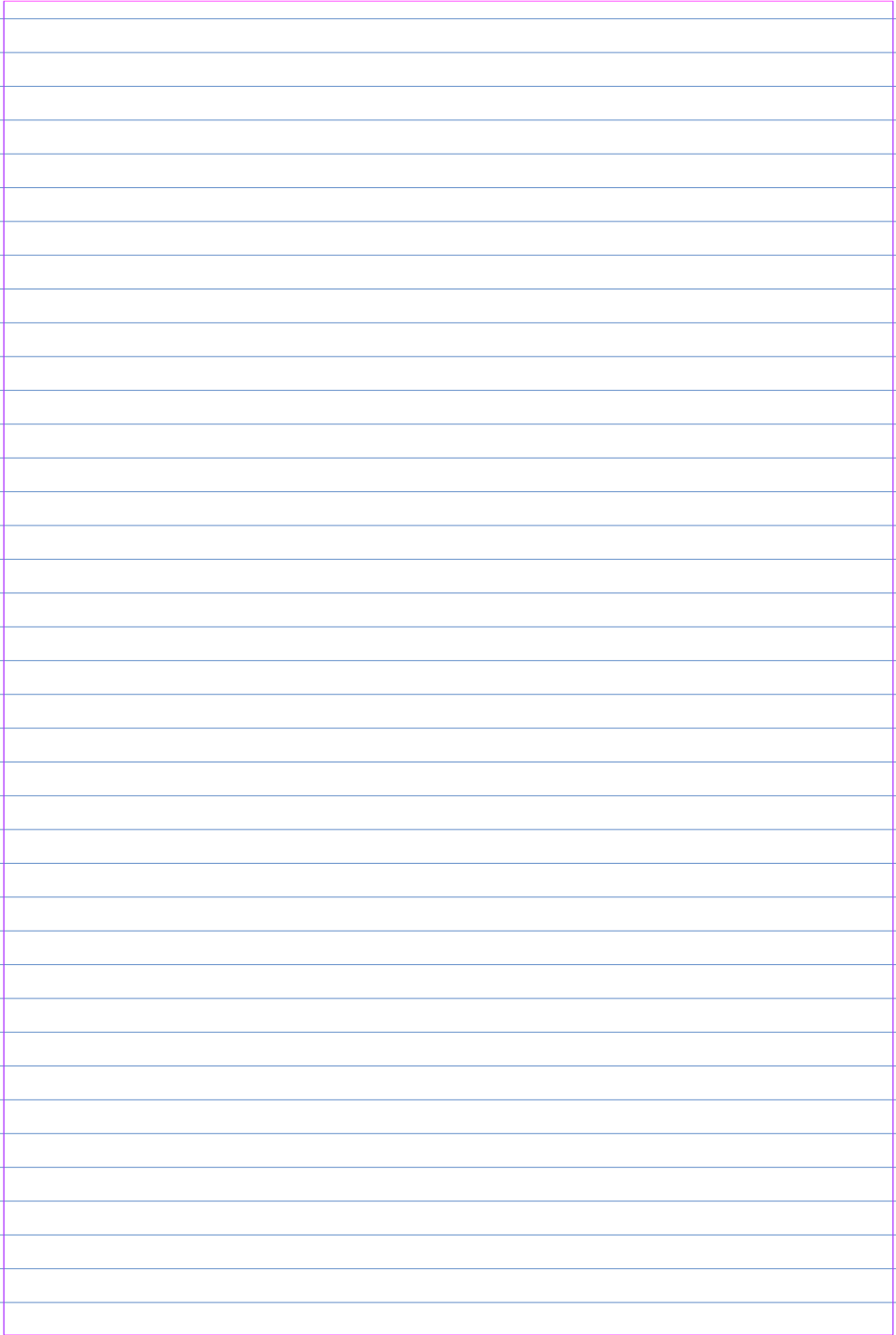
14. Colombo N, Berry I, Kucharczyk J, et al. Posterior pituitary gland: appearance on MR images in normal and pathological states. *Radiology* 1987;165:481-485.
15. Fujisawa I, Asato R, Nishimura K, et al. Anterior and posterior lobes of the pituitary gland: assessment by 1.5T MR imaging. *J Comp Assist Tomogr* 1987;11:214-220.
16. Fujisawa I, Nishimura K, Asato R, et al. Posterior lobe of the pituitary in diabetes insipidus: MR findings. *J Comp Assist Tomogr* 1987;11:221-225.
17. Kurakowa H, Fujisawa I, Nkano Y, et al. Posterior lobe of the pituitary gland: correlation between signal intensity on T1-weighted MR images and vasopressin concentration. *Radiology* 1998;207:79-83.
18. Duesberg CA, Feldman EC, Nelson RW, et al. Magnetic resonance imaging for diagnosis of pituitary macrotumors in dogs. *J Am Vet Med Assoc* 1995;206:657-662.
19. Bertoy EH, Feldman EC, Nelson RW, et al. Magnetic resonance imaging of the brain in dogs with recently diagnosed but untreated pituitary-dependent hyperadrenocorticism. *J Am Vet Med Assoc* 1995;206:651-656.
20. Bertoy EH, Feldman EC, Nelson RW, et al. One-year follow-up evaluation of magnetic resonance imaging of the brain in dogs with pituitary-dependent hyperadrenocorticism. *J Am Vet Med Assoc* 1996;208:1268-1273.
21. Graham JP, Roberts GD, Newell SM. Dynamic magnetic resonance imaging of the normal canine pituitary gland. *Vet Radiol US* 2000;41:35-40.
22. Kippenes H, Gavin PR, Kraft SL, et al. Mensuration of the normal pituitary gland from magnetic resonance images in 96 dogs. *Vet Radiol US* 2001;42:130-133.
23. Elster AD. Gradient-echo MR imaging: techniques and acronyms. *Radiology* 1993;186:1-8.
24. Brown MA, Semelka RC. MR imaging abbreviations, definitions and descriptions: a review. *Radiology* 1999;213:647-662.
25. Meij BP, Mol JA, Hazewinkel HAW, et al. Assessment of a combined anterior pituitary function test in beagle dogs: rapid sequential intravenous administration of four hypothalamic releasing hormones. *Domest Anim Endocrinol* 1996;13:161-170.
26. Katz DA, Marks MP, Napel SA, et al. Circle of Willis: evaluation with spiral CT angiography, MR angiography, and conventional angiography. *Radiology* 1995; 195:445-449.

27. Daniel PM, Pritchard MML. Studies of the hypothalamus and the pituitary gland. *Acta Endocrinol Suppl (Copenh)* 1975;80:S27-S63.
28. Hullinger RL. The endocrine system. In: Evans HE, ed. *Miller's anatomy of the dog*. 3rd ed. Philadelphia: WB Saunders Co, 1993;559-585.
29. Hamon-Kerautret M, Leclerc X, Dewilly D, et al. Pituitary microadenomas: experience with Gd-DOTA-enhanced MR imaging at 0.5 Tesla. *Eur J Radiol* 1994;18:185-190.
30. Stadnik T, Stevenaert A, Beckers A, et al. Pituitary microadenomas: diagnosis with two- and three-dimensional MR imaging at 1.5 T before and after injection of gadolinium. *Radiology* 1990;176:419-428.
31. Elster AD. Sellar susceptibility artifacts: theory and implications. *Am J Neuroradiol* 1993;14:129-136.
32. Dyce KM, Sack WO, Wensing CJG. The head and ventral neck of the carnivores. In: *Textbook of veterinary anatomy*. Philadelphia: WB Saunders Co, 2002;367-392.
33. Hesselink JR, Martin JF, Edelman RR. Fast Imaging. *Neuroradiol* 1990;32:348-355.
34. Kalender WA. Thin section three-dimensional spiral CT: Is isotropic imaging possible? *Radiology* 1995;197:578-580.
35. Mark L, Peck P, Daniels D, et al. The pituitary fossa: a correlative anatomic and MR study. *Radiology* 1984;153:453-457.
36. Terano T, Seya A, Tamura Y, et al. Characteristics of the pituitary gland in elderly subjects from magnetic resonance images: relationship to pituitary hormone secretion. *Clin Endocrinol* 1996;45:273-279.
37. Brooks BS, Gammal TE, Allison JD, et al. Frequency and variation of the posterior bright signal. *Am J Neuroradiol* 1989;10:943-948.
38. Sato N, Ishizaka H, Matsumoto M, et al. MR detectability of posterior pituitary high signal and direction of frequency encoding gradient. *J Comp Assist Tomogr* 1991;15:355-358.
39. Miki Y, Asato R, Okumura R, et al. Contrast enhanced area of posterior pituitary gland in early dynamic MRI exceeds hyperintense area on T1-weighted images. *J Comp Assist Tomogr* 1992;16:845-848.
40. Voorhout G. Cisternography combined with linear tomography for the visualization of the pituitary gland in healthy dogs: a comparison with computed tomography. *Vet Radiol* 1990;31:68-73.
41. Niebauer GW. Hypophysectomy. In: Slatter D, ed. *Textbook of small animal surgery*, 2nd ed. Philadelphia: WB Saunders Co, 1993;1496-1510.

# CHAPTER 7

**Summarizing discussion and conclusions**

## DIAGNOSTIC IMAGING OF THE PITUITARY GLAND IN DOGS



A large, empty rectangular box with a purple border, occupying the majority of the page below the title. This box is likely intended for a student to draw a diagram or insert an image related to the diagnostic imaging of the pituitary gland in dogs.

## Summarizing Discussion

Pituitary-dependent hyperadrenocorticism (PDH) is a frequently encountered endocrinopathy in dogs. Diagnosis and treatment options of PDH have been discussed in **Chapter 1**. Transsphenoidal hypophysectomy is an effective treatment of PDH in dogs.<sup>1-3</sup> However, for pituitary surgery to be successful information about the size of the pituitary gland and the exact location of the pituitary gland in relation to the surgical (bony) landmarks is essential.<sup>3,4</sup> Information about the size of the pituitary gland also has prognostic implications: survival and disease-free fractions after hypophysectomy were markedly higher in dogs with non-enlarged pituitary glands than in dogs with enlarged pituitary glands.<sup>3</sup>

In humans, conventional radiography has for many years been the standard methods to identify enlargement and osseous changes of the sella turcica in patients with space occupying lesions in the pituitary region.<sup>5-7</sup> However, many of the minor changes of the sella turcica later appeared to be normal variations.<sup>8,9</sup> In dogs the pituitary gland is not encompassed by bone, but is resting on the sella turcica. Expansion of the pituitary gland is usually seen in the dorsal direction.<sup>10</sup> Furthermore, the sella turcica in dogs cannot be visualised easily on conventional lateral radiographs of the skull. So, enlarged pituitary glands in dogs cannot be diagnosed with conventional survey radiographs of the skull. Other techniques, like cisternography in combination with linear tomography, have been described, but the magnitude of suprasellar extension cannot be assessed with this technique<sup>11</sup> At the start of this thesis, computed tomography (CT) and magnetic resonance imaging (MRI) were relatively new imaging techniques in veterinary medicine and only few studies on these imaging techniques were reported. Furthermore, most of the studies were performed with protocols specifically designed for humans. Part of this work was performed to obtain specific protocols for imaging the pituitary gland in dogs.

In order to fully understand the CT and MR images, detailed knowledge of the anatomy of the pituitary gland and the surrounding structures, like vasculature and the bony landmarks, is essential. Anatomy and vascularization have been described in **Chapter 1**. **Important anatomical differences between humans and canine pituitary glands have been highlighted.**

Transsphenoidal hypophysectomy is expected to have the best outcome when installed as primary treatment for dogs with normal-sized or moderately enlarged pituitary glands.<sup>3</sup> In veterinary radiology, adenomatous pituitary glands were initially classified as microadenomas (<10 mm) and macroadenomas (>10 mm) based on criteria used in humans.<sup>12</sup> Pituitary glands smaller than 10 mm were considered normal sized. However, the cut-off value of 10 mm that is used in humans cannot be used in dogs since the normal human pituitary gland, which measures 10 mm in diameter, is larger than the normal canine pituitary gland. Also, the size of the pituitary gland in healthy dogs varies greatly among breeds and even among individual dogs of the same breed.<sup>13</sup> Based on assessment of the dorsal contour of the pituitary gland in relation to the basal cisterns, many pituitary glands of dogs with PDH measuring smaller than 10 mm, were judged to be enlarged.<sup>10</sup> The pituitary height/brain area (P/B) ratio involves a correction for the size of the dog and had the highest discriminating power in distinguishing enlarged from non-enlarged pituitary glands. Normal-sized pituitary glands have P/B ratio's of 0.31 or smaller.<sup>10</sup> The CT dimensions of the pituitary gland in healthy dogs and dogs with pituitary disease have been reported,<sup>10,11,13,14</sup> but no information is available on the agreement within and between observers on CT measurements of the pituitary gland. Data on the accuracy of CT measurements of pituitary gland dimensions were not found in the literature. In **Chapter 2** the reproducibility of the CT measurements of pituitary gland dimensions is reported. In the same chapter the accuracy of CT measurements has been determined by use of a phantom study. It was found that the intra- and interobserver agreement for measuring pituitary gland dimensions on CT images was excellent, especially for measurement of pituitary gland height and the P/B ratio (which are the parameters that are most frequently used in other studies). The fixed window level (WL) and window width (WW) values used in this study led to an underestimation of the pituitary gland dimensions. The most accurate assessment of an object is obtained by setting the window level at half of the difference of Hounsfield Units between the object and the background (full width at half maximum).<sup>15</sup> Two different tissue interfaces are involved in measurement of height of the pituitary gland: the interface between pituitary gland and brain dorsally and the interface between pituitary gland and basisphenoid ventrally. Using different window settings for the pituitary gland-brain interface and pituitary gland-bone interface resulted in more accurate measurements.<sup>16</sup>

On CT images, the normal pituitary gland in human and dogs is homogenous and nearly isodense with brain tissue. After intravenous contrast medium injection, the pituitary gland is hyperdense as compared to brain tissue, which can be explained by the fact that the pituitary gland lies outside the blood-brain barrier.<sup>17</sup> Contrast-enhanced CT has been used in humans and dogs to evaluate pituitary tumors.<sup>10,12,18,19</sup> Large pituitary tumors with suprasellar expansion are readily diagnosed.<sup>10,12,18</sup> However, microadenomas, that do not affect the size and shape of the pituitary gland, may not be detected because of isoattenuation of the adenoma and the surrounding unaffected pituitary tissue.<sup>20-23</sup> In humans, microadenomas have been identified by use of dynamic CT.<sup>19,24,25</sup> Dynamic contrast-enhanced CT includes a series of scans of identical slice thickness, at the same slice position through the center of the pituitary gland, during and after IV injection of a bolus of contrast medium. In **Chapter 3** the dynamic CT enhancement pattern of the pituitary gland in healthy dogs has been described. After strong enhancement of the maxillary arteries, the intracavernous parts of the internal carotid arteries, and the communicating arteries of the arterial cerebral circle, there was a strong enhancement of the central part of the pituitary gland followed by enhancement of its peripheral part. In humans, a strong central enhancement of the pituitary gland has also been described and was explained by the enhancement of the centrally located secondary capillary bed (“pituitary tuft”) of the anterior lobe followed by centrifugal enhancement of the peripheral parts of the anterior lobe.<sup>24</sup> In dogs, the difference in timing of enhancement between the central and peripheral parts of the pituitary gland is a consequence of different vascularization of the neurohypophysis and the adenohypophysis, respectively. The neurohypophysis has a direct arterial blood supply, while the adenohypophysis receives its blood supply from the hypophyseal portal vessels.<sup>26,27</sup> The early and strong enhancement of the neurohypophysis in dogs was called the “pituitary flush”, to distinguish it from the “pituitary tuft” in humans.<sup>24</sup> This “pituitary tuft” should also exist in dogs, but has not been detected yet. This may be explained by the relatively small size and horse-shoe shape of the pars distalis adenohypophysis but detection also depends on the scanner used. CT equipment with higher resolution and shorter scanning times and interscan time delays, should make it possible to distinguish this “pituitary tuft” also in dogs.

As for the “tuft sign” in humans, displacement, distortion, or disappearance of the pituitary flush may be used for the detection and localization of microadenomas in dogs with PDH as was demonstrated in **Chapter 4**. Dynamic CT of the pituitary gland was performed in dogs with PDH that subsequently underwent transsphenoidal hypophysectomy. The aim of the study was to assess the contrast enhancement pattern of the pituitary gland on dynamic CT and to correlate the imaging findings with the findings at transsphenoidal hypophysectomy and findings of histopathological examination of the surgical specimens. In 82% of the dogs with PDH the pituitary gland appeared to be abnormal using dynamic CT, which is higher than in humans, in which the pituitary gland appeared to be abnormal in 54% of the patients.<sup>24</sup> However, if selective removal of the adenomatous adenohypophysis had been the aim of transsphenoidal surgery, it would have been successful in only 15% of the dogs. Separate removal of the adenoma (selective adenomectomy) is the aim of primary transsphenoidal pituitary surgery in humans. However, in a significant portion of these patients, one has to assume that the pituitary tissue that is left in situ has to contain some adenomatous tissue, which is most likely the cause of the recurrences after pituitary surgery in humans with Cushing’s disease. In contrast with the situation in dogs at our department, humans with Cushing’s disease are more often, in addition to the pituitary surgery, treated with medications aimed at the adrenocortical level and/or with conventional or focused radiation therapy aimed at the pituitary level.<sup>28,29</sup>

In dynamic CT, only one single 2-mm thick slice was examined and therefore small adenomas may have been outside the scan plane. Also, when the adenoma was detected in the scan plane no information was available about the rostral or caudal extension of the adenoma. So, for accurate pre-surgical localisation of the adenoma, a dynamic CT examination of the entire pituitary gland, rather than a single thin slice, should be performed. In **Chapter 5**, a dynamic CT examination of the entire pituitary gland has been described in healthy dogs, using helical CT. In this pilot study a protocol for dynamic imaging of the pituitary gland and its surrounding vasculature has been developed. A similar enhancement pattern was observed with dynamic helical CT as with single slice dynamic CT that was described in chapter 3 and 4. Furthermore, dynamic helical CT may give additional information on the vessels surrounding the pituitary gland. It was concluded that dynamic helical CT of the entire pituitary gland could be used for the visualisation of pituitary microadenomas

in dogs and may provide more detailed information about the size and shape of pituitary microadenomas.

Magnetic resonance imaging (MRI) is the imaging modality of choice for the evaluation of the pituitary gland in humans.<sup>19,30-32</sup> MRI allows for superior differentiation of soft tissue structures in all chosen scan planes.<sup>19,30,31,33</sup> Furthermore, the pituitary bright signal, a hyperintense signal on T1-weighted images, representing the neurohypophysis, can give additional anatomical and functional information.<sup>34-37</sup> MRI of the pituitary gland has also been described in dogs and in the studies MR images were made with a 1.5 Tesla (T) machine using spin echo sequences with 3 mm and 5 mm slice thickness.<sup>38-42</sup> Microadenomas in dogs with PDH may be as small as 1 to 2 mm in diameter.<sup>1</sup> On MR images of slices with a thickness of 3 mm or more pituitary pathology may go unnoticed. With 3D gradient echo (GE) sequences thinner slices can be made and quality may be improved significantly. **Chapter 6** describes the development of a protocol for pituitary gland imaging using thin slice 3D GE MRI with an 0.2 T open MRI scanner. It was concluded that MRI of the canine pituitary gland, using a 0.2 T open MRI scanner, should include a T1-weighted GE (flash 3D) sequence with 1 mm slice thickness and flip angle of 30°, before and after contrast-medium injection. The neurohypophysis, visible as the “pituitary bright signal”, was best visualized on the non-contrast images. MRI allows differentiation between the pituitary gland and the surrounding structures, but the specific surgical bony landmarks of the pituitary region were difficult to discern. Although the sphenoid bone itself was visible with MRI, the shape of the outer cortical lamina was difficult to discern on transverse MR images because of insufficient resolution. The hamular processes were visible on the transverse images of MRI series but their detection depended on the intensity of the surrounding tissues. Dynamic MRI of the pituitary gland has been considered but was not possible with the low-field equipment installed at our department. As already mentioned in chapter 1, an open MRI machine (0.2 T) was installed at our division because of the ability to perform MRI scans under general anesthesia in companion animals and of the head and legs horses. The increased interest in open systems is due mostly to the demand by patients for a more comfortable environment (e.g. claustrophobic feelings in closed MRI tunnels) and by the economic pressure for lower cost services. In addition, open systems will allow for interventional procedures, for which direct access to the patient is needed.<sup>43</sup> Another development stimulating open MRI scanner development is the intraoperative use of MRI. For example, real time MRI-guided neurosurgery of the brain in humans with neuronavigational

equipment and 100% MRI compatible surgical tools, requires a position of the surgeon and the operating table within the magnetic field of the MRI scanner and this is best achieved with an open MRI scanner. However, open MRI scanners remain limited in their maximum magnetic field strength, which, at this moment is approximately 0.6 T and is due to the resistive electromagnets and the difficulties in maintaining the homogeneous magnetic field. The open MRI scanner that was installed in 2000 in of our division had, at that time, the highest available magnet field strength (0.2 T) for an open MRI scanner.

Both dynamic helical CT and MRI of the pituitary gland may give valuable information on the pituitary gland in dogs. A comparative study should be performed in dogs with PDH to assess which of the two techniques gives the most valuable information, especially when pituitary surgery is considered. At this moment, complete hypophysectomy is the aim of pituitary surgery in dogs. Imaging may be able to change this when (dynamic) CT and/or MRI enables more precise localization of the adenoma and the neurohypophysis within the contours of the pituitary gland. Then separate removal of the adenohypophysis or the adenoma (adenomectomy) may become the goal of the surgery. This will become even more important when focused radiation therapy (linear accelerator) is available. MRI for pituitary gland imaging should also focus on visualising the pituitary gland in relation to the bony structures and landmarks. MRI of the pituitary gland can only outweigh (dynamic) helical CT when bone and soft tissue in and around the pituitary region are equally or better visualized with MRI than with helical CT.

## Conclusions

- CT measurements of the pituitary gland height and the P/B ratio have a low intra- and interobserver variability. The CT dimensions (specifically the height of the pituitary gland) were systematically underestimated when compared with true dimensions in a phantom study. For accurate measurements different window settings have to be used to identify the different tissue interfaces between pituitary gland, brain and bone.
- Transverse dynamic CT of the pituitary gland reveals the difference in enhancement between the neurohypophysis, seen as the pituitary flush, and the adenohypophysis.
- Displacement, distortion and disappearance of the pituitary flush is diagnostic for an abnormal pituitary gland. Displacement and distortion of the pituitary flush reveals the location, size and shape of the pituitary adenoma in dogs with PDH.
- Dynamic helical CT can be used for visualisation of the enhancement pattern of the entire pituitary gland and also gives information about the surrounding vasculature of the pituitary gland. Dynamic helical CT, in comparison with single slice dynamic CT, may provide more information about the size and shape of pituitary microadenomas.
- Thin slice MRI imaging of the pituitary gland in dogs using an open 0.2 Tesla MRI scanner is best performed using 3D gradient echo sequences in transverse and/or dorsal imaging planes, both before and after contrast medium injection.
- A comparative study between helical CT and MRI should be performed in dogs with PDH to assess which of the techniques gives the most valuable information, with special reference to the bony surgical landmarks.

## References

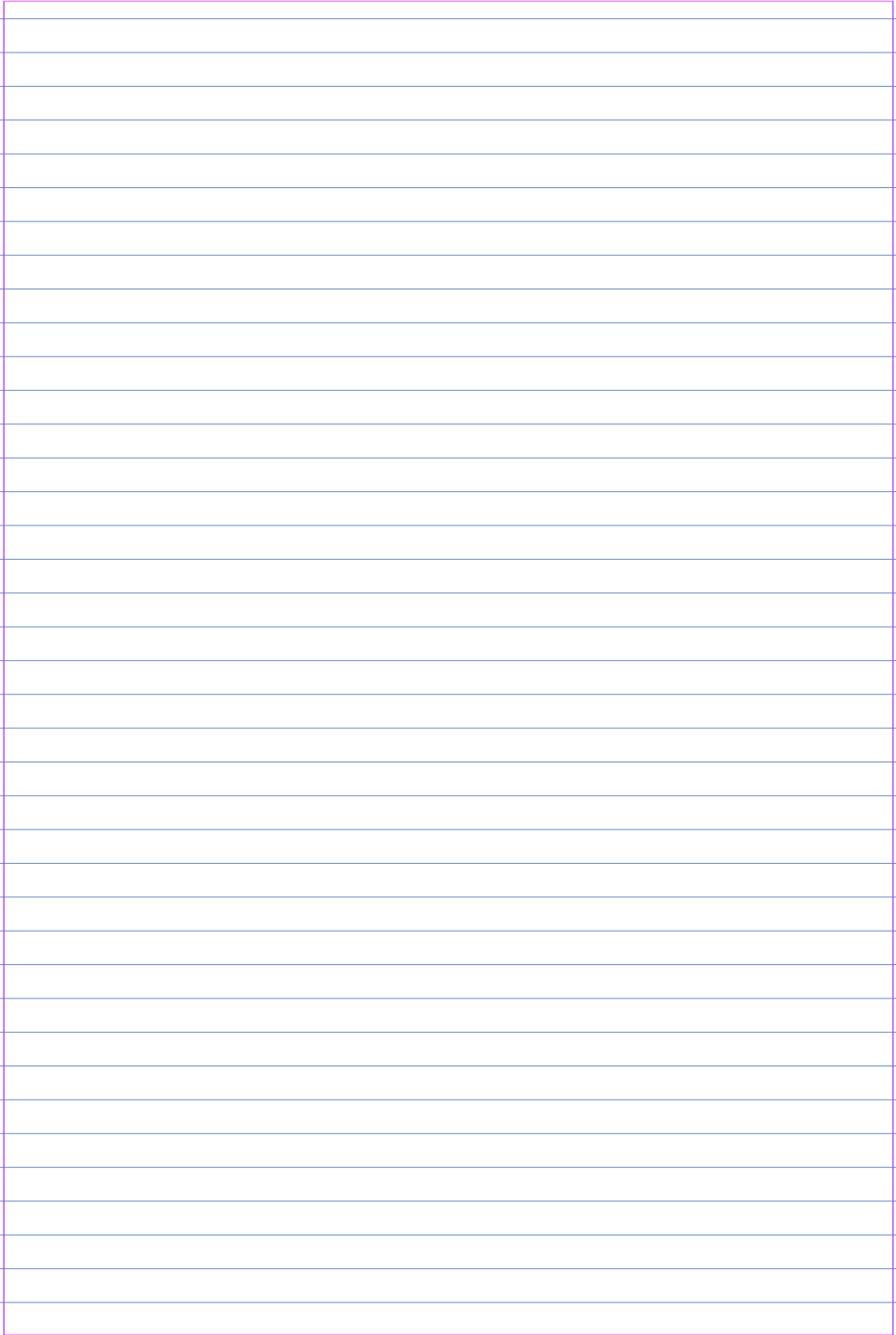
1. Meij BP, Voorhout G, Van den Ingh TSGAM, Hazewinkel HAW, Teske E, Rijnberk A. Results of transsphenoidal hypophysectomy in 52 dogs with pituitary-dependent hyperadrenocorticism. *Vet Surg* 1998;27:246-261.
2. Meij BP. Hypophysectomy as a treatment for canine and feline Cushing's disease. *Vet Clin North Am (Small Anim Pract)* 2001;31:1015-1041.
3. Hanson JM, van 't Hoofd MM, Voorhout G, Teske E, Kooistra HS, Meij BP. Efficacy of transsphenoidal hypophysectomy in treatment of dogs with pituitary-dependent hyperadrenocorticism. *J Vet Intern Med* 2005;19:687-694.
4. Meij BP, Voorhout G, Van den Ingh TSGAM, Hazewinkel HAW, Van 't Verlaat JW. Transsphenoidal hypophysectomy in beagle dogs: evaluation of a microsurgical technique. *Vet Surg.* 1997;26:295-309.
5. Di Chiro G, Nelson KB. The volume of the sella turcica. *Am J Roentgenol* 1962;87:989-1008.
6. McLachlan MSE, Wright AD, Doyle FH. Plain film and tomographic assessment of the pituitary fossa in 140 acromegalic patients. *Br J Radiol* 1970;43:360-369.
7. Robertson WD, Newton TH. Radiologic assessment of pituitary microadenomas. *Am J Roentgenol* 1978;131:489-492.
8. Muhr C, Bergström K, Grimelius L, Larsson S-G. A parallel study of the roentgen anatomy of the sella turcica and the histopathology of the pituitary gland in 205 autopsy specimens. *Neuroradiology* 1981;21:55-65.
9. Taylor CR, Jaffe CC. Methodological problems in clinical radiology research: pituitary microadenoma detection as a paradigm. *Radiology* 1983;147:279-283.
10. Kooistra HS, Voorhout G, Mol JA, Rijnberk A. Correlation between impairment of glucocorticoid feedback and the size of the pituitary gland in dogs with pituitary-dependent hyperadrenocorticism. *J Endocrinol* 1997;152:387-394.
11. Voorhout G, Rijnberk A. Cisternography combined with linear tomography for visualization of pituitary lesions in dogs with pituitary-dependent hyperadrenocorticism. *Vet Radiol* 1990;31:74-78.
12. Nelson RW, Ihle SL, Feldman EC. Pituitary macroadenomas and macroadenocarcinomas in dogs treated with mitotane for pituitary-dependent hyperadrenocorticism: 13 cases (1981-1986). *J Am Vet Med*

- Assoc 1989;194:1612-1617.
13. Hullinger RL. The endocrine system. In: Evans HE (ed.) *Miller's anatomy of the dog*. 3rd ed. Philadelphia: WB Saunders Co, 1993;559-585.
  14. Kippenes H, Gavin PR, Kraft SL, Sande RD, Tucker RL. Mensuration of the normal pituitary gland from magnetic resonance images in 96 dogs. *Vet Radiol Ultrasound* 2001;42:130-133.
  15. Baxter BS, Sorenson JA. Factors affecting the measurement of size and CT number in computed tomography. *Invest Radiol* 1981;16:337-341.
  16. Auriemma E, Voorhout G, Barthez P. Determination of optimal window width and level for measurement of the canine pituitary gland height on computer tomographic images using a phantom. Accepted *Vet Radiol US* 2006
  17. Brodie BB, Titus EO, Wilson CWM. The absence of the blood-brain barrier from special areas of the brain. *J Physiol* 1960;152:20P-22P
  18. Bonneville JF, Cattin F, Dietemann JL. Pituitary adenomas with suprasellar extension. In: Bonneville JF, Cattin F, Dietemann JL (eds.) *Computed tomography of the pituitary gland*. Berlin: Springer Verlag, 1986;47-51.
  19. Elster AD. Modern imaging of the pituitary. *Radiology* 1993;187:1-14.
  20. Davis PC, Hoffman JC, Tindall GT, Braun IF. CT-surgical correlation in pituitary adenomas: evaluation in 113 patients. *Am J Neuroradiol* 1985;6:711-716.
  21. Davis PC, Hoffman JC, Spencer T, Tindall GT, Braun IF. MR imaging of pituitary microadenomas: CT, clinical and surgical correlation. *Am J Neuroradiol* 1987;8:107-112.
  22. Gardeur D, Naidich TP, Metzger J. CT analysis of intrasellar pituitary adenomas with emphasis on patterns of contrast enhancement. *Neuroradiology* 1981;20:241-247.
  23. Hasegawa T, Ito H, Shoin K, Kogure Y, Kubota T, Yamamoto S. Diagnosis of an isodense pituitary microadenoma by dynamic CT scanning. *J Neurosurg* 1984;60:424-427.
  24. Bonneville JF, Cattin F, Moussa-Bacha K, Portha C. Dynamic computed tomography of the pituitary gland: the 'tuft sign'. *Radiology* 1983;149:145-148.
  25. Hemminghytt S, Kalkhoff RK, Daniels DL, Williams AL, Grogan JP, Haughton VM. Computed tomographic study of hormone-secreting microadenomas. *Radiology* 1983;146:65-69.
  26. Page RB. Pituitary blood flow. *Am J Physiol* 1982;243:E427-E442.

27. Bergland RM, Page RB. Can the pituitary secrete directly to the brain? (affirmative anatomical evidence). *Endocrinol* 1978;102:1325-1238.
28. Hofman BM, Fahlbusch R. Treatment of Cushing's disease: a retrospective clinical study of the latest 100 cases. *Front Horm Res* 2006;34:158-184.
29. Laws ER, Sheehan JP, Sheehan JM, Jagnathan J, Jane JA, Oskouian R. Stereotactic radiosurgery for pituitary adenomas: a review of the literature. *J Neurooncol* 2004;69:257-272.
30. Chong BW, Newton TH. Hypothalamic and pituitary pathology. *Radiol Clin North Am* 1993;31:1147-1183.
31. Escourelle H, Abecassis JP, Betagna X, Guilhaume B, Pariente D, Derome P, Bonnin A, Luton JP. Comparison of computerized tomography and magnetic resonance imaging for the examination of the pituitary gland in patients with Cushing's disease. *Clin Endocrinol* 1993;39:307-313.
32. Fitzpatrick M, Tartaglino LM, Hollander MD, Zimmerman RA, Flanders AE. Imaging of sellar and parasellar pathology. *Radiol Clin N-Am* 1999;37:101-121.
33. Lee BCP, Deck MDF. Sellar and juxtaseilar lesion detection with MR. *Radiology* 1985;157:143-147.
34. Colombo N, Berry I, Kucharczyk J, Kucharczyk W, De Groot J, Larson T, Norman D, Newton TH. Posterior pituitary gland: appearance on MR images in normal and pathological states. *Radiology* 1987;165:481-485.
35. Fujisawa I, Asato R, Nishimura K, Togashki K, Itoh K, Nakano Y, Itoh H, Hashimoto N, Takeuchi J, Torizuka K. Anterior and posterior lobes of the pituitary gland: assessment by 1.5 T MR imaging. *J Comp Assist Tomogr* 1987;11:214-220.
36. Fujisawa I, Nishimura K, Asato R, Togashi K, Itoh K, Noma S, Kawamura Y, Sago T, Minami S, Nakano Y, Itoh H, Torizuka K. Posterior lobe of the pituitary in diabetes insipidus: MR findings. *J Comp Assist Tomogr* 1987;11:221-225.
37. Kurakowa H, Fujisawa I, Nkano Y, Kimura H, Akagi K, Ikeda K, Uokawa K, Tanaka Y. Posterior lobe of the pituitary gland: correlation between signal intensity on T1-weighted MR images and vasopressin concentration. *Radiology* 1998;207:79-83.
38. Duesberg CA, Feldman EC, Nelson RW, Bertoy EH, Dublin AB, Reid MH. Magnetic resonance imaging for diagnosis of pituitary macrotumors in dogs. *J Am Vet Med Assoc* 1995;206:657-662.
39. Bertoy EH, Feldman EC, Nelson RW, Vaden SL, Scott-Moncrieff JCR.

- Magnetic resonance imaging of the brain in dogs with recently diagnosed but untreated pituitary-dependent hyperadrenocorticism. *J Am Vet Med Assoc* 1995;206:651-656.
40. Bertoy EH, Feldman EC, Nelson RW, Dublin AB, Reid MH, Feldman MS. One-year follow-up evaluation of magnetic resonance imaging of the brain in dogs with pituitary-dependent hyperadrenocorticism. *J Am Vet Med Assoc* 1996;208:1268-1273.
  41. Graham JP, Roberts GD, Newell SM. Dynamic magnetic resonance imaging of the normal canine pituitary gland. *Vet Radiol US* 2000;41:35-40.
  42. Kippenes H, Gavin PR, Kraft SL, Sande RD, Tucker RL. Mensuration of the normal pituitary gland from magnetic resonance images in 96 dogs. *Vet Radiol US* 2001;42:130-133.
  43. Grönemeyer DHW, Lufkin RB. *Open Field Magnetic Resonance Imaging*. Berlin: Springer Verlag, 2000.

## DIAGNOSTIC IMAGING OF THE PITUITARY GLAND IN DOGS

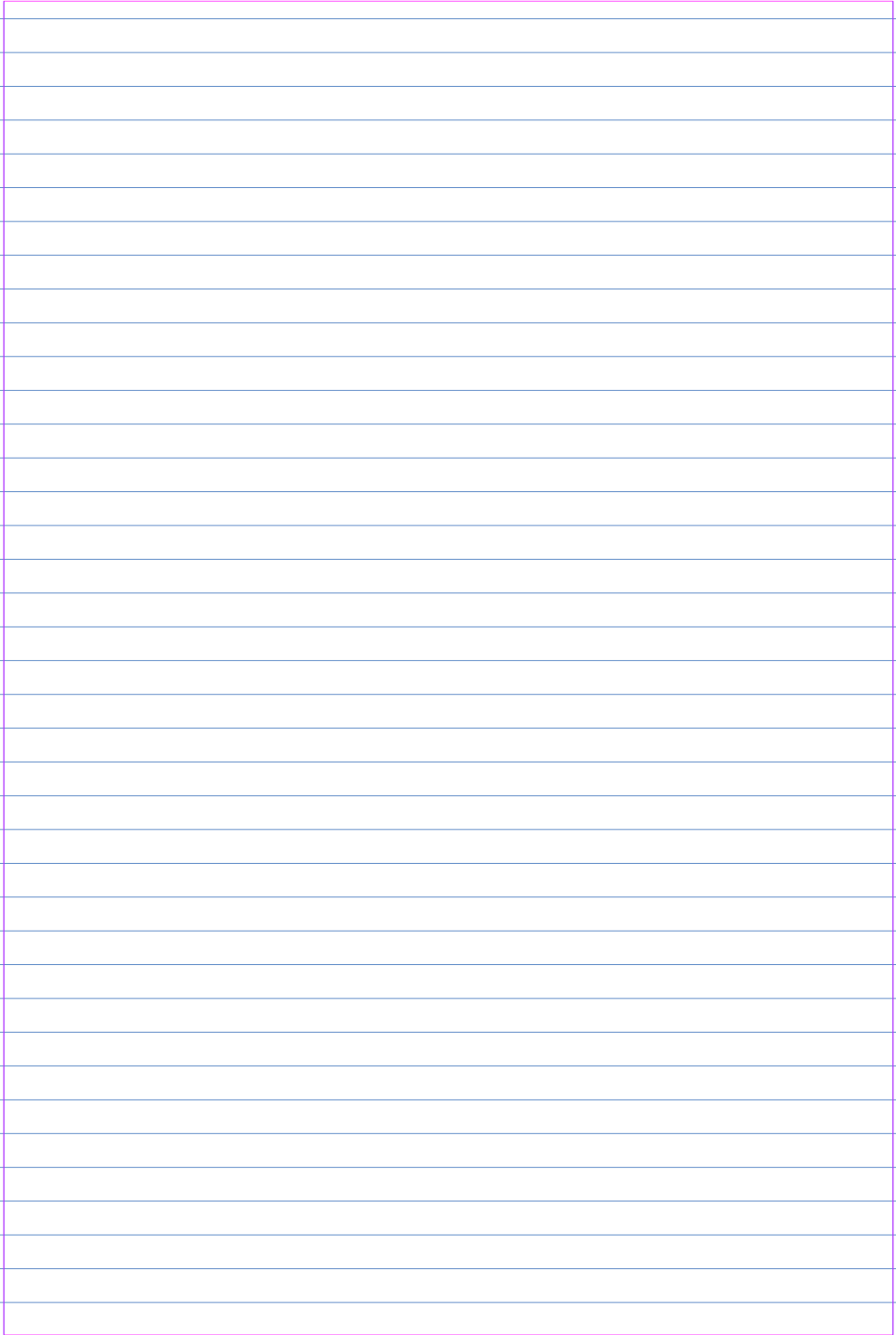


A large, empty rectangular box with a purple border, occupying the majority of the page below the title. This box is likely intended for a student to draw a diagram or insert an image related to the diagnostic imaging of the pituitary gland in dogs.

# CHAPTER 8

## Samenvatting en Conclusies

## DIAGNOSTIC IMAGING OF THE PITUITARY GLAND IN DOGS



A large, empty rectangular box with a purple border, occupying the majority of the page below the title. This box is likely intended for students to take notes, draw diagrams, or provide answers related to the topic of diagnostic imaging of the pituitary gland in dogs.

## Samenvatting

Hypofyse-afhankelijk hyperadrenocorticisme (HAH) is een veel voorkomende endocriene aandoening bij honden. Diagnose en behandelingsmogelijkheden van HAH werden besproken in **Hoofdstuk 1**. Transssphenoidale hypofysectomie is een effectieve behandelmethodes van HAH bij honden. Echter, voor een succesvolle hypofysechirurgie is het essentieel om informatie over de grootte van de hypofyse en de exacte locatie van de hypofyse ten opzichte van de benige oriëntatiepunten te verkrijgen. Informatie over de grootte van de hypofyse is niet alleen belangrijk voor de chirurg, maar geeft ook informatie over de prognose. De duur van overleving en remissie na hypofysectomie is duidelijk langer bij honden met niet vergrote hypofyses dan bij honden met vergrote hypofyses.

Bij mensen is het maken van conventionele röntgenfoto's heel lang de standaard methode geweest om vergroting en benige veranderingen van de sella turcica te identificeren bij patiënten met ruimte-innemende processen in de regio van de hypofyse. Echter, veel van de kleine veranderingen aan de sella turcica bleken later normale variaties te zijn. Bij honden is de hypofyse niet omringd door bot, maar ligt op de sella turcica. Vergroting van de hypofyse vindt vooral plaats in de hoogte, te weten de dorsale richting. Bovendien is bij de meeste honden de sella turcica op conventionele röntgenfoto's niet zichtbaar. Een vergrote hypofyse kan derhalve bij honden niet in beeld gebracht worden met behulp van conventionele röntgendiagnostiek. Andere technieken, zoals cisternografie in combinatie met lineaire tomografie, zijn beschreven maar de mate van uitbreiding in de hoogte kan hiermee niet worden vastgesteld. Bij de aanvang van dit promotieonderzoek waren CT en MRI nog relatief nieuwe technieken in de diergeneeskunde en waren er slechts enkele beschrijvingen van CT- en MRI-studies bij honden in de literatuur. Bovendien waren deze studies in de meeste gevallen uitgevoerd met protocollen die specifiek waren ontwikkeld voor mensen. Een gedeelte van dit promotieonderzoek is uitgevoerd om specifieke protocollen voor diagnostische beeldvorming van de hypofyse bij honden te ontwikkelen.

Om de CT- en MRI-beelden goed te kunnen begrijpen, is het essentieel om gedetailleerde anatomische kennis te hebben van de hypofyse en de omliggende structuren, zoals vaten en de benige oriëntatiepunten. Deze

zijn beschreven in **hoofdstuk 1**, waarin ook belangrijke verschillen tussen de hypofyse van mens en de honden worden benadrukt.

Transspheoidale hypofysectomie geeft het beste resultaat als het wordt uitgevoerd als eerste behandeling van honden met HAH en een hypofyse van normale grootte of met een gering vergrote hypofyse. In de veterinaire radiologie werden adenomateuse hypofyses in eerste instantie ingedeeld als microadenomen ( $< 10$  mm) of macroadenomen ( $> 10$  mm), gebaseerd op criteria die werden gebruikt bij mensen. Hypofyses kleiner dan 10 mm werden beoordeeld als normaal. Echter, de grenswaarde van 10 mm kan niet gebruikt worden voor honden omdat de normale hypofyse van de mens, die maximaal 10 mm in diameter is, groter is dan de hypofyse van de hond. Bovendien varieert de grootte van de hypofyse bij honden tussen de verschillende rassen en zelfs tussen honden van hetzelfde ras. Gebaseerd op de relatie tussen de dorsale contour van de hypofyse van de hond en de basale cisternen, werden veel hypofyses van honden met HAH die kleiner waren dan 10 mm toch beoordeeld als vergroot. De ratio tussen de hoogte van de hypofyse en de oppervlakte van de hersenen (P/B ratio), welke een correctie geeft voor de grootte van de hond, gaf het beste onderscheid tussen vergrote en niet-vergrote hypofyses. Niet-vergrote hypofyses hebben een P/B ratio van 0.31 of kleiner. De afmetingen van de hypofyse zijn beschreven bij gezonde honden en honden met HAH, maar er is geen informatie over de overeenstemming tussen de herhaalde metingen van één beoordelaar of tussen de metingen van verschillende beoordelaars. Verder is er geen informatie over de juistheid (accuratesse) van de metingen, d.w.z de overeenstemming tussen de metingen op de CT-beelden en de werkelijke afmetingen. In **Hoofdstuk 2** wordt een studie beschreven waarin de reproduceerbaarheid van het meten van de afmetingen van de hypofyse is onderzocht. In hetzelfde hoofdstuk is de juistheid van de metingen bepaald door middel van een fantoom. Het onderzoek liet zien dat de overeenstemming tussen de herhaalde metingen van één beoordelaar en tussen de metingen van twee beoordelaars uitstekend is, vooral voor de metingen van de hoogte van de hypofyse en voor de bepaling van de P/B ratio (wat de twee parameters zijn die het meest worden gebruikt in andere studies). Voor wat betreft de juistheid van de metingen liet het onderzoek zien dat het gebruikte CT-protocol een systematische onderschatting van de werkelijke hoogte van de hypofyse gaf. De meest exacte meting van een object wordt verkregen als de het vensterniveau (window level) wordt ingesteld op de helft van het verschil in Hounsfield eenheden tussen het te meten object en de achtergrond van het object. Bij de meting van de hoogte van de hypofyse spelen twee grenzen een

rol: de grens tussen de hypofyse en hersenen dorsaal en de grens tussen hypofyse en het benige basisphenoid ventraal. Bijstelling van het vensterniveau voor de overgang tussen hypofyse en bot levert een meer accurate meting op.

Op CT-beelden is de densiteit (dichtheid) van de normale hypofyse bij de mens en de hond homogeen en bijna identiek (isodens) aan de densiteit van hersenweefsel. Na intraveneuze toediening van contrastvloeistof neemt de densiteit van de hypofyse toe (hyperdens) ten opzichte van hersenweefsel, wat verklaard kan worden door het feit dat de hypofyse buiten de bloed-hersenenbarrière ligt. CT met gebruik van contrastvloeistof wordt bij de mens en de hond aangewend om hypofysetumoren in beeld te brengen. Grote hypofysetumoren met uitbreiding boven het dorsum sellae (suprasellair) kunnen op deze manier makkelijk worden gediagnosticeerd. Echter, microadenomen, die de grootte en de vorm van de hypofyse niet beïnvloeden, kunnen over het hoofd worden gezien wanneer het adenomateuze hypofyseweefsel even sterk aankleurt als het omliggende normale hypofyseweefsel. Bij mensen zijn microadenomen aangetoond met behulp van dynamische CT. Dynamische CT bestaat uit een serie scans op één en dezelfde positie door het centrum van de hypofyse, gedurende en volgend op een intraveneuze bolusinjectie met contrastvloeistof. In **Hoofdstuk 3** is het dynamische aankleuringspatroon van de hypofyse bij gezonde honden besproken. Na een sterke aankleuring van de arteria maxillaris, het intracaverneuze deel van de arteria carotis interna en de arteria communicans van de cerebrale arteriële cirkel, volgt een sterke aankleuring van het centrale deel van de hypofyse, hetgeen weer gevolgd wordt door aankleuring van het perifere gedeelte van de hypofyse. Ook bij mensen is een sterke aankleuring van het centrale gedeelte van de hypofyse beschreven en dit werd verklaard als de aankleuring van het secundaire capillaire bed ("hypofysaire tuft") van de lobus anterior van de adeno-hypofyse, gevolgd door een aankleuring van het perifere gedeelte van de hypofyse. Bij honden is het verschil in aankleuring tussen het centrale en perifere gedeelte van de hypofyse een gevolg van het verschil in bloedvoorziening van respectievelijk de neurohypofyse en de adeno-hypofyse. De neurohypofyse heeft een direct arteriële bloedvoorziening terwijl de adeno-hypofyse van bloed wordt voorzien door de hypofysaire portaalvaten. Om een onderscheid te maken met de "hypofysaire tuft" bij mensen wordt de vroege en sterke aankleuring van de neurohypofyse bij honden de "hypofysaire flush" genoemd. De "hypofysaire tuft" zou ook aanwezig moeten zijn bij honden, maar is nog niet aangetoond. Dit kan verklaard worden door de relatief kleine

afmetingen en de hoefijzervorm van het pars distalis van de adeno-hypofyse, maar de detectiegevoeligheid is ook afhankelijk van de apparatuur die wordt gebruikt. CT-apparatuur met hogere resolutie, kortere scantijden en kortere intervaltijden tussen de scans zou het mogelijk moeten maken om de “hypofysaire tuft” ook bij honden aan te tonen.

Zoals geldt voor het “hypofysaire tuft teken” bij mensen, zou verplaatsing, vervorming of het verdwijnen van de “hypofysaire flush” gebruikt kunnen worden om microadenomen in de hypofyse van honden met HAH te lokaliseren. In **Hoofdstuk 4** is het dynamisch CT-onderzoek van de hypofyse beschreven bij honden met HAH die vervolgens een transsphenoidale hypofysectomie ondergingen. Het doel van dit onderzoek was om het patroon van aankleuring van de hypofyse vast te stellen en de bevindingen te correleren met de bevindingen tijdens de transsphenoidale hypofysectomie en de bevindingen van het histopathologisch onderzoek van het chirurgisch verwijderde weefsel. Bij 82% van de honden met HAH was de hypofyse abnormaal tijdens het dynamisch CT-onderzoek, wat hoger was dan bij de mens, waar de hypofyse abnormaal was bij 54% van de patiënten. Echter, uit histopathologische gegevens bleek dat wanneer selectieve verwijdering van het adenomateuze weefsel het doel van de operatie zou zijn geweest, dit slechts bij 15% van de honden succesvol zou zijn geweest. Selectieve verwijdering van het adenoom (selectieve adenomectomie) is het doel van de primaire transsphenoidale hypofyse chirurgie bij mensen. Bij een significant deel van deze patiënten moet men er echter vanuit gaan dat er adenomateus hypofyseweefsel in de hypofyse achterblijft, hetgeen de meest waarschijnlijke oorzaak is van het relatief grote aantal recidieven dat wordt gezien na chirurgische behandeling van mensen met de ziekte van Cushing. In tegenstelling tot de situatie bij de hond, worden mensen met de ziekte van Cushing veel vaker aanvullend behandeld met medicaties die werken op het bijnierschorsniveau of behandeld met conventionele of gerichte radiotherapie van de hypofyse.

Met dynamische CT wordt slechts een enkele 2-mm dikke plak onderzocht en microadenomen kunnen buiten deze plak liggen. Wanneer het adenoom wel in beeld is gebracht zal er veelal onvoldoende informatie zijn over de rostrale of caudale uitbreiding van het adenoom. Voor volledige en accurate lokalisatie van het adenoom zou een dynamisch CT onderzoek van de gehele hypofyse, in plaats van slechts één plak, gemaakt moeten worden.

In **Hoofdstuk 5** wordt het dynamisch CT onderzoek van de gehele hypofyse met behulp van spiraal CT beschreven. In deze pilot-studie werd een protocol ontwikkeld voor de dynamische CT van de gehele hypofyse en de omringende vaten. Een vergelijkbaar patroon van aankleuring van de hypofyse werd gezien voor de gehele hypofyse zoals voor de dynamische CT van één plak door de hypofyse (hoofdstuk 3 en 4). Bovendien gaf de dynamische spiraal CT extra informatie over de vaten in de omgeving van de hypofyse. Er werd geconcludeerd dat de dynamische spiraal CT van de gehele hypofyse gebruikt moet kunnen worden voor het in beeld brengen van de adenomen in de hypofyse waardoor meer informatie gegeven kan worden over de grootte en vorm van de microadenomen.

Magnetic resonance imaging (MRI) is de eerste keuze voor de diagnostische beeldvorming van de hypofyse bij mensen. MRI zorgt voor een uitstekende differentiatie van de weke delen in alle scan-richtingen. Bovendien geeft het hypofysaire “bright signal”, het hyperintense signaal op de T1-gewogen opnamen dat overeenkomt met de neurohypofyse, aanvullende anatomische en functionele informatie. MRI van de hypofyse is ook beschreven bij honden. In die studies werd een 1.5 Tesla (T) MRI-scanner gebruikt met spin-echo sequenties en een plakdikte van 3 of 5 mm. Microadenomen bij honden met HAH kunnen een diameter hebben van niet meer dan 1-2 mm. Op MRI beelden gemaakt met een plakdikte van 3 mm of meer kunnen afwijkingen in de hypofyse gemist worden. Met 3D gradiënt echo (GE) sequenties kunnen dunnere plakjes gemaakt worden met een betere beeld kwaliteit. **Hoofdstuk 6** beschrijft de ontwikkeling van een MRI protocol voor het in beeld brengen van de hypofyse bij honden waarbij dunne plakken worden verkregen met behulp van een 3D GE sequentie. Dit protocol is ontwikkeld met een 0.2 T open MRI scanner die in 2000 is geïnstalleerd bij de afdeling Diagnostische Beeldvorming. Uit het onderzoek werd geconcludeerd dat MRI van de hypofyse bij honden, met gebruik van een 0.2 T open MRI scanner, moet bestaan uit een T1-gewogen GE (flash 3D) sequentie met een plakdikte van 1mm en een flip-angle van 30°, vóór en na een intraveneuze toediening van contrastvloeistof. De neurohypofyse, zichtbaar als het hypofysaire “bright signal” werd het beste in beeld gebracht op de sequenties zonder contrastvloeistof. MRI maakt onderscheid mogelijk tussen de hypofyse en de omringende structuren, maar de specifieke chirurgische benige oriëntatiepunten van de hypofysaire regio waren moeilijk in beeld te brengen. Hoewel het sphenoid zelf zichtbaar was op de

MRI-beelden, was het moeilijk om de vorm van de buitenste corticale botlaag te herkennen op de transversale beelden. De hamulae waren zichtbaar op de transversale MRI beelden, maar de detectie werd in grote mate beïnvloedt door de intensiteit van het omliggende weefsel. Het uitvoeren van een dynamische MRI-onderzoek is in overweging genomen, maar was niet mogelijk met de lage magneetveldsterkte van de gebruikte scanner. Zoals vermeld in hoofdstuk 1, werd de 0.2 T open MRI scanner geïnstalleerd op de afdeling vanwege de mogelijkheid om onder anesthesie MRI beelden van zowel gezelschapsdieren als van hoofd en benen van paarden te maken. De toegenomen interesse voor open MRI systemen is vooral veroorzaakt door de behoefte van humane patiënten aan een meer comfortabele onderzoeksomgeving (gevoel van claustrofobie in de gesloten MRI tunnels kwam veel voor) en door de vraag naar goedkopere apparatuur met minder onderhoudskosten. Nu worden de open MRI systemen meer en meer gebruikt vanwege hun rol bij interventieprocedures. Een voorbeeld hiervan is de MRI-geleide neurochirurgie van de hersenen van mensen, waarbij gebruik wordt gemaakt van speciale neuronavigatie apparatuur en chirurgische instrumenten die volledig "MRI-compatible" zijn. Hiervoor is het nodig dat de chirurg en de operatietafel bij de MRI-scanner staan, en dit is het beste mogelijk met een open MRI-scanner. Een nadeel van alle open MRI systemen is dat de magneetveldsterkte beperkt is. Op dit moment is de maximale magneetsterkte van open MRI systemen ongeveer 0.6 T omdat voor open MRI systemen elektromagneten worden gebruikt en het moeilijk is om het magneetveld homogeen te houden. Het open MRI systeem dat in 2000 geïnstalleerd is op onze afdeling was destijds alleen beschikbaar met een maximale veldsterkte van 0.2 T.

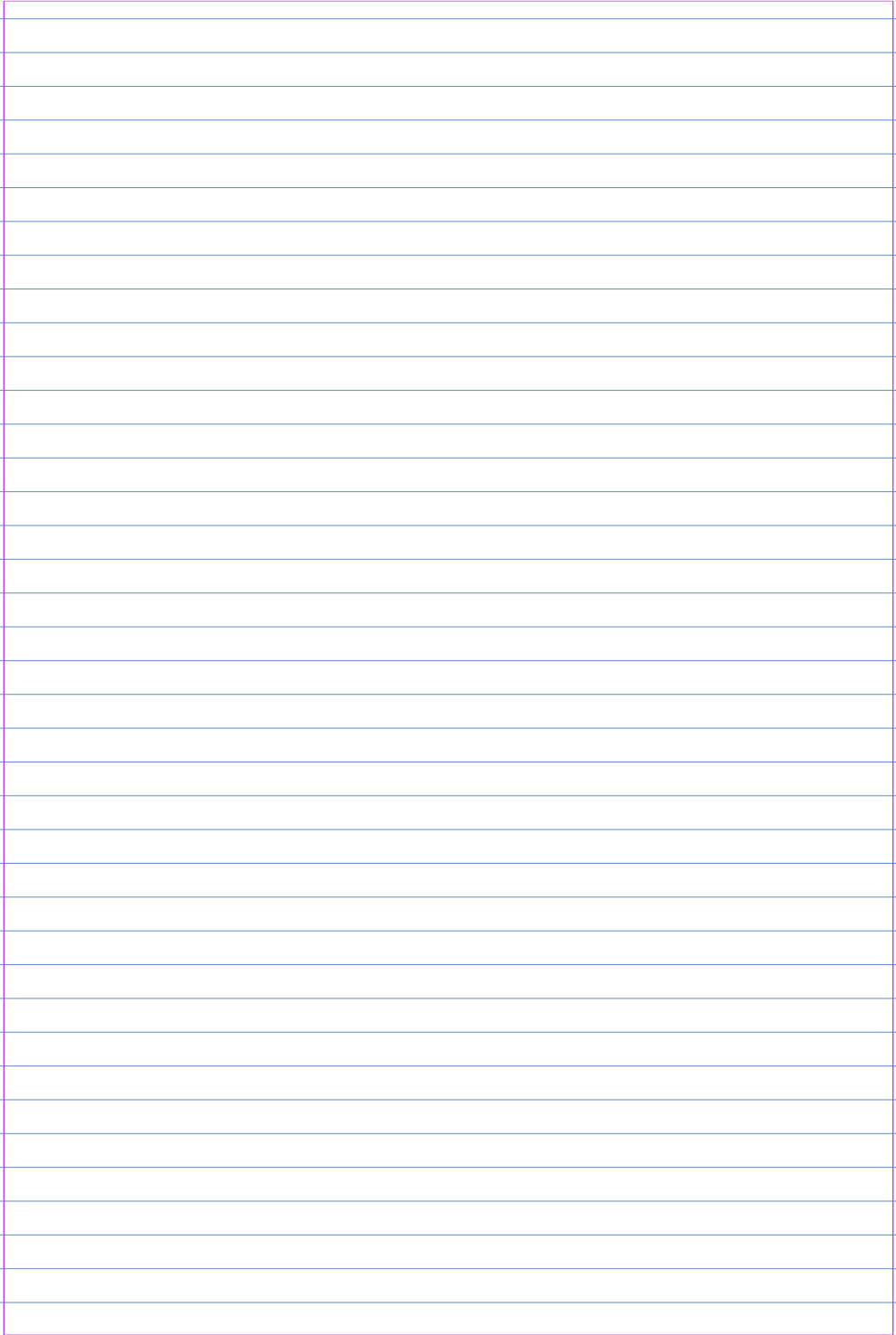
Zowel de dynamische spiraal CT als MRI van de hypofyse kunnen waardevolle informatie geven over de hypofyse bij honden. Een vervolg op het onderzoek in dit proefschrift zou een vergelijkende studie tussen spiraal CT en MRI kunnen omvatten bij honden met HAH om te bepalen welke van de twee technieken de meest waardevolle informatie geeft, vooral wanneer chirurgie van de hypofyse wordt overwogen. Op dit moment is complete hypofysectomie het doel van hypofysaire chirurgie bij de hond. Op het moment dat dynamische spiraal CT en/of MRI het adenoom, de normale adeno-hypofyse en de neurohypofyse beter kunnen lokaliseren binnen de contouren van de hypofyse, zou dit kunnen veranderen. Op dat moment zou het mogelijk kunnen zijn alleen de adeno-hypofyse of alleen het adenoom (selectieve adenomectomie) te

verwijderen. Dit zal nog belangrijker worden op het moment dat het mogelijk wordt om na de operatie gerichte bestraling (m.b.v. een lineaire versneller) toe te passen. Bij MRI van de hypofyse moet ook aandacht besteed worden aan het in beeld brengen van de hypofyse in relatie tot de benige structuren en oriëntatiepunten. MRI van de hypofyse kan alleen dan de (dynamische) spiraal CT van de hypofyse vervangen wanneer bot en weke delen rondom de hypofyse met MRI even goed of beter in beeld worden gebracht dan met spiraal CT.

## Conclusies

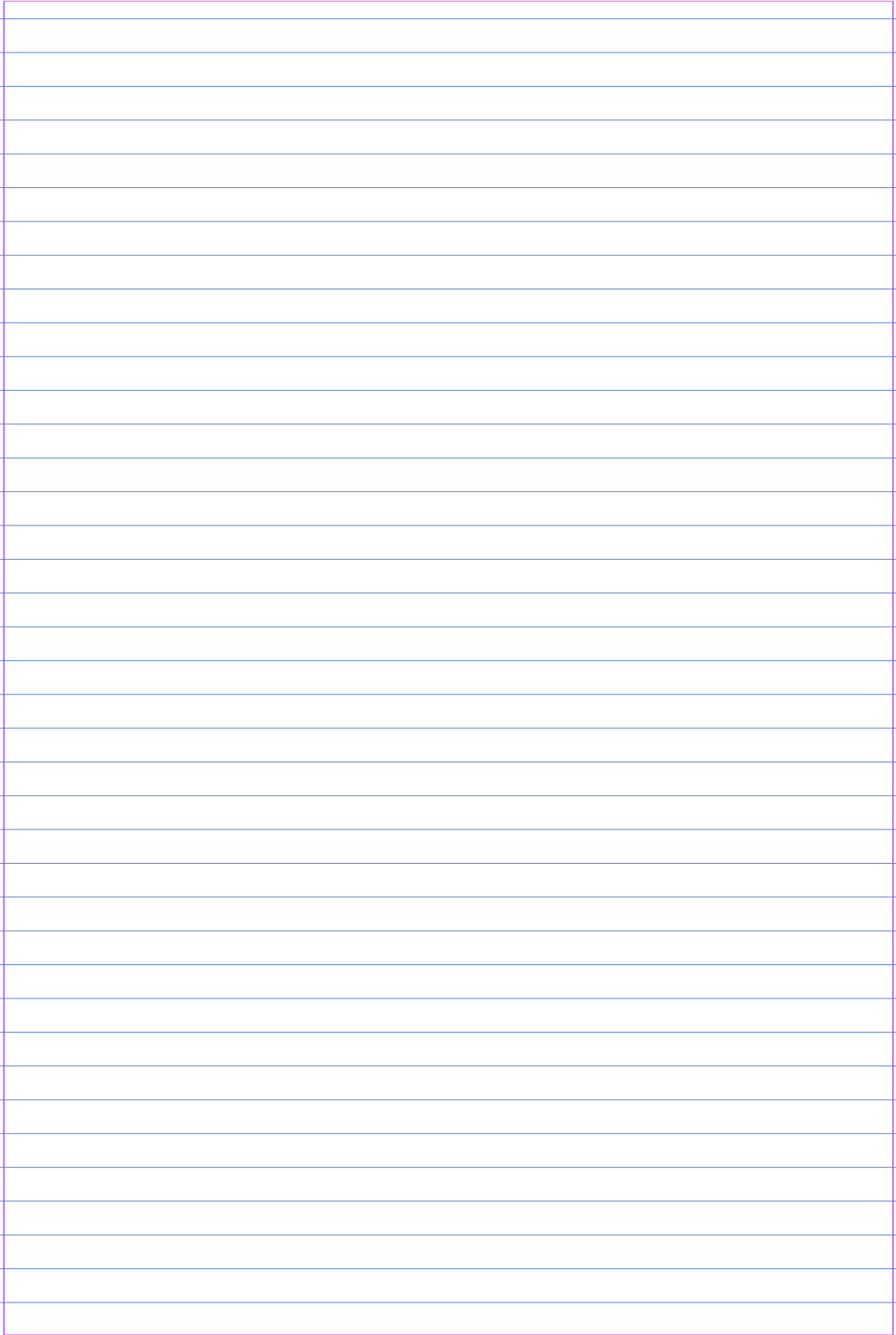
- Metingen van de hoogte van de hypofyse en de P/B ratio op CT beelden van gezonde honden, hebben een lage intra- en interwaarnemersvariatie. De afmetingen van de hypofyse, zoals gemeten op CT-beelden, worden systematisch onderschat in vergelijking met de werkelijke afmetingen van de hypofyse. Voor juiste metingen van de hoogte van de hypofyse moeten bij de hypofyse-hersenen en hypofyse-bot overgangen verschillende vensterniveaus gebruikt worden.
- Transversale dynamische CT van de hypofyse laat het verschil zien in de aankleuring van de neurohypofyse centraal, zichtbaar als de hypofysaire flush, en de adenoypofyse perifeer.
- Verplaatsing, vervorming of het verdwijnen van de hypofysaire flush is het bewijs van een abnormale hypofyse. Verplaatsingen vervorming van de hypofysaire flush geeft informatie over de locatie, grootte en vorm van hypofysaire adenomen bij de hond.
- Dynamische spiraal CT kan gebruikt worden voor het in beeld brengen van het aankleuringspatroon van de gehele hypofyse en geeft informatie over het omringende vaatbed. Dynamische spiraal CT van de gehele hypofyse zal in vergelijking met dynamische CT van één plak door de hypofyse meer informatie geven over de grootte en vorm van microadenomen in de hypofyse.
- Voor het verkrijgen van dunne plakjes van de hypofyse met een 0.2 T open MRI scanner kan het beste gebruikt worden gemaakt van een 3D gradiënt echo sequentie in transversale of dorsale richting, zowel vóór als na intraveneuze toediening van contrastvloeistof.
- Een vergelijkende studie tussen spiraal CT en MRI van de hypofyse bij honden met HAH is noodzakelijk om te bepalen welke van de 2 technieken de meest waardevolle informatie geeft, met speciale aandacht voor de benige chirurgische oriëntatiepunten.

## DIAGNOSTIC IMAGING OF THE PITUITARY GLAND IN DOGS



A large, empty rectangular box with a purple border, occupying the majority of the page below the title. This box is likely intended for a student to draw a diagram or insert an image related to the diagnostic imaging of the pituitary gland in dogs.

## DIAGNOSTIC IMAGING OF THE PITUITARY GLAND IN DOGS



A large, empty rectangular box with a purple border, occupying the majority of the page below the title. This box is likely intended for a student to draw a diagram or insert an image related to the diagnostic imaging of the pituitary gland in dogs.

# DANKWOORD

Al een tijdje heb ik over dit, niet onbelangrijke en veel gelezen, gedeelte van het proefschrift nagedacht. Een paar pagina's tekst schieten eigenlijk tekort om de dank die ik aan zoveel mensen verschuldigd ben goed over te brengen. Ik ga het echter toch proberen.

Dr. Voorhout, beste George, ik zie in jou een echte wetenschapper. Al vanaf het eerste gesprek heb jij mij met jouw enthousiasme voor het wetenschappelijke onderzoek aangestoken. Was een bepaalde vraag opgelost, dan was de volgende vraag bij jou alweer gerezen. Helaas hebben we, door het tijdsgebrek vanwege personele en bestuurlijke vernieuwingen, mijn/ons onderzoek niet kunnen afmaken zoals we beiden voor ogen hadden. Het is uiteindelijk toch gelukt en ik ben je dan ook erg dankbaar.

Dr. Meij, beste Björn, toen het afronden van het proefschrift stroef ging en alles stil lag, heb jij je ontpopt als de reddende engel. Je liet je niet afschepen en was altijd bereid om te helpen. Jouw altijd positieve mailtjes, waarin je aangaf dat je met veel plezier naar een manuscript had gekeken, gaven mij weer moed om door te gaan. Uiteindelijk heb jij ervoor gezorgd dat er weer schot in kwam en dat mijn proefschrift toch nog binnen niet al te lange tijd is afgerond.

Prof. Barthez, beste Paul, naast het feit dat ik natuurlijk een promotor nodig had, heeft u voor mij een waardevolle bijdrage geleverd aan de totstandkoming van het proefschrift. Tijdens discussies was u de waardevolle derde persoon en wist u ook spijkers met koppen te slaan. Ik ben vereerd uw eerste promovendus te zijn.

Drs. Boroffka, lieve Susanne, dank je wel voor je interesse en alle gesprekken. Ik zie uit naar jouw proefschrift, dat waarschijnlijk snel zal volgen.

Alle (oud)-medewerkers van de afdeling Diagnostische Beeldvorming wil ik hartelijk bedanken voor de 3 jaar dat ik deel heb mogen uitmaken van de vakgroep. Zonder anderen te kort te willen doen, wil ik het woord nog specifiek aan enkele van jullie richten. Maartje en Natasja, bedankt voor de gezelligheid op de sio-kamer en de wandelingen met onze honden. Anke, bedankt voor je hulp als ik die nodig had en voor jouw altijd stralende lach. Yvette, ik mis je Brabantse optimisme. Hans, omdat je altijd voor een praatje te vinden was. Lineke, bij jou kon ik, als het nodig was, altijd mijn hart luchten.

Nergens zijn de afbeeldingen zo belangrijk als bij de afdeling Radiologie en daarom ben ik Aart van der Woude, Yvonne Polak en Joop Fama dank verschuldigd voor de mooie afdrukken in mijn proefschrift. Karin Bosch wil ik graag bedanken voor het drukklaar maken van het proefschrift, meid wat ben jij daar goed in!

Zoals u in het proefschrift kunt lezen moeten de honden voor het onderzoek gedurende langere tijd heel stil blijven liggen en wie kunnen daar beter mee helpen dan de afdeling Anesthesiologie. Dat hebben zij ook perfect gedaan (er waren maar weinig taarten te verdienen), waarvoor mijn dank. Een speciaal woord wil ik hierbij richten tot Gert Haalboom, die veruit de meeste onderzoeken heeft begeleid, en voor een hoop gezelligheid heeft gezorgd op de CT en MRI kamers.

Van de afdeling Geneeskunde van Gezelschapsdieren ben ik dank verschuldigd aan een ieder die interesse heeft getoond voor mijn onderzoek; in het bijzonder de specialisten Endocrinologie: Prof. Rijnberk, Hans Kooistra, Montse Diaz en Sarah Galac.

Omdat wij gebruik hebben mogen maken van hun spiraal CT ben ik de hogeschool Haarlem, en in het bijzonder Tom Rhoding dankbaar.

Dank ben ik ook verschuldigd aan mijn huidige werkgevers, Bas Laméris en Cees van Veldhuizen, en mijn huidige collega's. Het feit dat ik mij bij ACE Pharmaceuticals BV zo thuis voel, maakte het makkelijker om mij 's avonds weer op de afronding van mijn proefschrift te kunnen storten.

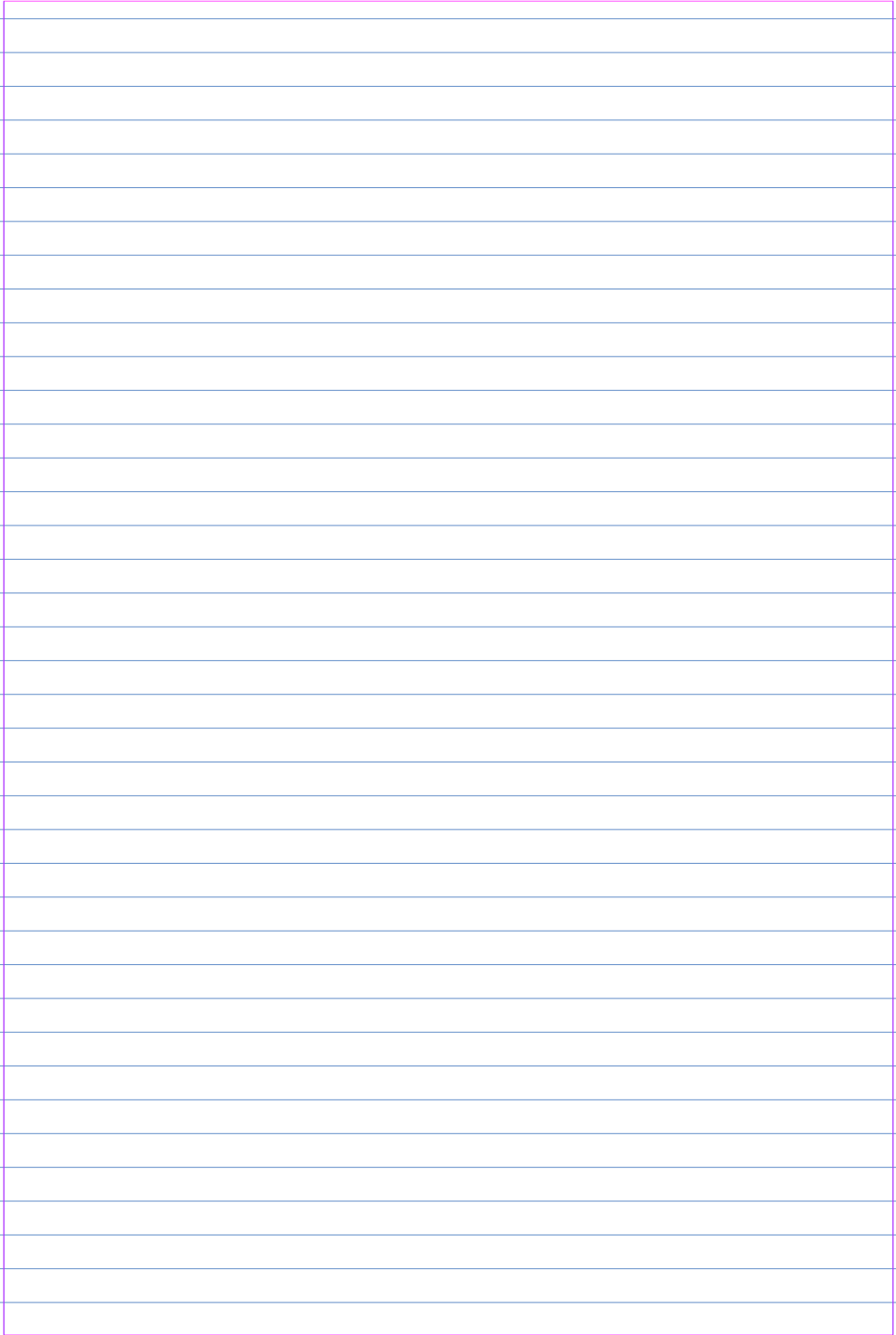
Waar zou ik zijn geweest zonder de altijd klaarstaande hulp van mijn oppasmoeders, Germa, Diana en Mieke. Heerlijk zo'n uitgebreide achterwacht!

Mama en papa, ik wil jullie bedanken voor de zelfstandigheid en het doorzettingsvermogen dat ik van jullie heb meegekregen. Papa, wat was je blij toen ik eindelijk ging studeren, helaas kun je dit niet meer lijfelijk meemaken, maar ik weet dat je nog ergens bent en dat zal mij op 9 november moed geven! Lieve ma, zussen, zwagers, schoonzus, neefjes en nichtjes, mijn familie is goud waard, dank jullie wel.

Allerliefste Vera en Alex, jullie komst heeft mij geleerd te relativeren en sterker gemaakt. Ook al begrijpen jullie nog niet helemaal wat promoveren betekent, blij zijn jullie wel, al is dat voornamelijk doordat ik nu weer meer tijd voor jullie kan vrijmaken.

Allerliefste Lex, mijn maatje, dank je wel voor de ruimte die je mij hebt gegeven om mijn eigen beslissingen te nemen. Ook ben ik je dankbaar dat jij altijd voor mij klaar stond, zowel tijdens de studie als tijdens het promotieonderzoek. Kinderen en promoveren zijn beide een test voor een relatie. Het feit dat onze relatie beide tegelijk met glans heeft doorstaan, geeft aan dat het goed zit tussen ons.

## DIAGNOSTIC IMAGING OF THE PITUITARY GLAND IN DOGS



A large, empty rectangular box with a purple border, occupying the majority of the page below the title. This box is likely intended for a student to draw a diagram or insert an image related to the diagnostic imaging of the pituitary gland in dogs.

# CV

De schrijfster van dit proefschrift is op 2 mei 1967 geboren te Hellevoetsluis. Na het behalen van haar VWO-diploma in 1985 is de schrijfster gaan werken op de afdeling Radiologie van het Dijkzigt ziekenhuis te Rotterdam. Hier heeft zij de opleiding tot Radiodiagnostisch laborante gevolgd, die zij in 1987 met een diploma heeft afgesloten. In 1989 heeft de schrijfster nog een jaar in het Amsterdam Medisch Centrum gewerkt en heeft vervolgens een jaar Informatiekunde in de Gezondheidszorg gestudeerd. In 1991 werd zij, na 4 keer, eindelijk ingeloot voor de studie Diergeneeskunde te Utrecht. In 1995, heeft de schrijfster, met genoegen, haar doctoraal gehaald en heeft zij, voordat ze verder is gegaan met haar post-doctoraal, een jaar onderzoek gedaan op de afdeling Diagnostische Beeldvorming in het kader van het Excellent Tracé. Voordat de schrijfster haar co-schappen is gaan volgen heeft zij nogmaals 8 maanden onderzoek gedaan op de afdeling Diagnostische Beeldvorming. Na het behalen van haar dierenartsdiploma in december 1999, is de schrijfster in dienst gekomen als aio op de afdeling Diagnostische Beeldvorming en werd het onderzoek zoals beschreven in dit proefschrift voltooid. Sedert Februari 2003 is de schrijfster in dienst van ACE Pharmaceuticals BV in de functie van medewerker Klinisch Onderzoek en Registratie.

The author of this thesis was born in Hellevoetsluis, the Netherlands on May 2<sup>nd</sup> 1967. After finishing her education in 1985, she started working at the department of Diagnostic Imaging at the Dijkzigt Academic hospital in Rotterdam. She followed the education for radiological technician which she completed in 1987. In 1989 the author worked for one year at the Amsterdam Medical Center. In 1991 the author was finally admitted to study Veterinary Medicine at the Faculty of Veterinary Medicine of the Utrecht University. In 1995, she completed her DVM, with a distinction, and performed research at the Division of Diagnostic Imaging for 1 year, before continuing with the practical educations. During the practical education, she performed research at the division of Diagnostic Imaging for another 8 months. After obtaining her Veterinary Surgeon Certificate, the author continued working as a researcher at the Division of Diagnostic Imaging in order to complete the research described in this thesis. In February 2003 the author started working at ACE Pharmaceuticals BV as employee of the department Clinical Research and Registration.

## Publications

- Meij BP, van der Vlugt-Meijer RH, van den Ingh TS, Flik G, Rijnberk A. Melanotroph pituitary adenoma in a cat with diabetes mellitus. *Vet Pathol.* 2005 Jan;42(1):92-7.
- Meij BP, van der Vlugt-Meijer RH, van den Ingh TS, Rijnberk A. Somatotroph and corticotroph pituitary adenoma (double adenoma) in a cat with diabetes mellitus and hyperadrenocorticism. *J Comp Pathol.* 2004 Feb-Apr;130(2-3):209-15.
- Spoormakers TJ, Ensink JM, Goehring LS, Koeman JP, Ter Braake E, van der Vlugt-Meijer RH, van den Belt AJ. Brain abscesses as a metastatic manifestation of strangles: symptomatology and the use of magnetic resonance imaging as a diagnostic aid. *Equine Vet J.* 2003 Mar;35(2):146-51.
- Van der Vlugt-Meijer RH, Voorhout G, Meij BP. Imaging of the pituitary gland in dogs with pituitary-dependent hyperadrenocorticism. *Mol Cell Endocrinol.* 2002 Nov 29;197(1-2):81-7.
- Van der Vlugt-Meijer RH, Meij BP, van den Ingh TS, Rijnberk A, Voorhout G. Dynamic computed tomography of the pituitary gland in dogs with pituitary-dependent hyperadrenocorticism. *J Vet Intern Med.* 2003 Nov-Dec;17(6):773-80.
- Van der Vlugt-Meijer RH, Meij BP, Voorhout G. Dynamic computed tomographic evaluation of the pituitary gland in healthy dogs. *Am J Vet Res.* 2004 Nov;65(11):1518-24.
- Van der Vlugt-Meijer RH. (Severe adverse effects of certain veterinary drugs in collies and collie-like dogs) *Tijdschr Diergeneeskd.* 2004 Sep 1;129(17):556-7.
- Van der Vlugt-Meijer RH, Meij BP, Voorhout G. Intraobserver and interobserver agreement, reproducibility, and accuracy of computed tomographic measurements of pituitary gland dimensions in healthy dogs. *Am J Vet Res* 2006; in press.
- Van der Vlugt-Meijer RH, Meij BP, Voorhout G. Thin-slice 3-dimensional gradient-echo magnetic resonance imaging of the pituitary gland in healthy dogs. *Am J Vet Res* 2006; in press.
- Van der Vlugt-Meijer RH, Meij BP, Voorhout G. Dynamic helical computed tomography of the pituitary gland in healthy dogs. *Vet Radiol US* 2006; in press.